Volume 71A
Number 5
Sept.–Oct. 1967

Physics and Chemistry

U.S. DEPARTMENT OF COMMERCE

SECTION A

JOURNAL OF RESEARCH

NATIONAL BUREAU OF STANDARDS

Journal of Research

of the

National Bureau of Standards

A. Physics and Chemistry

Sept.–Oct. • 1967

VOLUME • 71A

NUMBER • 5

Editor: C. W. Beckett

Associate Editors: D. D. Wagman
J. M. Richardson

Publication dates:
Feb. 1, Apr. 1, June 1, Aug. 1, Oct. 1, Dec. 1, 1967

JOURNAL OF RESEARCH

The National Bureau of Standards Journal of Research reports research and development in the fields of activity shown at right. Also included from time to time are survey articles on topics closely related to the Bureau's scientific and technical program.

The Journal is published in three separate sections as follows:

A. Physics and Chemistry

Contains papers of interest primarily to scientists working in these fields. Issued six times a year. Annual subscription: domestic, $5.00; foreign, $6.00. Single copy, $1.00.

B. Mathematics and Mathematical Physics

Presents studies and compilations designed mainly for the mathematician and the theoretical physicist. Issued quarterly. Annual subscription: domestic, $2.25; foreign, $2.75. Single copy, 75c.

C. Engineering and Instrumentation

Reports research and development results of interest chiefly to the engineer and the applied scientist. Issued quarterly. Annual subscription: domestic, $2.75; foreign, $3.50. Single copy, 75c.

The National Bureau of Standards is a principal focal point in the Federal Government for assuring maximum application of the physical and engineering sciences to the advancement of technology in industry and commerce. Its responsibilities include development and maintenance of the national standards of measurement, and the provision of means for making measurements consistent with those standards; determination of physical constants and properties of materials; development of methods for testing materials, mechanisms, and structures, and making such tests as may be necessary, particularly for government agencies; cooperation in the establishment of standard practices for incorporation in codes and specifications; advisory service to government agencies on scientific and technical problems; invention and development of devices to serve special needs of the Government; assistance to industry, business and consumers in the development and acceptance of commercial standards and simplified trade practice recommendations; administration of programs in cooperation with United States business groups and standards organizations for the development of international standards of practice; and maintenance of a clearinghouse for the collection and dissemination of scientific, technical and engineering information. The scope of the Bureau's activities is suggested in the following listing of its three Institutes and their organizational units.

Institute for Basic Standards. Applied Mathematics. Electricity. Metrology. Mechanics. Heat. Atomic Physics. Physical Chemistry. Laboratory Astrophysics.* Radiation Physics. Radio Standards Laboratory.* Radio Standards Physics & Radio Standards Engineering. Office of Standard Reference Data.

Institute for Materials Research. Analytical Chemistry. Polymers. Metallurgy. Inorganic Materials. Reactor Radiations. Cryogenics.* Materials Evaluation Laboratory. Office of Standard Reference Materials.

Institute for Applied Technology. Building Research. Information Technology. Performance Test Development. Electronic Instrumentation. Textile and Apparel Technology Center. Technical Analysis. Office of Weights and Measures. Office of Engineering Standards. Office of Invention and Innovation. Office of Technical Resources. Clearinghouse for Federal Scientific and Technical Information.**

*Located at Boulder, Colo. 80302.
**Located at 5285 Port Royal Road, Springfield, Va. 22151.

U.S. DEPARTMENT OF COMMERCE
Alexander B. Trowbridge, Secretary
NATIONAL BUREAU OF STANDARDS
A. V. Astin, Director

Order all publications from the Superintendent of Documents
U.S. Government Printing Office, Washington, D.C. 20402
Use of funds for printing this publication approved by the Director of the Bureau of the Budget (June 22, 1966).

JOURNAL OF RESEARCH of the National Bureau of Standards—A. Physics and Chemistry
Vol. 71A, No. 5, September–October 1967

Zeeman Effect in Positronium Annihilation at Low Temperatures

William C. Sauder* and Richard D. Deslattes

Institute for Materials Research, National Bureau of Standards, Washington, D.C. 20234

(May 10, 1967)

The annihilation of positronium is discussed as a means of obtaining a precise measurement of the Compton wavelength of the electron. In particular the spectral line shape of the annihilation radiation is calculated for positronium thermalized in helium gas cooled to the region of its critical point with an applied magnetic field sufficient to yield a three photon to two photon branching ratio of unity for the $^3S_0$ component. Under such conditions the rapid thermalization of the positronium and the long half-life of two photon decay out of the predominantly triplet state make possible the production of rather narrow spectral distributions. An exact solution of the Zeeman effect in positronium is included. This study suggests that a wavelength determination beyond the one part per million level is attainable within the range of present technology.

Key Words: Annihilation radiation, Compton wavelength of the electron, positronium, quenching.

1. Introduction

X-ray data have been excluded from recent adjustments of the atomic constants [1][1] since at their then current precision they would have carried typically about one fifth the weight assigned to other measurements. Simply improving the precision of the x-ray data by a factor of three would lead to equal weight. Recent improvements in the internal consistency of the x-ray scale by Bearden et al. [2], permit a further sharpening by x-ray determinations of the constants to limits set by the uncertainty in the conversion factor between the x-ray wavelength scale and the defined length. Were these potentialities realized today, then the x-ray data would be significant in an adjustment of the fine structure constant and the proton moment [3].

The precision of x-ray measurements of the atomic constants is limited by the precision with which it is possible to define an x-ray wavelength scale. The scale, of course, depends on the precision with which it is possible to establish the wavelength of an individual x-ray line. Ordinary x-ray lines have full widths at half maximum upwards of some 300 ppm (parts per million). We have no theoretical model for their shape and hence little hope of specifying the wavelength of any of their features (peak, centroid, or median) to better than 1 ppm. This problem has been studied by J. S. Thomsen and F. Y. Yap [4].

Beside the traditional x-ray determinations of the constants there are phenomena which either occur spontaneously or can be provoked to occur which are considerably sharper than natural x-ray lines. For example, there are nuclear transitions which have quite narrow profiles [5] and there are crystal lattices of extraordinary perfection [6] which occur as, so to speak, spontaneous phenomena. Other phenomena which are also quite sharp can be produced by experimental design. One of these, namely radiation from the annihilation of positronium as narrowed by thermalization in a magnetic field is the subject of the present paper.

2. Positron-Electron Annihilation

If a positron and an electron initially at rest annihilate with the emission of two photons, then by conservation of energy,

$$2\frac{hc}{\lambda_A} = 2m_0c^2, \tag{1}$$

since conservation of linear momentum implies that the wavelengths of the two photons are equal. Solving eq (1) for λ yields the Compton wavelength:

$$\lambda_A = \frac{h}{m_0c} \tag{2}$$

where m_0 is the rest mass of either the electron or the positron.

*Associate Professor of Physics, Virginia Military Institute, Lexington, Virginia 24450. Consultant to the Crystal Chemistry Section, Inorganic Materials, Division, National Bureau of Standards, Washington, D.C. 20234.

[1] Figures in brackets indicate the literature references at the end of this paper.

If, however, the positron-electron system has nonzero momentum at the instant of annihilation, the two photons in general will not have the same wavelength, so that spectroscopic observation of the radiation shows a broadened annihilation line. Examination of this process shows that the line widths resulting from the annihilation of free positrons with electrons in matter are much too great (typically in excess of 1000 ppm) to allow a precision (i.e., approx. 1 ppm) measurement.

If a flux of positrons is incident upon certain materials, a significant fraction of these incoming particles will combine with electrons in the substance to form hydrogen-like atoms of positronium [7]. The peak of the annihilation line is shifted because the right-hand side of eq (1) is reduced by the binding energy of the positronium atom, while the width of the line is determined by the momentum of the positronium atom at the time of annihilation.

Positronium exists in either singlet (para-) or triplet (ortho-) states; the lifetime against annihilation of ortho-positronium is two orders of magnitude greater than that of para-positronium. The triplet lifetime is sufficiently great to allow an ortho-positronium atom to reach thermal equilibrium with its surroundings before annihilating. If this thermalization process is carried out in the presence of an external magnetic field, then an appreciable fraction of the long-lived positronium component will decay via the two photon channel because the field causes mixing of the singlet and triplet states. If the temperature of the surroundings is sufficiently low, then the resulting annihilation line will be narrow.

It is the purpose of this paper to examine in detail the line shape of the radiation produced in this process. In particular we shall consider the lifetime of the two photon annihilation of positronium in the presence of a magnetic field; combining this with appropriate expressions for the thermalization of the positronium and for the thermal distribution function of the surroundings yields an expression for the line shape.

3. Zeeman Effect of Positronium

The hyperfine separation between the singlet and triplet energy levels of positronium in its ground state is much greater than the corresponding splitting in the hydrogen atom for two reasons [8]. In the first place the dipole-dipole interaction between the electron and positron is proportional to the magnetic moment of the positron, and therefore is increased over the interaction in hydrogen by the ratio of the Bohr magneton to the nuclear magneton. Furthermore, the hyperfine splitting is increased by an amount that is approximately equal in magnitude to the dipole-dipole term by quantum electrodynamic effects involving virtual annihilation of the pair.

If $\mathcal{H}_0$ represents the Hamiltonian (including the hyperfine interaction) of the positronium, then one can represent the stationary ground state as an eigenstate

$$\mathcal{H}_0 u_{Fm} = E_F u_{Fm} \tag{3}$$

where $F=0$, 1 is the quantum number denoting the spin state of the atom, and m is the quantum number associated with z-component of the spin angular momentum. The states u_{Fm} are eigenfunctions of the spin operators $(S_e+S_p)^2$ and $(S_{ez}+S_{pz})$, where the subscripts e and p denote the electron and positron, respectively. These states, written in terms of the spin states of the individual particles, are

$$u_{11} = \Psi_0 u_e(\uparrow) u_p(\uparrow) \tag{4a}$$

$$u_{10} = \frac{\Psi_0}{\sqrt{2}}[u_e(\uparrow)u_p(\downarrow) + u_e(\downarrow)u_p(\uparrow)] \tag{4b}$$

$$u_{1-1} = \Psi_0 u_e(\downarrow) u_p(\downarrow) \tag{4c}$$

and

$$u_{00} = \frac{\Psi_0}{\sqrt{2}}[u_e(\uparrow)u_p(\downarrow) - u_e(\downarrow)u_p(\uparrow)] \tag{4d}$$

where Ψ_0 is the hydrogenic ground state wave function which results if spin is neglected. The hfs separation has been evaluated to be

$$\Delta E = E_1 - E_0 = 8\times 10^{-4}\text{eV}.$$

If an external magnetic field H is applied to the positronium atom, then the Hamiltonian becomes

$$\mathcal{H} = \mathcal{H}_0 + \mathcal{H}_H \tag{5}$$

where, in terms of magnetic moment operators μ for the positron and electron,

$$\mathcal{H}_H = -(\boldsymbol{\mu}_e + \boldsymbol{\mu}_p)\cdot \mathbf{H}. \tag{6}$$

Since the magnetic moments of the electron and positron are equal (approximately) in magnitude to the Bohr magneton but opposite in direction with respect to the spin vectors, and since their g factors are equal, then $\mathcal{H}_H$ can be written in terms of Pauli spin matrices σ_z as

$$\mathcal{H}_H = \frac{\mu_0 g H}{2}(\sigma_{ez} - \sigma_{pz}). \tag{7}$$

Some treatments [9] of the Zeeman effect in positronium have employed perturbation theory; however, an exact solution is readily obtained by well-known methods [10].

One can write down the Hamiltonian matrix by employing the fact that $\sigma_z u(\uparrow) = u(\uparrow)$ and $\sigma_z u(\downarrow)$

$=-u(\downarrow)$; the operation of $\mathfrak{H}_H$ in eq (7) on the wave functions in eq (4a-d) yields

$$\mathfrak{H}_H|u_{11}=\mathfrak{H}_H|u_{1-1}>=0$$

$$\mathfrak{H}_H|u_{10}>=\mu_0 gH|u_{00}>$$

and

$$\mathfrak{H}_H|u_{00}>=\mu_0 gH|u_{10}>. \tag{8}$$

As a result, the Hamiltonian matrix including the magnetic interaction is

$$\langle\mathfrak{H}\rangle=\begin{pmatrix} E_1 & 0 & 0 & 0 \\ 0 & E_1 & 0 & \mu_0 gH \\ 0 & 0 & E_1 & 0 \\ 0 & \mu_0 gH & 0 & E_0 \end{pmatrix} \tag{9}$$

The secular equation for $\langle\mathfrak{H}\rangle$ is

$$(E_1-\lambda)^2\{(E_1-\lambda)(E_0-\lambda)-(\mu_0 gH)^2\}=0 \tag{10}$$

with roots

$$\lambda=E_1, E_1, \overline{E}\pm\frac{1}{2}\Delta E\sqrt{1+x^2} \tag{11}$$

where

$$\overline{E}=\frac{1}{2}(E_1+E_0)$$

and

$$x=\frac{\mu_0 gH}{\Delta E/2}.$$

Thus the diagonalized matrix is

$$\langle\mathfrak{H}\rangle_{\text{diag}}=\begin{pmatrix} E_1 & 0 & 0 & 0 \\ 0 & \overline{E}+\frac{\Delta E}{2}\sqrt{1+x^2} & 0 & 0 \\ 0 & 0 & E_1 & 0 \\ 0 & 0 & 0 & \overline{E}-\frac{\Delta E}{2}\sqrt{1+x^2} \end{pmatrix} \tag{12}$$

Note that the degeneracy between the triplet $m=\pm 1$ states is not removed by $\mathfrak{H}_H$. Furthermore, the energy of these states is not affected by the field, since these states have zero net magnetic moment because the positron and electron are oppositely charged particles. The lack of a linear Zeeman effect, and the existence of a quadratic effect in the $m=0$ state can be described qualitatively as follows. The triplet $m=0$ state as mentioned above has no magnetic moment and is not affected in first order. The singlet state, though it possesses a magnetic moment, is a zero spin state; since there is no axis of quantization, the atom "tumbles" in the field. Both states do exhibit an energy shift because the applied field induces a preferential alinement of the individual particle magnetic moments as is indicated by the H^2 variation (in the limit, this induced alinement becomes the Paschen-Back effect).

The wave functions for the perturbed positronium atom can now be determined by carrying out the matrix multiplication

$$\langle S\rangle\langle\mathfrak{H}\rangle=\langle\mathfrak{H}\rangle_{\text{diag}}\langle S\rangle \tag{13}$$

where $\langle S\rangle$ is the transformation matrix that diagonalizes $\langle\mathfrak{H}\rangle$, and employing the fact that $\langle S\rangle$ must be unitary. This operation leads to the following wave functions:

$$\begin{pmatrix} u_{11} \\ u_{10} \\ u_{1-1} \\ u_{00} \end{pmatrix} \xrightarrow{\mathfrak{H}_m} \begin{pmatrix} \psi_{11} \\ \psi_{10} \\ \psi_{1-1} \\ \psi_{00} \end{pmatrix} = \langle S\rangle \begin{pmatrix} u_{11} \\ u_{10} \\ u_{1-1} \\ u_{00} \end{pmatrix} = \begin{pmatrix} u_{11} \\ au_{10}+bu_{00} \\ u_{1-1} \\ au_{00}-bu_{10} \end{pmatrix} \tag{14}$$

where

$$a=\frac{1}{\sqrt{2}}\left(1+\frac{1}{\sqrt{1+x^2}}\right)^{1/2} \tag{15a}$$

and

$$b=\frac{1}{\sqrt{2}}\left(1-\frac{1}{\sqrt{1+x^2}}\right)^{1/2} \tag{15b}$$

Equation (14) shows that the application of a magnetic field mixes the states u_{10} and u_{00}. Thus ψ_{10} and ψ_{00} each decay by both the two- and three-photon channels.

If the annihilation rate of the state u_{10} is γ_T and that for the state u_{00} is γ_s, then the mean annihilation rate for the mixed state ψ_{10} is

$$\gamma_{10}=a^2\gamma_T+b^2\gamma_s. \tag{16}$$

Substitution of eq (15) into the above yields

$$\gamma_{10}=\left(\frac{\gamma_T+\gamma_s}{2}\right)+\frac{1}{\sqrt{1+x^2}}\left(\frac{\gamma_T-\gamma_s}{2}\right) \tag{17}$$

The branching ratio for the ψ_{10} state (i.e., the ratio of the number of two photon decays to three photon decays) is

$$B_{10}=\left(\frac{b}{a}\right)^2\frac{\gamma_s}{\gamma_T}=\frac{(2+x^2)-2\sqrt{1+x^2}}{x^2}\frac{\gamma_s}{\gamma_T}. \tag{18}$$

In figure 1 are plotted eqs (17) and (18) as functions of the applied field H up to 2177 G, at which point B_{10} equals unity.

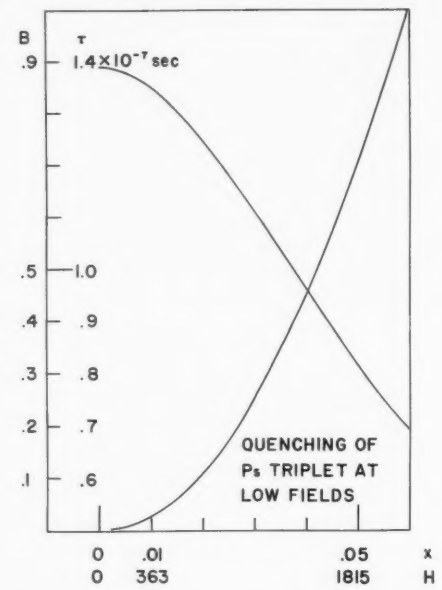

FIGURE 1. *Quenching of triplet positronium at low fields.*

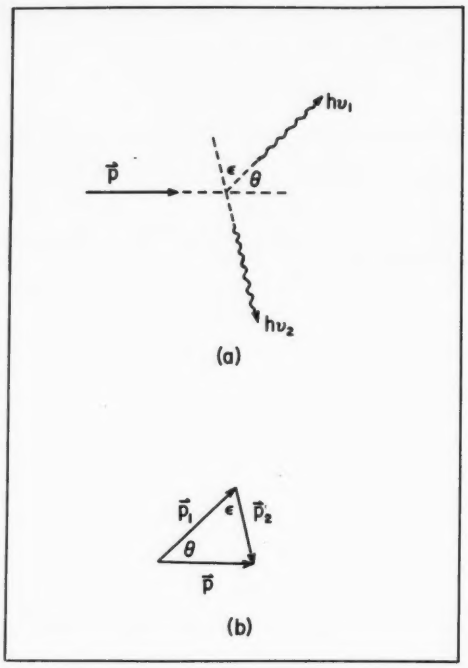

FIGURE 2. *(a) Two-photon annihilation of positronium in motion. (b) Momentum triangle for the process (a).*

4. Line Profile for Positronium in a Monoenergetic Moderator

In this section we shall consider the case in which a flux of positronium atoms is incident in a moderating medium possessing a single thermal energy. We must first relate the energy separation of the two photons to their emission directions. Figure 2a is a representation of the annihilation of a positron atom with linear momentum $\mathbf{p}$ into photons $h\nu_1$ and $h\nu_2$ which are emitted at an angle ϵ with respect to each other. The photon $h\nu_1$ is emitted at an angle θ with respect to the direction of the incident positronium atom. From the momentum triangle of figure 2b one can write

$$p_2^2 - p_1^2 = p^2 - 2pp_1 \cos\theta. \tag{19}$$

Letting $h\nu_1$ be the photon of greater energy, then one can write

$$h\nu_1 = \tfrac{1}{2}E_0 + \delta \tag{20a}$$

and

$$h\nu_2 = \tfrac{1}{2}E_0 - \delta, \tag{20b}$$

where E_0 is the total energy of the positronium atom prior to annihilation. Thus multiplying eq (19) by c^2 and subsequently substituting eqs (20) into the result leads to

$$\delta = -\frac{pc}{2}\left\{\frac{pc}{E_0} - \left(1 + \frac{2\delta}{E_0}\right)\cos\theta\right\}. \tag{21}$$

If the positronium atom is nearly in thermal equilibrium with its surroundings at annihilation, then

$$\frac{pc}{E_0} \ll 1$$

and

$$\frac{2\delta}{E_0} \ll 1;$$

as a result, eq (21) can be written

$$\delta \simeq \frac{pc}{2}\cos\theta = \delta_{\max}\cos\theta. \tag{22}$$

It has been shown by Heitler [11] that the emission of annihilation photons is spherically symmetric in the limit $\mathbf{p}=0$; thus the distribution will be very nearly isotropic in the case at hand—that of thermalized positronium. The intensity distribution as a function

of θ will thus be proportional to the solid angle subtended at the annihilation site:[3]

$$I_\theta d\theta = \tfrac{1}{2} \sin\theta \, d\theta, \; \theta < \frac{\pi}{2} \tag{23}$$

Then the intensity distribution for δ can be written

$$I_\delta d\delta = I_\theta d\theta = I_\theta \frac{d\theta}{d\delta} d\delta, \; \delta < \delta_{\max}. \tag{24}$$

The quantity $d\theta/d\delta$ can be evaluated from eq (22) so that the distribution function $I_\delta d\delta$ in eq (24) becomes

$$I_\delta d\delta = \frac{d\delta}{pc}, \; \delta < \delta_{\max}. \tag{25}$$

Thus the annihilation of a positronium atom traveling with momentum **p** is equally likely to produce photons in the range from $E_0/2$ up to $E_0/2 + pc/2$.

It is now possible to determine the annihilation line shape from a positronium flux in a monoenergetic moderator. The number of *Ps* atoms annihilating during the time interval $(t, t+dt)$ is

$$N_t dt = \gamma_{10} N_0 e^{-\gamma_{10} t} dt. \tag{26}$$

Annihilations during this time interval contribute an increase of intensity dI_δ which is uniform for all δ from 0 up to $\delta_{\max}$, according to eq (25). Since the area under the distribution curve is equal to the number of atoms annihilating, then

$$N_t dt = \delta_{\max} dI_\delta. \tag{27}$$

We can determine the total intensity distribution by adding up all the dI_δ's from $t=0$ up to t_δ such that $\delta = \delta_{\max}$:

$$I_\delta = \int_0^{t_\delta} \frac{N_t dt}{pc}. \tag{28}$$

The momentum $p = \sqrt{2mE}$ is a function of the time; this thermalization function has been found [12] to be

$$E = E_m \coth^2(\beta + \alpha t) \tag{29}$$

where E_m is the moderator energy, β depends upon the energy of the positronium atoms at $t=0$, and α depends upon the properties of the moderator. Defining

$$u = \beta + \alpha t$$

eq (28) can be written as

$$I_\delta = K \int_0^{t_\delta} e^{-\frac{\gamma_{10} u}{\alpha}} \tanh u \, du. \tag{30}$$

[3] In reality θ does not quite reach $\pi/2$; this is merely an indication of the approximation of spherical symmetry, and will not affect the results significantly.

This integral can be approximated in the case for which γ_{10}/α is small. The details of this calculation appear in the appendix. The resulting distribution function is

$$\begin{aligned} I_\delta &= I_0 \left\{ 1 - \left[1 - \left(\frac{\delta_T}{\delta} \right)^2 \right]^{\frac{\gamma_{10}}{2\alpha}} \right\} && \delta > \delta_T \\ &= I_0 && 0 < \delta < \delta_T \end{aligned} \tag{31}$$

where δ_T is the maximum energy shift for the annihilation of a completely thermalized positronium atom.

In the case of two-photon annihilation of the ψ_{10} component of positronium using helium at its critical point ($T_c = 5.2$ °K, $p = 2.3$ atm) as a moderator and an applied magnetic field of 2177 G (so that $B_{10} = 1$), the quantity γ_{10}/α is quite small:

$$\left. \frac{\gamma_{10}}{\alpha} \right|_{\substack{\text{He crit} \\ 2177 \text{ G}}} = 8.5 \times 10^{-3}.$$

As a result the function I_δ (eq (31)) falls very rapidly for $\delta > \delta_T$, so that this leads to a distribution function that is nearly rectangular; viz, at $\delta/\delta_T = 1$, $I = I_0$, while at $\delta/\delta_T = 1.001$, $I = I_0 \times 10^{-3}$.

The physical interpretation of this result is fairly simple. Since γ_{10} is the two photon annihilation rate of the long-lived component of positronium, then γ_{10}^{-1} is the mean lifetime of the atom; similarly, α^{-1} represents the characteristic time required for the *Ps* atom to thermalize with its surroundings. Thus the ratio $\gamma_{10/\alpha}$ is just the ratio of thermalization time to mean life. When this ratio is small, then thermalization usually is completed long before the positronium atom decays. Since the calculations of this section concern the somewhat artificial case of a monoenergetic moderator, the resulting rectangular distribution in the preceding paragraph indicates that the vast majority of the positronium atoms decay after they have become fully thermalized, so that the resulting intensity distribution is simply the characteristic rectangular distribution arising from monoenergetic positronium.

5. Line Profile for Thermalized Positronium

Let us now consider annihilation in a moderator at temperature T characterized by a Maxwell distribution of velocities:

$$N_v dv = A v^2 e^{-\frac{mv^2}{2kT}} dv. \tag{32}$$

If the thermalization time α^{-1} is much less than the mean life γ_{10}^{-1}, then most *Ps* atoms are in thermal equilibrium with the moderator at the time of annihilation. As a result there will be a Maxwell distribution of positronium atoms; atoms with velocities

in the interval $(v, v+dv)$ will produce a rectangular distribution according to eq (31), so that

$$\delta dI = N_v dv \tag{33}$$

where δ is the width of the distribution and is the maximum energy shift for photons produced in the decay of a *Ps* atom moving with velocity v. If one makes the substitution $\delta = 1/2\ mvc$, eq (33) can be integrated to yield the intensity distribution of annihilation photons:

$$I = \int_{\delta/mc}^{\infty} \frac{2A}{mvc} e^{-\frac{mv^2}{2kT}} dv$$

$$= Ke^{-\frac{m}{2kT}\left(\frac{\delta}{mc}\right)^2}. \tag{34}$$

The quantity δ can be expressed in terms of the positronium kinetic energy as

$$\delta = c\sqrt{2mE}. \tag{35}$$

Denoting as δ_T that value of δ corresponding to the mean thermal energy at T, then one can write that

$$\delta_T = c\sqrt{2m\left(\frac{3}{2}kT\right)} = \sqrt{\left(\frac{3}{2}kT\right)E_0}. \tag{36}$$

Since $E_0 \simeq 2m_0c^2$, then eq (34) becomes

$$I = Ke^{-\frac{3}{2}\left(\frac{\delta}{\delta_T}\right)^2} \tag{37}$$

The line profile resulting from the annihilation process is a Gaussian with a half width at half intensity of

$$\delta_{1/2} = \delta_T\sqrt{\frac{2}{3}\ln 2} = 0.68\ \delta_T. \tag{38}$$

6. Summary

It has been demonstrated that if a moderator is such that the thermalization time of positronium is much less than the mean life against annihilation, the two photon annihilation of positronium in this moderator at temperature T results in an annihilation line that is a Gaussian, the width of which depends upon T. These conditions are fulfilled for helium near its critical point for positronium lifetimes of the order of magnitude of the triplet state lifetime. Since triplet positronium decays with the emission of three photons, whereas a determination of the Compton wavelength is feasible only in the case of two photon decay, one must carry out such an experiment in the presence of a magnetic field so that the mixing of singlet and triplet states give rise to a long-lived two photon process. It has been shown that for fields of approximately 2 kG, one half of the long-lived decays will occur via the two photon channel with a life time sufficiently great to fulfill the conditions for the Gaussian line shape described above. It would thus appear possible to carry out an annihilation experiment in which the line width is sufficiently narrow to allow a 1 ppm determination of λ_A.

7. Appendix

In order to evaluate the integral of eq (30),

$$\Im = \int e^{-\frac{\gamma_{10}u}{\alpha}} \tanh u du, \tag{A-1}$$

for the case in which $\epsilon = (\gamma_{10}/\alpha) \ll 1$, we make the substitution

$$\eta = \ln \cosh u. \tag{A-2}$$

The expression $\tanh u du$ can be expressed in terms of η:

$$\tanh u du = \frac{d(\cosh u)}{\cosh u} = d(\ln \cosh u) = d\eta. \tag{A-3}$$

From (A-2) we can write

$$e^{\eta} = \cosh u \tag{A-4}$$

which leads to

$$u = \cosh^{-1} e^{\eta} \tag{A-5}$$

and therefore (A-1) becomes

$$\Im = \int e^{-\epsilon \cosh^{-1} e^{\eta}}\ d\eta. \tag{A-6}$$

Employing an identity for $\cosh^{-1}$ yields

$$\cosh^{-1} e^{\eta} = \ln\left(e^{\eta} + \sqrt{e^{2\eta}-1}\right)$$

$$= \eta + \ln\left(1 + \sqrt{1-e^{-2\eta}}\right) \tag{A-7}$$

and therefore

$$e^{-\epsilon \cosh^{-1} e^{\eta}} = e^{-\epsilon\eta}\left(1 + \sqrt{1-e^{-2\eta}}\right)^{-\epsilon}. \tag{A-8}$$

Since ϵ is small, eq (A-8) can be expanded:

$$\left(1 + \sqrt{1-e^{-2\eta}}\right)^{-\epsilon} = 1 - \epsilon \ln\left(1 - \sqrt{1-e^{-2\eta}}\right)$$

$$+ \frac{\epsilon^2}{2}\ln^2\left(1 + \sqrt{1-e^{-2\eta}}\right) - \ldots. \tag{A-9}$$

But note that

$$\ln\left(1 + \sqrt{1-e^{-2\eta}}\right) = \sum_{s=1}^{\infty} \frac{(-1)^{s+1}}{s}\left(1-e^{-2\eta}\right)^{s/2} \tag{A-10}$$

and that one can write

$$\left(1 + \sqrt{1-e^{-2\eta}}\right)^{-\epsilon} = 1 + \Phi\epsilon \tag{A-11}$$

in which

$$|\Phi|\epsilon \leq \epsilon \ln\left(1+\sqrt{1-e^{-2\eta}}\right) \leq \epsilon(1-e^{-2\eta})^{1/2}.$$

Now the integral (A–6) becomes

$$\Im = \int e^{-\epsilon\eta}(1+\Phi\epsilon)d\eta = -(1+\bar{\Phi}\epsilon)\,\frac{e^{-\epsilon\eta}}{\epsilon} \qquad \text{(A–12)}$$

where

$$\bar{\Phi} = \int \Phi e^{-\epsilon\eta}d\eta \Big/ \int e^{-\epsilon\eta}d\eta, \qquad 0 < \bar{\Phi} < 1.$$

Rewriting (A–12) in terms of u yields eq (31) in section 3.

8. References

[1] E. R. Cohen and J. W. M. DuMond, Rev. Mod. Phys. **37,** 537 (1965).

[2] J. A. Bearden, A. Henins, J. G. Marzolf, W. C. Sauder, and J. S. Thomsen, Phys. Rev. **135,** A899 (1964).

[3] This situation is rapidly changing, see, e.g., W. H. Parker, B. N. Taylor and D. N. Langenberg, Phys. Rev. Letters, **18,** 287 (1967).

[4] J. S. Thomsen and F. Y. Yap, to be published.

[5] J. A. Bearden, Phys. Rev. **137,** B181 (1965).

[6] This is most graphically demonstrated by U. Bonse and M. Hart, Appl. Phys. Letters **7,** 99 (1965).

[7] M. Deutsch, Prog. Nuc. Phys. **3,** 131 (1953); P. R. Wallace, Solid State Physics, **10,** 1 (Academic Press, New York, 1960).

[8] V. W. Hughes, S. Marder and C. S. Wu, Phys. Rev. **106,** 934 (1957).

[9] O. Halpern, Phys. Rev. **94,** 904 (1954); Hughes et al., ibid.

[10] E. V. Condon and G. H. Shortley, The Theory of Atomic Spectra, p. 152 (Cambridge University Press, New York, 1953).

[11] W. Heitler, The Quantum Theory of Radiation, 3d ed. (Oxford University Press, New York, 1954).

[12] William C. Sauder, J. Res. NBS **72A** (Phys. and Chem.) No. 1 (1968).

(Paper 71A5–464)

JOURNAL OF RESEARCH of the National Bureau of Standards—A. Physics and Chemistry
Vol. 71A, No. 5, September–October 1967

Surface-Layer Relaxation in the Dielectric Spectrum of CaF_2 Doped With GdF_3

A. D. Franklin, S. Marzullo, and J. B. Wachtman, Jr.

Institute for Materials Research, National Bureau of Standards, Washington, D.C. 20234

(May 10, 1967)

CaF_2 crystals doped with 0.1 percent GdF_3 were observed to develop surface layers when annealed above 700 °C in air, during application of Pt paste electrodes. The conductivity in these surface layers was much higher than in the bulk, due presumably to the large numbers of anion vacancies produced by dissolved oxygen. The presence of these high conductivity surface layers produced a relaxation in the dielectric spectrum with (1) an approximately temperature-independent magnitude, $\Delta\kappa$, (2) a relaxation time controlled by the conductivity of the surface layers, and influenced therefore by heat treatment of the specimen, and (3) an activation energy equal to that for conductivity of the surface layers, about 0.9 eV. This relaxation is sufficiently similar to dielectric relaxations observed previously in ionic crystals and ascribed to defect pairs to suggest that great care must be taken in interpreting dielectric measurements in these materials. What is thought to be dipole relaxation may in fact be due to the presence of thin layers accidentally present on the crystal. There is a marked electrode polarization effect in these crystals. The electrode capacitance at not-too-low frequencies depended upon the frequency and both the number and mobility of the charge carriers with 3/2 power laws.

Key Words: CaF_2, conductivity, crystals, defect pairs, dielectric relaxation, electrode capacitance, surface layers.

1. Introduction

Dielectric relaxation has been an important tool in studying point defect pairs in ionic crystals. Considerable work has been done on divalent cations (anions) paired with cation (anion) vacancies in alkali halides [1].[1] More recently, such dipole relaxation ascribed to impurity cations paired with interstitial fluoride ions has been reported [2] in CaF_2 doped with trivalent cations. This interpretation of the dielectric relaxation data as due to coupled pairs of defects rests on several grounds: most notably, comparison between doped and pure crystals; the observation of a single relaxation time, to be expected from reorienting independent dipoles; the observation of activation energies that are (1) similar to but somewhat lower than the activation energies for d-c conduction in the same compounds, and (2) of the same general magnitude as activation energies calculated for coupled defect reorientation on theoretical grounds; and, in several cases, examination of the same crystal by dielectric relaxation and spin resonance or by dielectric and an elastic relaxation.

The unambiguous interpretation of the dielectric relaxation can be somewhat complicated by the existence of several other effects, arising from other causes but giving rise to very similar data. In particular, when two distinct phases are present, with different conductivities and dielectric constants, a dielectric relaxation can be observed. If the minor phase is distributed as dispersed particles of uniform shape [3], or if it forms a thin layer [4], the resulting relaxation will obey the Debye equations. An examination of possible effects of this sort in materials of interest for coupled-defect studies can therefore help in sorting out the latter effects.

In this spirit, we present here a study of such a relaxation, observed in single-crystal CaF_2 containing 0.1 mole percent GdF_3. Similar layers were formed on pure CaF_2 but were not studied in detail. Thin surface layers of high conductivity were formed by annealing the crystals in air during the application of platinum paste electrodes. Disregarding electrode blocking effects, the specimen could then be represented by the sketch and equivalent circuit in figure 1. B denotes the bulk, l the layer on the surface under the electrodes, and l' the exterior surface layer from electrode to electrode. The parallel impedance of such a circuit exhibits a relaxation describable by the Debye [5] equation with a single relaxation time.

[1] Figures in brackets indicate the literature references at the end of this paper.

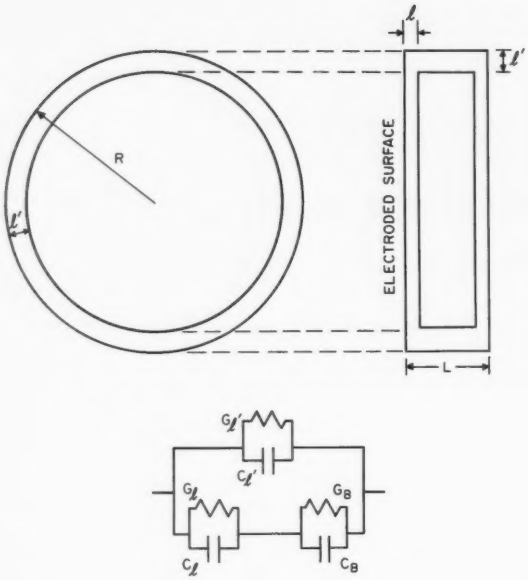

FIGURE 1. *Sketch of layered specimen, with equivalent electrical circuit.*

2. Specimens

Four pieces were cut from a crystal, obtained from the Harshaw Chemical Company, with nominal 0.1 mole percent GdF_3 present. On one, here designated A, gold electrodes were evaporated, and the specimen was subject to no heat treatment. On three, platinum paste was applied in several doses to the major faces, during which the specimens were annealed in air at about 700 °C for each dose. It has been shown [6] that under this sort of anneal oxygen diffuses into CaF_2 and then precipitates as the crystal cools, producing well-defined surface layers containing CaO particles. Similar layers were observed under the microscope in our specimens as shown by figure 2. Table 1 gives dimensions of the specimens, together with the thickness of the surface layers taken as the precipitated zones observed under the microscope. Note that specimen A is essentially free of precipitate while specimen D contains precipitate throughout. The properties of specimen D are therefore some measure of the properties of the surface layers on specimens B and C, while for the properties of their interior portions, between the surface layers, specimen A provides a measure.

3. Comparison Between Observed Behavior and Predictions of the Surface-Layer Model

3.1. Low-Frequency Conductivity

At frequencies well below the critical frequency of the relaxation, but high enough to avoid blocking effects at the electrodes, the apparent conductivity should approach a low-frequency limit given by

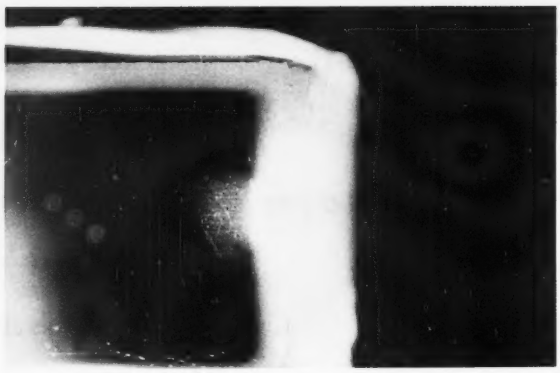

FIGURE 2. *Optical micrograph of cross section of specimen C.*

$$\sigma = \left\{ \frac{(1-A)\sigma_B + A\sigma_l}{(1-2l/L)\sigma_l + (2l/L)\sigma_B} \right\} \sigma_l \qquad (1)$$

where l is the thickness of the layer under the electrodes, L the total thickness of the specimen, σ_l and σ_B the true conductivities of the surface layer and the bulk, respectively, and

$$A = (l'/R)(2 - l'/R)(1 - 2l/L)$$

with l' the thickness of the layer on the outer edge of the specimen. For l and l' equal to zero (specimen A), σ becomes σ_B, while for $2l$ equal to L (specimen D) σ becomes σ_l.

Specimens B, C, and D were originally very slowly cooled after the anneal involved in applying the Pt electrodes. Figure 3 shows ln (σT) plotted as a function of T^{-1}. Straight lines were drawn through the data for specimens A and D, to produce values for σ_B and σ_l as a function of temperature. These, with the data in table 1, were then inserted into eq (1) to produce estimates of σ for the layered specimens B and C. The lines on figure 3 labeled B and C are the results of these calculations. Although the scatter, much of it in the measuring temperatures, is large, the calculations describe the data reasonably well.

The conductivity of the partially oxidized specimens was found to depend upon the rate of cooling from a temperature above about 500 °C. The effect was studied using specimen C. By removing the specimen from the furnace to provide a rapid cool, the apparent conductivity was increased by almost an order of magnitude, with no apparent change in activation energy. A second slow-cooling returned the apparent conductivity to close to its former value, so that the effect of this heat-treatment is approximately reversible. A similar anneal (at 400 °C) and rapid cooling produced no effect in the gold-electroded specimen.

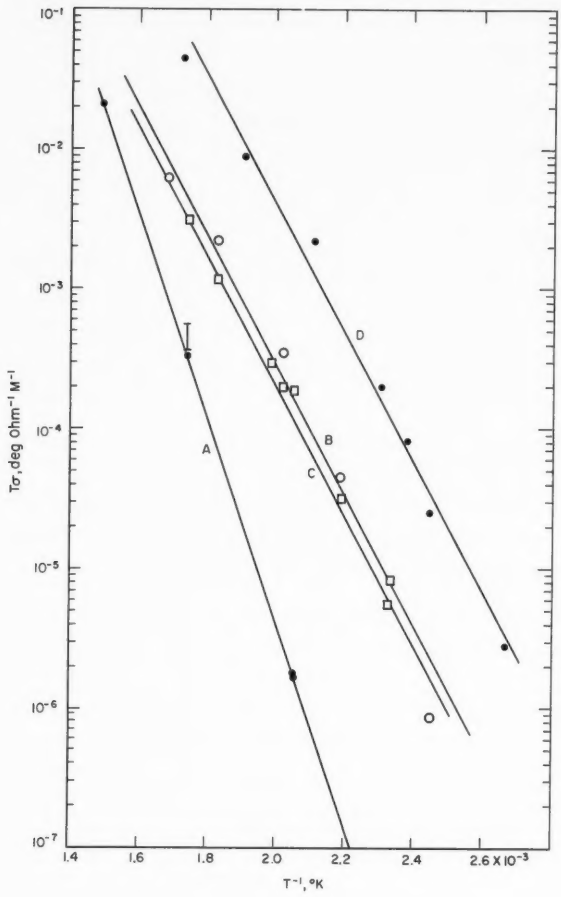

FIGURE 3. *Temperature dependence of apparent low-frequency conductivity of specimens A, B, C, and D.*

3.2. Dielectric Relaxation

The layered model of figure 1 should exhibit a relaxation in the dielectric spectrum with a single relaxation time. In interpreting our data, we assume that the true dielectric constant of the material, κ_T, is the same for all parts of the specimen. Then the model predicts the following:

(i) The high-frequency limit, κ_∞, of the apparent real part of the dielectric constant is

$$\kappa_\infty = \kappa_T. \tag{2}$$

(ii) The magnitude, $\Delta\kappa$, in the dispersion in κ' is

$$\Delta\kappa = \kappa_T(1 - l'/R)^2 \left\{\frac{(1-2l/L)\sigma_l^2 + (2l/L)\sigma_B^2}{[(1-2l/L)\sigma_l + (2l/L)\sigma_B]^2} - 1\right\}. \tag{3}$$

With the data in table 1 and σ_l and σ_B derived as in the last section, it is evident the terms in σ_B are negligible, and eq (3) reduces to

$$\Delta\kappa = \kappa_T \frac{(1-l'/R)^2(2l/L)}{(1-2l/L)}. \tag{4}$$

(iii) The relaxation time of the model is

$$\tau = \kappa_T[(1-2l/L)\sigma_l + (2l/L)\sigma_B]^{-1}. \tag{5}$$

Combining eq (5) and eq (1), and again dropping the negligibly small terms in σ_B,

$$\tau = \frac{\kappa_T}{1.13 \times 10^{11}} \frac{A}{\sigma(1-2l/L)^2} \tag{6}$$

with σ in $(\text{ohm} \cdot \text{m})^{-1}$ and τ in sec. A has the meaning of the last section.

For temperatures from about 135 °C to about 300 °C, a relaxation appeared in the dielectric spectrum of specimens B and C between 20 and 10^5 Hz. Figure 4 shows a plot of the real and the imaginary parts of the parallel dielectric constant for specimen *C* in the slowly cooled condition at 214 °C. These data when plotted as an Argand diagram, in the manner of Cole and Cole [7], are shown in figure 5. Good semicircles

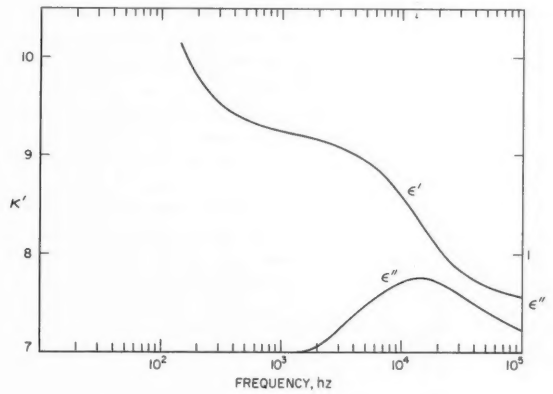

FIGURE 4. *Portion of the dielectric spectrum of specimen C at 214 °C.*

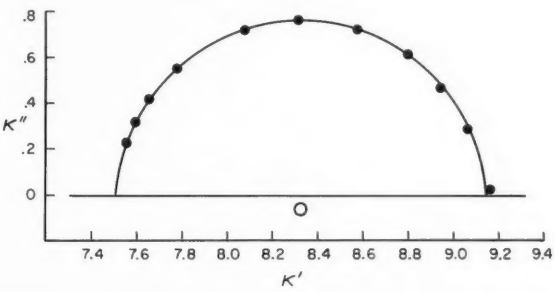

FIGURE 5. *Argand diagram for specimen C at 214 °C.*

were formed in most cases, with approximately single-relaxation-time behavior. Reasonable estimates of κ_∞, the high-frequency dielectric constant, and $\Delta\kappa$, the magnitude of the dispersion, could be obtained from these diagrams. To obtain the relaxation times, τ, of the dispersion, use was made of the Cole-Cole relation in the form

$$\left[\frac{(\kappa_0-\kappa')^2+\kappa''^2}{(\kappa'-\kappa_\infty)^2+\kappa''^2}\right]^{1/2}=(\omega\tau)^{1-\alpha} \qquad (7)$$

where κ_0 is the low-frequency limit for the dielectric constant in the Argand diagram and α is a parameter describing the breadth of the distribution of relaxation times. A plot of the left-hand side as a function of the circular frequency, ω, produces a straight line. The value of τ is the inverse of ω when the function on the left equals unity.

Figure 6 shows the temperature dependence of κ_∞, with the data of Rao and Smakula [8] measured at 10^{10} Hz, plotted for comparison. All specimens show roughly the same temperature dependence as do the data of Rao and Smakula, which were measured on pure CaF_2 in the absence of any dispersion effects. The discrepancy between our data and those of Rao and Smakula *could* arise from overestimating the thickness of our specimens, but it seems unlikely that our errors could be as large as required to bring all the data into coincidence. It seems more reasonable to suppose an additional relaxation exists in our dielectric spectra, at frequencies above our measuring range. Defect pairs, such as $Gd^{3+}-F^-$ interstitials, could give rise to such a relaxation.

In figure 7 we show the temperature dependence of $\Delta\kappa$. This dispersion was observed only in specimens B and C, the specimens containing two layers. With specimen A, gold-electroded with no visible oxide layer, a much smaller relaxation with quite different characteristics was observed, but may not be related to that observed in the dielectric spectra of specimens B and C. None was observed with specimen D (fully precipitated).

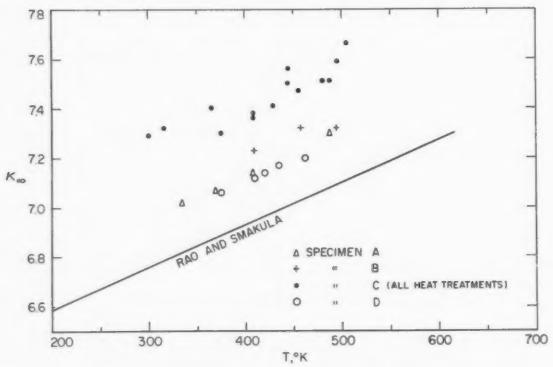

FIGURE 6. *Temperature dependence of κ_∞, the high-frequency limit of the real part of the relative dielectric constant.*

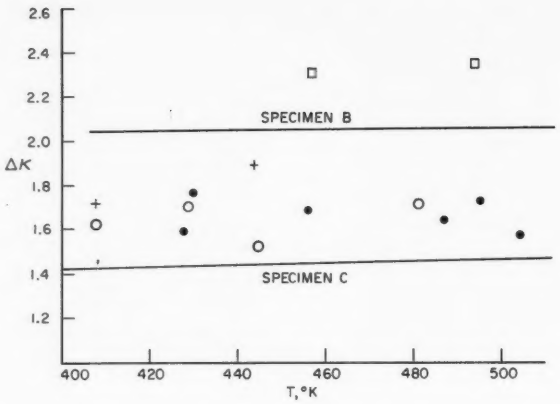

FIGURE 7. *Temperature dependence of $\Delta\kappa$, the magnitude of the dispersion in the real part of the relative dielectric constant, for specimens B and C.*

Specimen B, □; Specimen C, slowly cooled, mild quench ○, rapid quench +.

The lines drawn on figure 7 show values of $\Delta\kappa$ calculated with eq (4) and the appropriate values of κ_∞ substituted for κ_T. The calculations reproduce the general lack of dependence of $\Delta\kappa$ upon temperature, but underestimate the magnitude by 10 to 15 percent. The calculated value for $\Delta\kappa$ depends directly upon the thickness of the layers under the electrodes. The estimate of this thickness by microscopic examinations can easily be in error by this amount, in view of the fact that (1) a judgment must be made as to the edge of the precipitated zone, and (2) the region of high conductivity can be expected to extend inward from the precipitated zone, so that the thickness of the latter must underestimate somewhat the thickness of the *electrical* layer of high conductivity.

A dispersion of this magnitude cannot, on the other hand, be accounted for by $Gd^{3+}-F^-$ interstitial pairs, even if all the Gd ions present were associated with interstitial ions. Use may be made of the simple relation for dipole polarization [9]

$$\Delta\kappa=\frac{n\mu^2}{3kT\epsilon_0} \qquad (8)$$

where n is the number of dipoles/cm^3, $\mu=ea$ is the dipole moment, with a the $F^- - F^-$ distance, and T is taken as 450 °K; a value of $\Delta\kappa$ of 0.3 results. However, had the surface layers been thinner by a factor of 10, the relaxation arising from their presence would have been of the same order of magnitude as the observed dipole relaxation.

The observed relaxation time of the relaxation found in specimens B and C is closely related to the apparent low-frequency conductivity as called for by eq (6). Figure 8 shows a log-log plot of τ versus $A/(1-2l/L)^2\sigma$ for both specimen B and specimen C heat treated in various ways. Equations 6 and 7 appear in fact to describe these data rather well. The correspondence is in fact very strong. By varying the measurement temperature of specimen C for a given

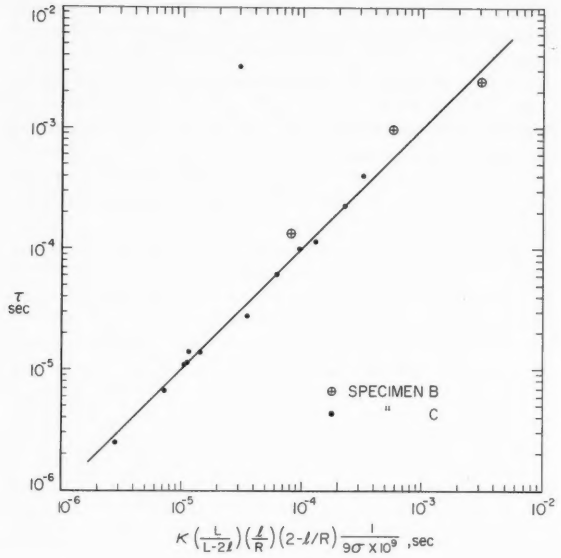

FIGURE 8. *Relation between relaxation time and apparent conductivity in specimens B and C.*

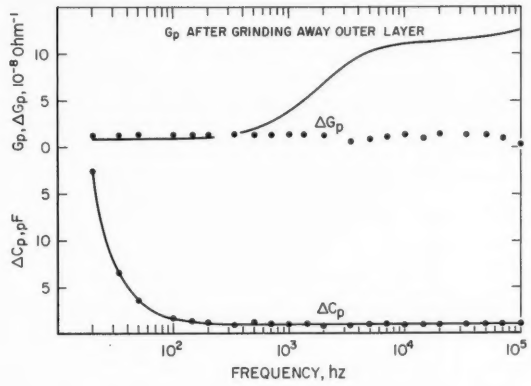

FIGURE 9. *Effect upon parallel capacitance and conductance of grinding away outer surface of layered specimen similar to specimen C.*

Measurements made at 183 °C.

heat-treatment, the mobility of a constant number of charge carriers was varied. Measurements at a given temperature of the specimen with varying heat treatments corresponded to varying the number of charge carriers with constant mobility. Regardless of which mechanism was used to vary σ, eq (6) described the accompanying variation in τ. The result appears completely to rule out dipoles as a source of the relaxation.

According to the model, the cylindrical surface layer on the outside of the specimen contributes the elements represented by $G_{l'}$ and $C_{l'}$ in figure 1. These should have no influence on the relaxation, so that grinding off the layer should reduce both the parallel conductance and the parallel capacitance of the specimens by quantities that are independent of frequency (except at the low frequencies where electrode effects occur). Figure 9 shows the change in parallel capacitance and conductance at 183 °C produced by grinding off this outer surface of a layered specimen, of dimensions similar to specimen C, save for the expected electrode effect in ΔC_p, the changes produced by grinding are frequency independent. The figure also shows the conductance of the specimen after grinding. The relaxation is centered around 115×10^3 Hz. The change in the conductance at low frequencies produced by grinding is larger than the conductance remaining, again in accordance with the model.

The correspondence between the predictions of the layer model and the nature of the dielectric dispersion in these specimens is good. Using layer thickness obtained from microscopic examination and conductivities obtained from specimens composed entirely of one layer or the other, it has been possible to account quantitatively, to within 10 to 15 percent, for the low-frequency conductivity, high-frequency dielectric constant, magnitude of the dispersion, and relaxation frequency.

4. Electrode Polarization

At very low frequencies, as figure 3 demonstrates, a large increase in capacitance occurs with decreasing frequency, accompanied by a decrease in conductance. For not too low frequencies, the capacitance varied as $\omega^{-3/2}$ and the decrease in conductance as $\omega^{-1/2}$, in accordance with Friauf's [10] model for two mobile charge carriers, one of which is blocked at the electrodes, or Ninomiya and Sonoike's [11] model with one blocked carrier. In actual fact, d-c measurements showed that only part of the current is blocked. If only one mobile carrier is present, it is only partially blocked at the electrodes.

Models such as those of Friauf and of Ninomiya and Sonoike suggest that the increment in capacitance depends upon both the density of charge carriers and their mobilities, as well as geometrical factors:

$$\Delta C = \frac{KA}{L^2} f(\mu, n, \omega), \tag{11}$$

where μ is the mobility and n the density of the charge carriers, A the area, L the thickness of the specimen, and K a constant containing the dielectric constant.

The experiments on specimen C, in which quenching could be used to vary the density of the charge carriers independently of their mobility, allow the separate dependence upon n and μ to be studied. Figure 10 shows the log of the slopes of capacitance versus $\omega^{-3/2}$ plots, in the form

$$\frac{L^2}{(\pi R^2)} \frac{\partial C_p}{\partial \omega^{-3/2}}$$

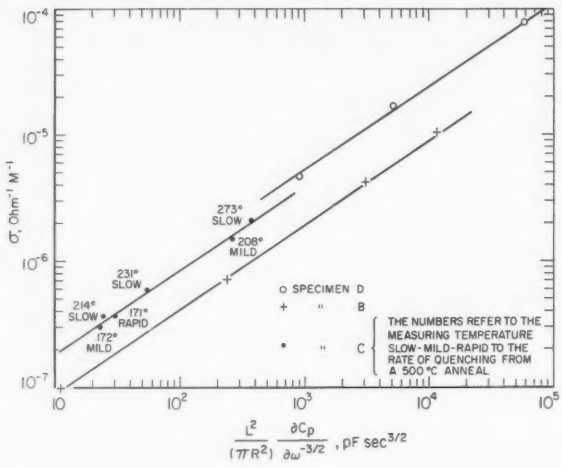

FIGURE 10. *Relation between electrode capacitance and apparent conductivity in specimens B, C, and D.*

plotted versus the log of the apparent conductivity, σ, at frequencies below the relaxation discussed above, but above the onset of the electrode polarization effects discussed here. The data for specimen C show that the electrode polarization effect depends upon σ and not upon n and μ separately. Equation (11) can be written for this specimen

$$\frac{L^2}{A}\,\Delta C = K(n\mu)^{3/2}\omega^{-3/2}. \tag{12}$$

Since in the specimens B and C only the thin outer shell carries appreciable low-frequency current, it seems reasonable to use the area of this shell and the conductivity, σ_l, of the oxidized layers in eq (12) for these specimens. Then using eq (1) to replace σ_l by σ, the apparent conductivity

$$\frac{L^2}{(\pi R^2)}\,\frac{\partial C_p}{\partial \omega^{-3/2}} = \frac{KR\sigma^{3/2}}{(2Rl-l^2)^{1/2}} \tag{13}$$

while for specimen D, with no interior part,

$$\frac{L^2}{(\pi R^2)}\,\frac{\partial C_p}{\partial \omega^{-3/2}} = K\sigma^{3/2}. \tag{14}$$

According to these equations, the lines representing the data for specimens B and C should be separated from that for D by appropriate values of log $R(2Rl-l^2)^{-1/2}$. The following table gives values for $R(2Rl-l^2)^{-1/2}$ calculated from the data in table 1 compared to those derived from the displacements of the lines in figure 9 from the line for specimen D:

Specimen	Calculated	Observed
B	3.8	4.3
C	4.5	1.6

These electrode polarization effects are known to depend rather sensitively upon the nature of the electrode contact. The electrodes were applied to specimens B and D at the same time, both receiving the same series of heat-treatments in the course of applying the electrodes, while specimen C was treated separately. This may account for the reasonable correspondence between calculated and observed factors in the table for specimen B and the discrepancy for specimen C.

The results on specimen C show that ΔC depends upon $\sigma_l^{3/2} = (n\mu)^{3/2}$ and not upon n and μ separately. In a study of alkali halides containing divalent impurities (both anions and cations), Wintle and Rolfe [12] also found a dependence on $\sigma^{3/2}$, but in addition found an independent dependence upon μ, with a negative exponent. This dependence was missing here. It should be noted that our results refer only to the temperature and frequency region in which ΔC exhibited $\omega^{-3/2}$ behavior. At lower frequencies the increase of ΔC with decreasing ω became less rapid. At higher temperatures (above about 250 °C) this effect became more pronounced, and ΔC at temperatures above about 300 °C exhibited an ω^{-1} behavior.

5. Discussion

5.1. Relation to Dipole Relaxation Measurements

The comparison between our experimental data and the behavior expected from the simple surface-layer model establishes clearly the importance of these layers for the electrical properties of these specimens.

In particular, the surface layers are responsible for the presence of a very significant relaxation in the dielectric spectrum. Dielectric relaxation has been extensively used as a means of studying coupled point defects; our results suggest that great care must be taken to eliminate the relaxation due to surface layers from such studies. In the present study, the surface layers were very thick and obvious. Layers with the same properties but thinner by a factor of 10 would be only a few tens of microns thick, and therefore quite easy to overlook, and yet would produce a relaxation comparable to that expected from the approximately 0.1 mole percent of dipoles expected to be present.

The outstanding characteristics of high-conductivity-layer dielectric relaxation are an approximately temerature-independent magnitude, $\Delta\kappa$, and a relaxation time determined by the conductivity of the layer. Since the layer will probably obtain its high conductivity as a result of a high doping level, the activation energy of its conductivity, and hence of the relaxation time, is apt to be the motional activation energy of the majority carrier in the layer. Under special circumstances, which obtained in the present experiments, the layer conductivity may be influenced by thermal treatment of the specimen. This will result in a sensitivity of the relaxation time to thermal treatment.

Published results of dielectric relaxation experiments often exhibit some of these characteristics. The temperature independence of $\Delta\kappa$ is not only com-

mon in these experiments, it is almost the rule. It was remarked upon for NaCl containing $CaCl_2$ by Haven [1b] and for NaCl containing $MnCl_2$ by Watkins [1d]. It is exhibited by the data Dryden and Meakins [1c] for several alkali halides containing divalent cations. The same effect was noted for KBr crystals containing *F*-centers by Krasnopevtsev [1h], who also observed a decrease in relaxation time with increasing concentration of *F*-centers, an effect difficult to understand in terms of reorienting dipoles. Jacobs et al. [1f], in a study of KBr containing K_2S, not only found $\Delta\epsilon$ essentially independent of temperature, but also observed that thermal treatment of the samples produced much the same effect as observed here, a shift in the low-frequency conductivity accompanied by an inverse shift in the relaxation time.

Kessler and Mariani [1j] observed in NaCl doped with $CaCl_2$ a high-temperature relaxation, in addition to the one described by Haven and others, the characteristics of which correspond rather well to surface-layer relaxation. The magnitude $\Delta\epsilon$ appeared to be independent of temperature. Increasing the concentration of $CaCl_2$ decreased the relaxation time but did not change $\Delta\epsilon$. It is particularly interesting to note that Kaderka [1i] reports much the same results for NaCl doped with NaOH or $NaCO_3$, except that increasing the concentration of the divalent anion increased the relaxation time. If τ were related to either σ_I or σ_B as in eq (5) and if the dominant conductivity were controlled by the number of cation vacancies, then the results of both Kessler et al., and of Kaderka would follow.

In all of these studies, the activation energy for the relaxation process is about the same as or slightly smaller than the motional activation energy for the major charge carrier present. This finds a natural explanation in the coupled-defect model, since reorientation of the pair involves jumps of the mobile charge-carrying defect around the impurity by which it has been trapped, and the activation energy for these jumps could be similar to that for jumps of the free carrier. It also finds a natural explanation in the surface layer model, where it is the jump of the free carrier, in a rather heavily doped layer, that determines the relaxation time.

In the present case, the high-conductivity layers were formed on CaF_2 by diffusing oxygen into the crystal from the atmosphere, consistent with the accepted picture [13] of anion vacancies as the rapidly moving intrinsic defect in CaF_2. Ure [13] observed the formation of oxidized layers on CaF_2 crystals heated to 1000 °C in a purified He atmosphere. He also observed the formation of very thin layers of very high conductivity on his specimens when heated during measurements to temperatures above 650 °C, although it is not clear whether the high conductivity was produced by oxygen. Jacobs [14] found a dielectric relaxation in some CaF_2 crystals accompanied by high measured conductivity. The magnitude of the relaxation was approximately independent of temperature. The activation energy reported by Jacobs was 0.74 eV, somewhat lower than that found in the present work.

Crystals such as CaF_2, in which anion vacancies are the mobile species and can be produced by dissolved oxygen, should be particularly sensitive to contamination by the atmosphere. The work of Bontinck [15] suggests that water vapor may enhance the rate of contamination. Dielectric relaxation in rare-earth-doped CaF_2 ascribed to defect pairs has exhibited activation energies ranging from 1.7 to 1.2 eV, in magnitude similar to or somewhat lower than the motional energy (1.7 eV) attributed by Ure [13] to anion interstitials. That this activation energy depends upon the dissolved cation argues in favor of the interpretation in terms of the reorientation of defect pairs, as does the observation that the magnitude of the relaxation increases with the concentration of impurity cation. On the other hand, Viegele and Bevan have interpreted the narrowing observed above 400 °C in the nmr spectrum of F [19] in CaF_2 containing 0.05 percent Sm as due to diffusion of F^- interstitials, presumably trapped at Sm^{3+} ions. They find an activation energy for the process of 0.26 eV, very much lower than that for either motion of free interstitials or of dielectric relaxation.

There appears to be sufficient similarity between the properties of the surface-layer model and the observations of dielectric relaxation made on various ionic crystals expected to contain defect pairs to suggest great care should be taken in interpreting the experiments. What appears to be dipole relaxation may in fact be due to surface layers. If the layers possess lower conductivity than that of the bulk, then the relaxation time will depend on the thickness, but for high conductivity layers this is not the case. In either case, dependence of the relaxation time upon heat treatment or other factors influencing conductivities may sometimes be used to test whether surface layers are responsible for the relaxation.

5.2. Low-Frequency Conduction

In figure 3, the straight lines for specimens A and D correspond to

$$T\sigma = (T\sigma)_0 \exp(-Q/kT).$$

Simply theory [17] equates $(T\sigma)$ to

$$T\sigma = \frac{e^2 a_0^2}{6k} n_0 \nu_0 \exp[(-(g_n + g_m)/kT)]$$

where e is the electronic charge, a_0 the unit jump distance (equal to the anion-anion distance in CaF_2 for anion vacancy motion), $n_0 \exp(-g_n/kT)$ the number of charge carriers, ν_0 a vibrational frequency $\sim 10^{13}$ sec^{-1}, and g_m the free energy of activation for motion of the charge carriers. Fitting this equation to the data for specimens A and D produces the result

	n_0	g_n+g_m
Specimen A (bulk)	$4.4 \times 10^{24}/cm^3$	1.5 eV
Specimen D (oxidized layer)	$1.5 \times 10^{22}/cm^3$	0.9 eV

Ure [13] has shown that the anion vacancy is mobile, with an activation energy of ~ 0.9 eV at temperatures in the range studied here. It seems reasonable to suggest that during the course of these measurements the major charge carriers in the oxidized layers were anion vacancies whose concentrations were fixed by the amount of oxygen in the lattice. Since this was saturated, the concentration is of the order of the number of unit cells/cm^3, 2×10^{22}.

In the bulk, the defect concentrations can be expected to be dominated by the GdF_3 present. On the basis of Ure's results, the mobile species in our temperature range is again expected to be the anion vacancy. In the presence of the large concentration of GdF_3 (0.1 mole percent) and assuming strong association between Gd^{3+} ions and F^- interstitials, the anion vacancy concentration should be

$$n=\frac{2N\exp\left[-(g_f-g_p/2)/kT\right]}{6\left[\text{mole fraction } Gd^{3+}\right]^{1/2}}$$

where N is the number of unit cells/cm^3, g_f the anion Frenkel formation free energy, and g_p the free energy of association of the Gd^{3+} ions with F^- interstitials. Using the nominal mole fraction GdF_3, this produces a value for n_0 of about $5\times10^{23}/cm^3$, accounting for the fact that the observed n_0 exceeds N. However, this interpretation would equate $g_f-g_p/2$ with $1.47-0.92=0.55$ eV, which cannot be reconciled with Ure's numbers, $2.8-0.7=2.1$ eV. In his study of CaF_2 containing YF_3, Ure found in the temperature range used here that σ did not increase with Y^{3+} content and suggested that some mechanism other than volume charge transport might have dominated his measurements. He observed an activation energy for conduction in this range similar to the one found here for the bulk.

It seems probable that anion vacancies are the major charge carrier in the oxidized layer, and that in the bulk the charge carriers are related to the impurity concentration somewhat as outlined above. However, a positive identification cannot be made on the basis of the present data.

6. Summary

Surface layers differing in conductivity from the bulk are easy to produce in CaF_2, and may be common in general on ionic crystals. They are known to be responsible for dielectric relaxation effects similar to those expected from reorienting defect pairs. Such layers are produced in CaF_2 by an anneal in air during the application of Pt paste electrodes, but would probably result from any high temperature treatment of the crystal in the presence of even small amounts of oxygen or water vapor.

The layers on CaF_2 produced a relaxation dispersion in the dielectric spectrum with characteristics similar to those of dispersions associated in other work with orienting defect pairs:

(i) Temperature independent magnitude of the same order as produced by a few mole percents of dipoles

(ii) Relaxation time changing with the conductivity, or with factors such as defect or impurity concentration known to affect the conductivity

(iii) Activation energy close to the activation energy of motion of the dominant charge carrier, in this case anion vacancies.

TABLE 1. *Dimensions of* CaF_2: *0.1 percent* GdF_3 *Specimens*

Specimen	Diameter	Thickness	Layer thickness	
			Electrode, l	Outer edge, l'
A	1.760 cm	0.127 cm	Not observed	Gold electrodes
B	1.698	.254	0.030 cm	0.038 cm
C	1.981	.193	.016	.017
D	1.698	.0635	Completely precipitated	

7. References

[1.a] R. G. Breckenridge, J. Chem. Phys. **16,** 959 (1948); **18,** 913 (1950).
[b] Y. Haven, J. Chem. Phys. **21,** 171 (1953).
[c] J. S. Dryden and R. J. Meakins, Disc. Far. Soc. **23,** 39 (1957).
[d] G. D. Watkins, Phys. Rev. **113,** 91 (1959).
[e] R. W. Dreyfus, Phys. Rev. **121,** 1675 (1961).
[f] G. Jacobs, L. G. Vandewiele, and A. Hamerlinck, J. Chem. Phys. **36,** 2946 (1962).
[g] R. W. Dreyfus and R. B. Laibowitz, Phys. Rev. **135,** A1413 (1964).
[h] V. V. Krasnopevtsev, Sov. Phys.-Sol. State **4,** 1327 (1963).
[i] M. Kaderka, Czech J. Phys. **B13,** 378 (1963).
[j] A. Kessler and E. Mariani, Czech J. Phys. **B14,** 757 (1964).
[2.a] J. H. Chen and M. S. McDonough, Bull. Am. Phys. Soc. **9,** 647 (1964); **11,** 195 (1966).
[b] P. D. Southgate, Bull. Am. Phys. Soc. **11,** 195 (1966).
[3] See, for instance, R. W. Sillars, J. Instn. Elect. Engrs. **80,** 378 (1937).
[4] See, for example, A. A. Fairweather and E. J. Frost, Symposium on Insulating Materials, p. 15 (Instn. of Elect. Engrs., London, 1953).
[5] P. Debye, Polar Molecules, p. 94 (Chemical Catalog Co., New York, 1929).
[6] W. L. Phillips, Jr. and J. E. Hanlon, J. Am. Ceram. Soc. **46,** 447 (1963).
[7] K. S. Cole and R. H. Cole, J. Chem. Phys. **10,** 98 (1942).
[8] K. V. Rao and A. Smakula, J. Appl. Phys. **37,** 319 (1966).
[9] See Ref. 5, p. 29.
[10] R. J. Friauf, J. Chem. Phys. **22,** 1329 (1954).
[11] T. Ninomiya and S. Sonoike, Symposium on Photographic Sensitivity, Tokyo, p. 81, ed. S. Fujisawa (Maruzen, Tokyo, **2,** 1958).
[12] N. J. Wintle and J. Rolfe, Can. J. Phys. **44,** 965 (1966).
[13] R. W. Ure, Jr., J. Chem. Phys. **26,** 1363 (1957).
[14] G. Jacobs, J. Chem. Phys. **27,** 1441 (1957).
[15] W. Bontinck, Physica **24,** 650 (1958).
[16] W. J. Viegele and A. W. Bevan, Jr., Phys. Rev. **131,** 1585 (1963).
[17] H. G. Van Bueren, Imperfections in Crystals, p. 537 (North Holland, Amsterdam, 1961).

(Paper 71A5–465)

JOURNAL OF RESEARCH of the National Bureau of Standards—A. Physics and Chemistry
Vol. 71A, No. 5, September–October 1967

Thermal Expansion of Rutile from 100 to 700 °K*

Richard K. Kirby

Institute for Basic Standards, National Bureau of Standards, Washington, D.C. 20234

(June 15, 1967)

The thermal expansion of a single crystal of rutile (TiO_2) was determined in directions parallel to its crystallographic axes. A unique macroscopic technique was used wherein a cube-shaped specimen was cut from the anisotropic crystal, each of its six faces polished flat and nearly parallel to the face opposite it, and the expansion measured along each of its three body axes with an Abbe-Pulfrich interferometer. The relationship between the expansion along the body axes of the specimen and that in the crystallographic directions was determined from a Laue x-ray pattern. The unusual behavior of the thermal expansion that was observed can be explained by assuming an acoustical and optical contribution where the corresponding Grüneisen constants are 2.80 and 0.75 respectively.

Key Words: Anisotropic crystal, Grüneisen's constant, interferometer, rutile, thermal expansion.

1. Introduction

Thermal expansion is the dimensional change of a body which occurs with change in temperature. Grüneisen [1][1] has shown that the thermal expansion of a Debye solid should be approximately proportional to the internal energy. It has been found experimentally [2, 3, 4] that Grüneisen's relation is generally true for those elements that crystallize in face-centered-cubic, body-centered-cubic, close-packed-hexagonal, and tetragonal structures.

At present, interest [5] is being shown in solids which deviate from Grüneisen's relation. These solids include those that crystallize in a diamond-cubic structure (Ge, Si, diamond, InSb, etc.) and some glasses (vitreous silica, borosilicate, etc.). Theories have been proposed to explain the unusual behavior of these materials. Diamond-structure solids for instance are said to have a low-lying transverse acoustic mode which at low temperatures is predominant in absorbing energy. Glasses that have negative expansivity are said to have a low-lying transverse optical mode which also absorbs energy at low temperatures. The large effect of the transverse modes in all of these materials is due to open structures which result in large values of the shear elastic compliances associated with the modes [6].

The analysis of recent measurements of thermal expansion of rutile (TiO_2) with an x-ray technique [7] and a dilatometric technique [8] has indicated that the expansion of this material also deviates from the simple Grüneisen relation. This deviation is opposite to that of the above mentioned materials in that the expansivity at low temperatures seems larger than expected. Because these measurements were not of high precision, a precise determination of length, of the order of one part per million, was desired. This paper describes a unique set of thermal expansion measurements on a single crystal of rutile from 100 to 700 °K to obtain the desired precision.

2. Apparatus

X-ray techniques are often the preferred way, and for certain crystals (triclinic and monoclinic) perhaps the only way, to measure the thermal expansion of an anisotropic crystal. The difficulty of obtaining accurate measurements of lattice spacings versus temperature [9], however, occasionally makes the use of macroscopic techniques preferable. Determinations of anisotropic expansion with macroscopic techniques [10, 11] have almost always been made on two or more single crystals of the material having different orientations between the specimen axis and the crystallographic axis. In the case of materials like rutile, which are grown at high temperatures, differences in residual strain and lattice defects may occur between specimens grown in different crystalline directions. To eliminate some errors that might be caused by such differences, an Abbe-Pulfrich interferometer [12] was used to measure the thermal expansion along three nearly orthogonal directions of a single-crystal specimen of rutile. The only known use of this technique was by Benoit [13] in 1888 on a cube-shaped specimen of crystal quartz used in his determination of the density of water.

*This paper is based in part on a thesis submitted to the Department of Physics and Astronomy of the University of Maryland in partial fulfillment of the requirements for an M.S. degree, 1964.

[1] Figures in brackets indicate the literature references at the end of this paper.

267-984 O-67—2

The assembled interferometer and its individual parts are shown in figure 1. Three ruby spheres, each

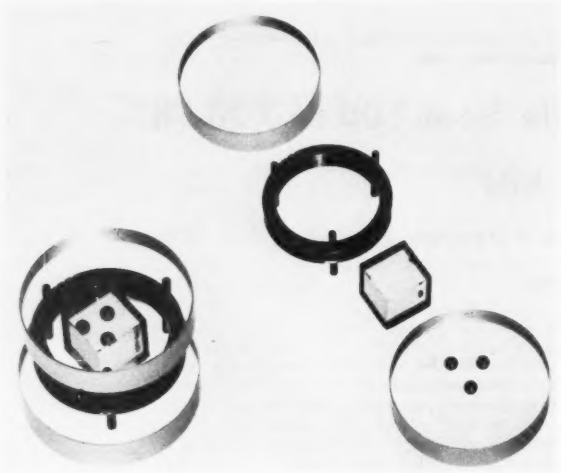

FIGURE 1. *Assembled interferometer and the individual parts.*

resting on a small flat area polished on one side, are placed on an optical flat. The cube-shaped specimen, about 12 mm on a side, rests on the three ruby spheres. An etalon made from recrystallized W–1 tool steel supports the top flat. The dimensions of the ruby spheres (about 3 mm) are adjusted so that Fizeau fringes, fringes of equal thickness, can be obtained between optical flats when separated by them. The dimensions of the steel etalon (about 16 mm) are adjusted in the same way. Parallelism between opposing faces of the rutile specimen is such that Fizeau fringes are also obtained in the completely assembled interferometer between the specimen's upper face and the top flat.

The fringes were observed with a Pulfrich viewer and their displacement from a reference point engraved on the lower surface of the top flat was measured with a filar-micrometer eyepiece. The filtered green line of a natural mercury discharge lamp was used for illumination.

Temperatures below 300 °K were measured with a copper-constantan thermocouple while higher temperatures were measured with a chromel-alumel thermocouple. A potentiometer was used to measure the emf of the thermocouples to 1 μV. The thermocouples had been calibrated by the Temperature Physics Section of the National Bureau of Standards. The cryostat and furnace used are shown in figures 2 and 3.

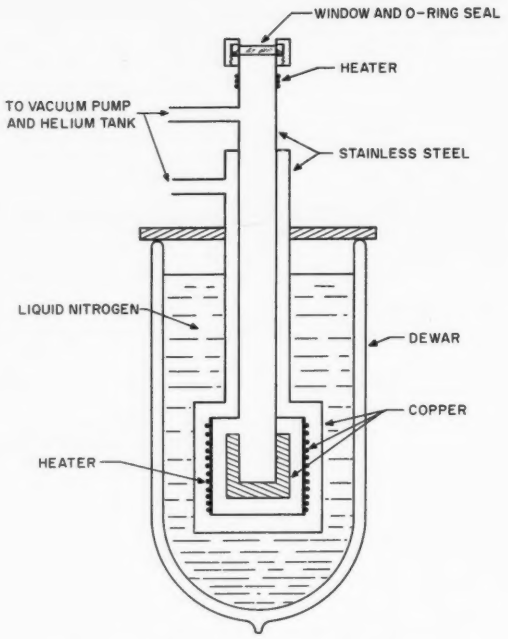

FIGURE 2. *Schematic drawing of the cryostat.*
The heavy copper block in which the interferometer is placed is suspended by three thin strips of stainless steel, only one of which is shown.

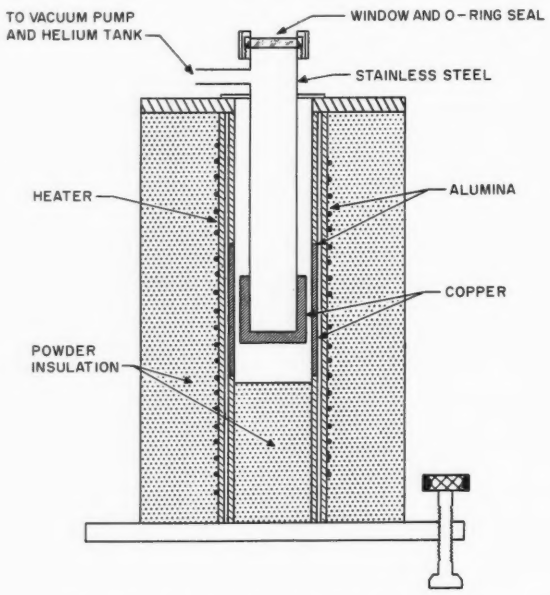

FIGURE 3. *Schematic drawing of the furnace.*

3. Specimen

The rutile crystal, obtained from the National Lead Company, was grown by the Verneuil flame fusion technique and may contain as much as 0.1 percent of impurities. The color of the crystal is faintly yellowish which indicates that it is nearly stoichiometric. The specimen was cut from the boule with a diamond saw and the opposite faces were made nearly parallel by

precision grinding. The six faces were then carefully lapped to optical flatness. When interference was observed between opposite faces of the specimen the fringes were distorted by local variations in the index of refraction. The ordinary and extraordinary rays, however, could be clearly extinguished with a polaroid filter and a grid pattern was not visibly distorted when viewed through the specimen. The density of the specimen was determined by a direct measurement of its mass and dimensions and was found to be 4.24 g/cm^3.

The body axes normal to the faces of the specimen are nearly orthogonal to one another. The angles between them as determined with an autocollimator are $\phi_{XY}=89°51'$, $\phi_{YZ}=89°30'$, and $\phi_{ZX}=90°2'$. A back-reflection Laue x-ray pattern was used to determine the inclination, ω, of the body axes from the crystallographic c direction. Values of ω are given in table 1.

TABLE 1. *Angle of inclination between the crystallographic c direction of the rutile specimen and each of its body axes*

Body axis	ω
X	17.2°
Y	72.9°
Z	86.9°

4. Experimental Procedure

Measurements of temperature and of fringe positions were made at intervals of about 50 °K only when the system was at constant temperature as indicated by the fringes remaining stationary for at least 15 min. The expansion observed in the complete interferometer is the difference between the expansion of the steel etalon and the sum of the expansions of the ruby spheres and the specimen. Since fringes could be obtained between the optical flats when separated by either the ruby spheres or the steel etalon the values for their expansion were determined in separate tests with the same equipment.

The expansion is measured by determining the number of fringes, N, passing the reference point.

$$\Delta L=\frac{N\lambda_r}{2}+A_c$$

where $\lambda_r=0.54623$ micrometer is the wavelength of the green line of mercury in vacuum. The apparent expansion, A_c, caused by the change in the index of refraction of the gas when subjected to a temperature change may be estimated from the following equation based on the ideal gas laws [14].

$$A_c=\frac{(n_0-1)288LP(T_2-T_1)}{760T_1T_2}$$

where n_0 is the index of the gas at standard conditions, L is the separation of the optical flats, P is the pressure (torr), and T_1 and T_2 are the initial and final temperatures (degrees Kelvin). This apparent expansion may be made small by operating at a low pressure. Since the index, n_0, of helium is 1.000036, the value of A_c will be negligible for the measurements presented here when the pressure is less than 5 torr. All of the measurements of expansion were made in a helium atmosphere at a pressure of about 2 torr which is sufficient to support good heat transfer.

While heating between observation temperatures the number of fringes that passed the reference point was carefully observed. The length at each temperature was measured with a precision of ± 0.03 of a fringe (± 0.008 micrometers). Each run was repeated until the measurements of length at each temperature did not differ by more than 1/10 of a fringe. A smoothed curve of the expansion for each direction in the specimen, for the ruby spheres, and for the steel etalon was obtained by a procedure such that there was overall agreement with the observed data as well as agreement between coefficients taken from it at 50 degree intervals and the coefficients calculated from the observed data.

5. Experimental Results

Smoothed curves representing the expansion of the ruby spheres, the steel etalon, and the specimen are shown in figure 4. No attempt was made to determine

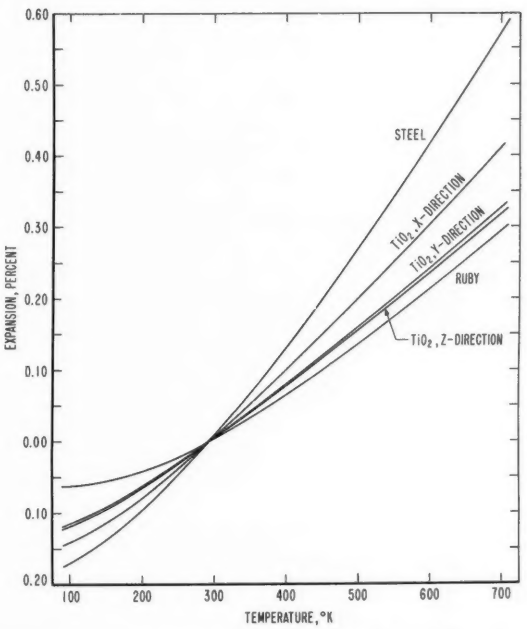

FIGURE 4. *Linear thermal expansion of the cube-shaped rutile specimen in the direction of its body axes* X, Y, *and* Z, *of the W–1 tool-steel etalon, and of the ruby spheres.*

the crystallographic orientation of the ruby spheres but their average expansion as determined is in excellent agreement with the results of Wachtman et al. [10] on the expansion of polycrystalline aluminum oxide. Values obtained for the thermal expansion of the W–1 tool steel, given in table 2, are in good agreement with results obtained on other medium-carbon steels [15].

TABLE 2. *Thermal expansion of recrystallized W–1 tool steel*

Temperature	Linear thermal expansion
°K	*Percent*
100	−0.1703
150	−.1386
200	−.0958
250	−.0465
293	.0000
300	.0079
350	.0670
400	.1303
450	.1976
500	.2683
550	.3420
600	.4182
650	.4965
700	.5767

It can be shown for rutile, which has a tetragonal crystal structure (P4/mnm), that only two coefficients are needed, α_a and α_c, to represent the expansion of the crystal. Volume expansivity is given by

$$\beta = 2\alpha_a + \alpha_c$$

while expansivity in a direction inclined at an angle ω from the c axis is given [16] by

$$\alpha_\omega = \alpha_a + (\alpha_c - \alpha_a)\cos^2\omega.$$

The linear expansion is given by

$$\left(\frac{\Delta L}{L}\right)_\omega = \left(\frac{\Delta L}{L}\right)_a + \left[\left(\frac{\Delta L}{L}\right)_c - \left(\frac{\Delta L}{L}\right)_a\right]\cos^2\omega. \quad (1)$$

Values of $\left(\frac{\Delta L}{L}\right)_a$ and $\left(\frac{\Delta L}{L}\right)_c$ were obtained by fitting equation (1) to the smoothed values of $\left(\frac{\Delta L}{L}\right)_X$, $\left(\frac{\Delta L}{L}\right)_Y$, $\left(\frac{\Delta L}{L}\right)_Z$, and the corresponding values of ω by the method of least squares. These values are given in table 3.

The results of this investigation are in good agreement with results of other investigators [7, 8, 17, 18, 19] as indicated in figure 5 where values of the expansivities α_a and α_c are plotted against temperature.

TABLE 3. *Thermal expansion of rutile* (TiO_2)

Temperature	Body axis			Crystallographic direction		Volume
	X	*Y*	*Z*	*c*	*a*	
°K	*Percent*	*Percent*	*Percent*	*Percent*	*Percent*	*Percent*
100	−0.1414	−0.1184	−0.1157	−0.1439	−0.1158	−0.3751
150	−.1140	−.0941	−.0921	−.1161	−.0920	−.2999
200	−.0782	−.0642	−.0625	−.0797	−.0626	−.2049
250	−.0375	−.0307	−.0299	−.0383	−.0299	−.0981
293	.0000	.0000	.0000	.0000	.0000	.0000
300	.0063	.0051	.0050	.0064	.0050	.0164
350	.0526	.0428	.0416	.0537	.0417	.1372
400	.1007	.0817	.0793	.1029	.0795	.2621
450	.1503	.1212	.1177	.1535	.1179	.3899
500	.2010	.1611	.1567	.2052	.1568	.5197
550	.2526	.2019	.1966	.2579	.1966	.6524
600	.3049	.2436	.2373	.3114	.2372	.7878
650	.3576	.2861	.2785	.3653	.2785	.9251
700	.4106	.3290	.3201	.4193	.3202	1.0635

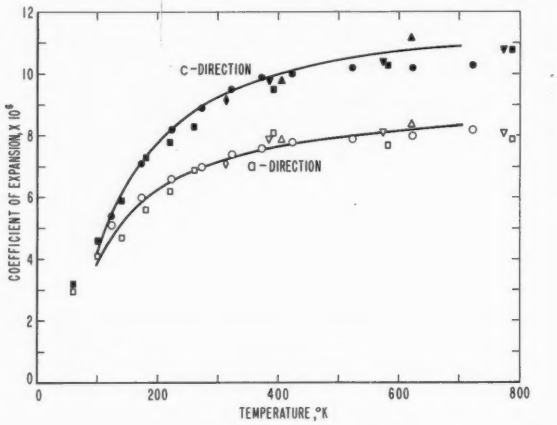

FIGURE 5. *Expansivity of rutile in the crystallographic directions.*
The results of this investigation, as represented by the curves, are compared with the results obtained by Mauer and Bolz □, Kirby ○, Grain and Campbell △, Merz ▽, and Fizeau ◇.

6. Discussion

The usual expression for Grüneisen's parameter is

$$\gamma(T) = \frac{\beta V}{C_p \kappa_s}$$

where β is the coefficient of volume thermal expansion, V is the molar volume, C_p is the molar heat capacity at constant pressure, and κ_s is the adiabatic compressibility. The value of $\gamma(T)$ for well-behaved materials increases slightly from low to high temperatures such that $\gamma(\infty) - \gamma(0) \leq 0.3$ [20]. The unusual behavior of rutile is indicated in figure 6 where the experimentally determined value of $\gamma(T)$ decreases from 2.6 at 100 °K to a high-temperature value of 1.47. Values of $\gamma(T)$ plotted in this figure are listed in table 4. The molar volume at room temperature was calculated from unit cell parameters as determined by Baur [21], the molar heat capacity was calculated by averaging the data of Shomate [22], McDonald and Seltz [23], and Naylor [24], and the compressi-

bility was calculated from the measurements of Chung [25].

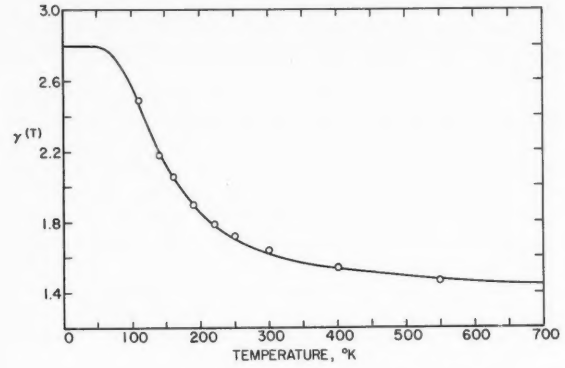

FIGURE 6. *Grüneisen parameter for rutile.*

TABLE 4. *Grüneisen parameter and values for expansivity, volume, heat capacity, and compressibility*

Temperature (T)	Coefficients of linear thermal expansion (α_a)	(α_c)	Coefficient of volume thermal expansion (β)	Molar volume (V)	Molar heat capacity (1 cal = 4.1840J) (C_p)	Adiabatic compressibility (κ_s)	Grüneisen parameter (γ)
°K	10^{-6}/°K	10^{-6}/°K	10^{-6}/°K	cm³/mol	cal/mol °K	10^{-12} cm²/dyn	
110	4.30	4.89	13.49	18.74	5.10	4.750	2.49
140	5.07	6.04	16.18	18.75	7.00	4.753	2.18
160	5.51	6.66	17.68	18.76	8.09	4.756	2.06
190	6.02	7.43	19.47	18.77	9.64	4.761	1.90
220	6.43	8.04	20.90	18.78	10.97	4.768	1.79
250	6.76	8.55	22.07	18.79	12.10	4.776	1.72
300	7.18	9.21	23.57	18.81	13.51	4.795	1.64
400	7.67	10.00	25.34	18.86	15.29	4.851	1.54
550	8.11	10.56	26.78	18.93	16.56	4.961	1.47

Grüneisen's relation can be expressed as

$$\beta=\frac{\gamma C_v \kappa_T}{V}=\kappa_T\left(\frac{\partial S}{\partial V}\right)_T$$

where C_v is the molar heat capacity at constant volume, κ_T is the isothermal compressibility, and S is the entropy. Since entropy is an additive function of state Grüneisen's relation can be interpreted as a sum

$$\beta=\frac{\kappa_T}{V}\sum_i \gamma_i C_i. \qquad (2)$$

This approach has been successfully used to determine the contributions to thermal expansion from conduction electrons [26] and magnetic spin interactions [27] as well as from the lattice. In order to make sense out of the expansion data for rutile it is suggested that for polyatomic crystals eq (2) can also be used to determine the contributions to thermal expansion from the acoustical and optical modes of lattice vibrations.

Since the heat capacity of rutile can be represented to within a few percent from 50 to 600 °K by the combination of a Debye and a single Einstein expression it was hoped that by analogy only two terms for the expansion would be sufficient,

$$\beta=\frac{\kappa_T}{V}(\gamma_{aco}C_{aco}+\gamma_{opt}C_{opt}), \qquad (3)$$

instead of three that might be expected (one acoustical and two optical). The validity of eq (3) for rutile has been tested graphically by plotting ($\beta V/C_{aco}\kappa_T$) against (C_{opt}/C_{aco}), see figure 7. It can be seen that a straight line fits the data as hoped. The intercept of the line with the vertical axis at $C_{opt}/C_{aco}=0$ gives a value of 2.80 for γ_{aco} while the slope of the line gives a value of 0.75 for γ_{opt}.

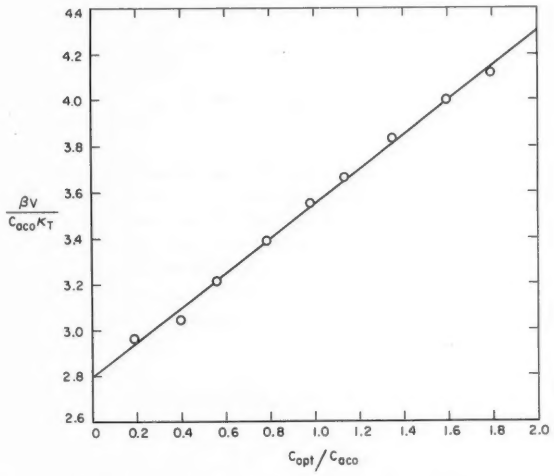

FIGURE 7. *Confirmation that the contributions of the acoustical and optical modes of lattice vibrations to the thermal expansion of rutile can be separated.*

Values for C_{opt} were calculated from the Einstein expression for heat capacity, $C_{opt}=2C\left(\frac{\theta_E}{T}\right)$, using 706 °K as the characteristic temperature. This value for θ_E agrees very closely with the infrared resonance frequency at the absorption maximum [28]. Values for C_{aco} were calculated by taking the difference between observed values of C_v and calculated values of C_{opt}.

The temperature variation of $\gamma(T)$ can be calculated from

$$\gamma(T)=\frac{\gamma_{aco}C_{aco}+\gamma_{opt}C_{opt}}{C_v}$$

and is represented by the solid line in figure 6. At temperatures below 60 °K, $\frac{\theta_E}{T}\sim 12$, the values of C_{opt} are very small and in the limit as $T\rightarrow 0$ °K,

$C_{opt}/C_{aco}=0$, it can be seen that $\gamma(0)\sim\gamma_{aco}=2.80$. At high temperatures $C_{aco}\rightarrow 1/3C_v$ and $C_{opt}\rightarrow 2/3C_v$ and in the limit as $T\rightarrow\infty$, $C_{opt}/C_{aco}=2$, it can be seen $\gamma(\infty)=1/3(\gamma_{aco}+2\gamma_{opt})=1.43$.

The plots of $\frac{3\alpha_c V}{C_{aco}\kappa_T}$ and $\frac{3\alpha_a V}{C_{aco}\kappa_T}$ versus C_{opt}/C_{aco} can also be represented by straight lines with the resulting values at 1.06 and 0.60 for γ_{opt} and 3.04 and 2.68 for γ_{aco} respectively. These results indicate that the value of α_c will always be larger than the corresponding value of α_a.

Using the definition of expansivity as the temperature derivative of the elastic strain tensor at constant stress it can be shown [29] that the principal γ-values for a tetragonal crystal are represented by

$$\gamma_1=\frac{V}{C_p}[(c_{11}+c_{12})\alpha_a+c_{13}\alpha_c]$$

$$\gamma_3=\frac{V}{C_p}(2c_{13}\alpha_a+c_{33}\alpha_c).$$

Since the values of the elastic constants are only known at room temperature [30] the temperature dependence of γ_1 and γ_3 can not be evaluated. Their values at 300 °K, however, are 1.5 and 2.1 respectively.

According to Barron and Leadbetter [31] the volume dependence of certain properties of a crystal, for instance the characteristic temperature for the entropy,

$$\frac{\theta^s(V_0)}{\theta^s(V)}\sim\left(\frac{V}{V_0}\right)^{\gamma_n}\text{where } n=0,$$

and the characteristic temperature for the Debye-Waller factor for x rays,

$$\frac{\theta^M(V_0)}{\theta^M(V)}\sim\left(\frac{V}{V_0}\right)^{\gamma_n}\text{where } n=-2,$$

depend in a direct manner on individual moments of the frequency distribution, $\overline{\nu^n}$. The dimensionless parameters, γ_n, are defined as

$$\gamma_n=-\frac{1}{n}\frac{d\ln\overline{\nu^n}}{d\ln V}.$$

It can be shown that $\gamma_{-3}=\gamma(0)=2.80$ and $\gamma_0=\gamma(\infty)=1.43$, the low and high temperature limiting values of the Grüneisen parameter. At intermediate temperatures

$$\gamma_n=\int_0^\infty\gamma(T)C_vT^{n-1}dT\Big/\int_0^\infty C_vT^{n-1}dT$$

where $-3<n<0$. Using Simpson's rule to evaluate these integrals it was found that γ_{-2} and γ_{-1} are equal to 2.58 and 2.07 respectively.

7. Conclusions

The thermal expansion of an anisotropic crystal, rutile, has been determined from 100 to 700 °K with a unique macroscopic technique. These measurements of expansion (length) are estimated to be accurate to within 4 ppm.

In analyzing these measurements it has been shown that the expansion of rutile is the result of contributions from the acoustical and optical modes of lattice vibrations. Acoustical vibrations seem to be about twice as effective as optical vibrations in causing the volume expansion of the crystal while the optical vibrations are slightly more effective in the direction parallel with the c axis than in a perpendicular direction.

There is reason to assume that the thermal expansion of polyatomic crystals in general will to some degree be dependent upon optical modes of vibration as well as upon acoustical modes [32].

The author is indebted to J. B. Wachtman, Jr., for supplying the rutile crystal and information on its crystallographic orientation and to D. H. Chung for allowing the use of his unpublished elasticity data without which the analysis could not have been made. The author is also grateful to T. A. Hahn for interesting and helpful discussions about this work and to J. W. McDermott for the difficult job of preparing the specimen.

8. References

[1] E. Grüneisen, U.S. NASA Publ. No. RE2-18-59W (translation of Handbuch der Physik **10,** 1 (1926)).
[2] G. K. White, Proc. Eighth Int. Conf. on Low Temp. Phys., Butterworths, London, 1963, p. 394.
[3] R. D. McCammon and G. K. White, Phil. Mag. **11,** 1125 (1965).
[4] G. K. White, Phys. Letters **8,** 294 (1964).
[5] G. K. White, J. Australian Inst. Metals **8,** 134 (1963).
[6] M. Blackman, Phil Mag. **3,** 831 (1958).
[7] F. A. Mauer and L. H. Bolz, National Bureau of Standards; unpublished report.
[8] R. K. Kirby, National Bureau of Standards, unpublished report.
[9] W. J. Campbell, Bureau of Mines Rept. of Investigations 6115 (1962).
[10] J. B. Wachtman, Jr., T. G. Scuderi, and G. W. Cleek, J. Am. Ceram. Soc. **45,** 319 (1962).
[11] E. V. Vernon and S. Weintroub, Proc. Phys. Soc. (London) **66,** 887 (1953).
[12] C. Pulfrich, Z. Instrumentenk. **13,** 365 (1893).
[13] R. Benoit, Trav. et Mem. du Bureau Int. Poids et Mes. **6,** 3 (1888).
[14] C. G. Peters and C. H. Cragoe, B. S. Sci. Pap., No. 393 (1920).
[15] Handbook of Thermophysical Properties of Solid Materials, Volume **2** (The MacMillan Co., New York, 1961).
[16] J. F. Nye, Physical Properties of Crystals—Their Representation by Tensors and Matrices (Oxford University Press, New York, 1957).
[17] C. F. Grain and W. J. Campbell, Bureau of Mines Rept. of Investigations 5982 (1962).
[18] K. M. Merz, Cornell Aeronautical Laboratory, Inc., Report No. PI-1273-M-8 (1960).
[19] H. Fizeau, Comptes Rendus **62,** 1101 (1866).
[20] T. H. K. Barron, Phil. Mag. **3,** 831 (1958).
[21] W. H. Baur, Acta Cryst. **9,** 515 (1956).

[22] C. H. Shomate, J. Am. Chem. Soc. **69,** 218 (1947).
[23] H. J. McDonald and H. Seltz, J. Am. Chem. Soc. **61,** 2405 (1939).
[24] B. F. Naylor, J. Am. Chem. Soc. **68,** 1077 (1946).
[25] D. H. Chung, Materials Research Laboratory, Pennsylvania State University, private communication.
[26] G. K. White, Phil. Mag. **6,** 815 (1961).
[27] G. K. White, Proc. Phys. Soc. (London) **86,** 159 (1965).
[28] T. Liebisch and H. Rubens, Preuss. Akad. Wiss. Ber. **8,** 211 (1921).
[29] J. G. Collins and G. K. White, Prog. Low Temp. Phys. **4,** 450 (1964).
[30] J. B. Wachtman, Jr., W. E. Tefft, and D. G. Lam, Jr., J. Res. NBS **66A** (Phys. and Chem.), No. 6, 465 (1962).
[31] T. H. K. Barron and A. J. Leadbetter, Proc. Roy. Soc. **A279,** 62 (1964).
[32] R. K. Kirby, Bull. Am. Phys. Soc. Series II, **12,** No. 3, 371 (1967).

(Paper 71A5–466)

JOURNAL OF RESEARCH of the National Bureau of Standards—A. Physics and Chemistry
Vol. 71A, No. 5, September–October 1967

Mass Spectrometric Study of Photoionization. VII. Nitrogen Dioxide and Nitrous Oxide*

Vernon H. Dibeler, James A. Walker, and Susan K. Liston

Institute for Basic Standards, National Bureau of Standards, Washington, D.C. 20234

(June 14, 1967)

Photoionization efficiency curves are obtained for the molecule and fragment ions of NO_2 and N_2O from ionization threshold to 600 Å. Features of the molecule ion curves are ascribed to autoionization and the Rydberg levels are correlated with reported spectroscopic observations. The minimum onset of ionization for NO_2 occurs at 1272 Å (9.75 eV). The threshold value of 12.34 eV for the NO^+ fragment results in D(NO–O) of 3.09 eV in good agreement with that calculated from thermochemical heats of formation. The O^+ ion is apparently formed with 0.1 eV excess energy. The minimum threshold energy for the N_2O^+ ion is 962 Å (12.89 eV). The N_2^+ fragment ion curve has a threshold at 17.29 eV corresponding to the thermochemical bond energy, $D(N_2-0)=1.67$ eV. However a lower-energy threshold at 15.57 eV is ascribed to ionization of molecular nitrogen from an unknown source. There is no evidence for an ion-pair process. The ground state transition for NO^+ is forbidden by spin conservation rules. The observed threshold is 0.8 eV in excess of the calculated value and suggests a vibrationally excited state of the ion. The N^+ ion is also formed with excess energy.

Key Words: Dissociation, fragment ions, ionization, mass spectrometer, molecule, NO_2, NO_2^+ N_2O^+, photoionization, threshold, ultraviolet, vacuum.

1. Introduction

Studies of ionization and dissociation processes of NO_2 and N_2O are of interest both in theory and in application, particularly to the physics and chemistry of the upper atmosphere. As a result, numerous workers have reported on absorption spectra, thresholds of ionization and bond dissociation energies for both molecules.

In the case of NO_2, Mulliken [1][1] first postulated a molecular ionization threshold somewhat higher than that of nitric oxide and adopted [2] the value of 10 eV. No Rydberg series converging near this value has yet been detected [3, 4] for reasons now believed understood [5, 6]. However, two photoionization studies [4, 7] obtained thresholds of 9.78 eV and 9.8 eV, respectively; the former without mass analysis and the latter with mass analysis but an optical resolution of about 6 Å.

Of the many electron impact measurements reported on NO_2 in the last decade [8–12], only the ionization energies derived from fragment-ion measurements of nitroalkyls have resulted in a value near the theoretical and photoionization values 9.91 eV [11, 12]. Apparently all other measurements (including several other photoionization studies [13, 14, 15] refer to thresholds of states other than the ground state of the ion.

Recent attempts to determine the minimum ionization threshold of the N_2O^+ ion by electron impact have resulted in values ranging from 12.6 to 13.1 eV; a variation which is considerably larger than the quoted uncertainties in most of the measurements [8, 16, 17]. Unlike NO_2, however, Rydberg absorption series converging to the first ionization threshold of N_2O have been detected and analyzed [18, 19]. In addition, photoionization measurements with [13] and without [20, 21] mass analysis indicate that the minimum ionization threshold is about 12.89 eV. Ionization thresholds for states above the ground state of the ion have been reported by electron impact, Rydberg series, and photoelectron spectroscopy [15, 22]. Of the data reported, those from the latter two sources are probably most reliable, although the first ionization threshold reported by Al-Joboury, May, and Turner [22] would appear to be too low by about 0.07 eV.

Measurements of fragment-ion thresholds have been obtained both by electron impact [8, 16] and by photoionization using mass analysis [13]. However, several inconsistencies and ambiguities appeared in the calculations of bond dissociation energies, some of which were ascribed to pyrolysis on filaments used in the electron impact studies. Of particular interest is the $D(N_2-O)$ value and its relation to the exo- or endothermic nature of certain possible atmospheric reactions [23].

The purpose of the present work, part of a continuing program [24] on mass spectrometric studies of photoionization, is to obtain improved photoionization

*Supported in part by the U.S. Atomic Energy Commission.

[1] Figures in brackets indicate the literature references at the end of this paper.

efficiency curves for the molecule and fragment ions of nitrogen dioxide and nitrous oxide and to reexamine the threshold values and the energies of dissociative ionization occurring in these molecules.

2. Experimental Procedure

The combined vacuum ultraviolet monochromator and mass spectrometer described in detail in the first paper of this series [25] was used in the present work with only the minor modifications previously reported [24]. The argon continuum was excited by a 2450 MHz, 800-W microwave discharge and used as a photon source for the NO_2^+ ion from threshold to about 1060 Å. The hydrogen many-line spectrum excited by microwave discharge or in a Hinteregger lamp was used from 1060 to 950 Å. The Hopfield continuum of helium obtained in the Hinteregger lamp was employed from 950 to 600 Å. Portions of these wavelength ranges were used for the other ions as required. Gratings, intensities of photons and ions, and probable errors were essentially as described in earlier reports. Conversion factors used are 1 eV = 8065.73 cm^{-1}, and 1 eV molecule = 23.0609 kcal mol^{-1}.

Both nitrogen dioxide and nitrous oxide were obtained as research grade materials from a commercial supplier. Immediately before using, they were purified of more nearly permanent gases by simple bulb to bulb distillation in a vacuum system made a part of the mass spectrometer inlet system. In addition, periodic examination of mass spectra and relative intensities of significant ions in the spectra were made during the course of all measurements to affirm the absence of changes in composition of the purified material. It is estimated from mass spectral data that impurities were less than 1 mole percent. There was no evidence for N_2O_4 in NO_2.

Several experiments were made on NO_2 and N_2O to determine the possible occurrence of bimolecular reactions in the ion source or formation of products resulting from multiple photon impact even at the assumed low pressures existing in the ion source. All observed ion currents were simple functions of the intensity of the photon beam (at 584 Å) varied over a factor of 10 and of the sample pressure varied over a factor of 20.

As molecular nitrogen, a common residual gas in mass spectrometers, interferes with the measurements of the N_2^+ ion in N_2O, special care was taken to to maintain background gases at the lowest practical value. It was frequently determined that the background ion count at $m/e = 28$ remained a small fraction < 0.1 percent of the maximum ion count for the principal ion in each gas admitted to the mass spectrometer.

3. Results and Discussion

NO_2: The relative intensities of the NO_2^+, NO^+, O^+, and N^+ ions at 584 Å (21.23 eV) are 0.49, 1.0, 0.18, and 0.003, respectively. The abundance of the N^+ ion was too low to permit an accurate threshold determination. Also, an unsuccessful search was made for negative ions at all accessible frequencies. It is estimated that the maximum relative intensity for any ion-pair process is less than 0.01.

Figure 1 shows typical ionization efficiency curves for the NO_2^+ and NO^+ ions. The O^+ ion curve, observable only over a short wavelength range is omitted in order to simplify the figure. The abscissa is wavelength in angstroms with the equivalent energy in electron-volts given at convenient points. The ordinate is the ionization yield (ions per photon transmitted through the ionization chamber) given in arbitrary units. The ordinate scale for the NO^+ ion is one-half that of the molecule ion. The initial portion of the NO_2^+ ion curve is replotted in the inset using an ordinate scale 25 times that of the complete curve. Data points are plotted in the form of error bars; the length indicating the estimated uncertainty. Included in the figure are vertical lines of uniform length designating the location of Rydberg absorption series and progressions observed by Tanaka and Jursa [26], and the vibrational structure of a Rydberg series reported by Nakayama, Kitamura, and Watanabe [4]. In addition, vertical arrows locate ionization thresholds of nitrogen dioxide as observed by Al-Joboury and Turner [14] and Vroom [15], using photoelectron spectroscopy.

With the exception of the minimum threshold for ionization, the major features of the molecule ion curve are generally in agreement with the curves published by Weissler et al. [13], and by Frost et al. [7], although detailed comparison is not possible as those authors made observations at relatively few wavelengths and with poorer optical resolution. Our curve also shows features similar to those observed in the total ionization curve obtained by Nakayama et al., in the wavelength region 1275 to 1100 Å. The appearance of the photoionization curve in this region explains the failure of electron impact measurements and low-sensitivity techniques to observe the minimum onset of ionization.

It has been shown [5, 6] that the ground state of NO_2 is bent whereas the ion, isoelectronic with CO_2 is undoubtedly linear. Thus, the slowly rising ion yield curve appears to be characteristic of molecules undergoing structural change on ionization as noted in previous studies.

The inset of figure 1 shows the initial onset plotted on an expanded ordinate. The minimum onset definitely appears at 1272 Å (9.75 ± 0.01 eV). The uncertainty here and in following thresholds is estimated from the experimental conditions with the value of 9.78 eV selected by Nakayama et al. [4], and 9.80 ± 0.05 eV reported by Frost et al. [7]. It indicates the approximate correctness of the indirect determinations of 9.91 eV by Kandel [11] and 9.93 eV by Collin [12] although indicating that these derivations probably include some excess energy. It also supports the predicted [1, 2] low value for the ionization threshold of NO_2 and the view that all values so far obtained by Rydberg extrapolation refer to the several inner ioniza-

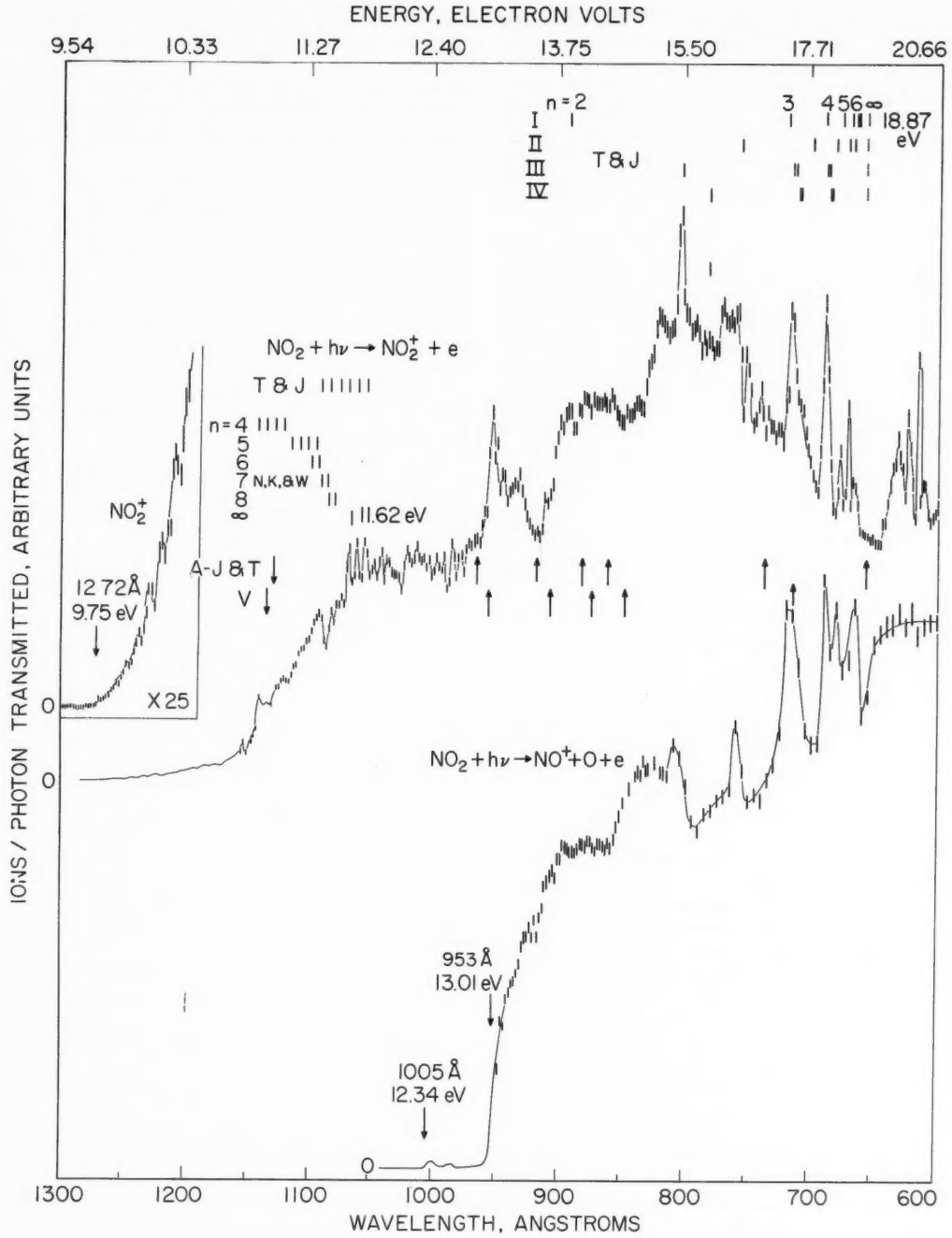

FIGURE 1. *Photoionization yield curves for the* NO_2^+ *and* NO^+ *ions of* NO_2.

The inset shows a replot of the threshold of NO_2^+ at a sensitivity 25X the complete curve. The sensitivity for the NO^+ ion is twice that of the NO_2^+ ion

tion thresholds. From the absence of a strong, sharp onset, it is not surprising that spectroscopists have failed to observe the initial onset.

The initial rise of the ionization yield curve exhibits weak structure at intervals of 10 Å attributed to autoionization. Although Rydberg levels have not been reported in the wavelength region 1251 to 1144 Å, the intervals are in good agreement with the $\Delta\nu$'s observed in the 1280, 1135, and 1080 Å absorption bands and attributed to the ν_2 vibration.

The slowly rising ion yield curve in the region of 1150 to 900 Å shows partially resolved peaks attributed to autoionization. Good correlation is possible with a progression reported by Tanaka and Jursa in the 1093 to 1056 Å region, but only fragmentary evidence is obtained for the progressions reported by Nakayama et al. Furthermore, the convergence reported at 11.62 eV cannot be confirmed by our results due to the interfering autoionization peaks. The band at 940 Å has not been reported previously. It apparently converges to an onset at 915 Å (13.55 eV). Further autoionization is observed in the region of 810 to 660 Å, much of which can be correlated with the Rydberg absorption series I to IV. An additional autoionizing band is apparent below 650 Å, perhaps converging at about 20.6 eV.

Comparison of the present molecule-ion curve structure with inner ionization thresholds obtained by means of photoelectron spectroscopy is difficult because of interference from autoionization. In addition, there is a certain lack of agreement between the two sets of photoelectron data. It is apparent, however, that the latter do not include observations of the ion ground-state threshold. Also, the reported threshold at about 12.8–12.9 eV coincides with a sudden increase in a dissociative ionization process which could not be identified without mass analysis. The photoelectron threshold at 13.5 to 13.6 eV seems to be supported by a rise in the photoionization curve at that energy. Other thresholds can not be confirmed. There seems to be some inconclusive evidence from Rydberg series of ionization thresholds in NO_2 between 9.76 and ~ 17.5 eV. Unfortunately, only one instance of agreement is reported for photoelectron threshold with the well-established Rydberg convergence at 18.87 eV.

The photoionization yield curve for the NO^+ ion (fig. 1) shows a very weak onset at 1005 Å (12.34 eV) and includes evidence for autoionization. It is followed by a much more intense onset at 953 Å (13.01 eV). The latter increase coincides with a peak in the molecule ion curve attributed to an autoionizing Rydberg level. It is suggested that this level may autoionize either to the parent ion or to a fragment ion. Similar instances of competing processes have been observed in previous studies and the conclusion is further supported by the intense autoionization observed in the region 810 to 600 Å, some of which can be correlated directly with similar peaks in the molecule ion curve.

The threshold value of 12.34 eV, less 9.25 eV for the ionization energy of NO [21], gives 3.09 eV for the heat of reaction at 0 °K for the process, $NO_2 \rightarrow NO + O$. We find this in very satisfactory agreement with the value of 3.115 eV calculated from the appropriate heats of formation [27] at 0 °K. There is no evidence for a lower-energy threshold such as would correspond to an ion-pair process, $NO_2 + h\nu \rightarrow NO^+ + O^-$.

The shape of the ionization efficiency curve (not shown) for the O^+ ion from $NO_2 + h\nu \rightarrow O^+ + NO$ is quite similar to the NO^+ curve. A very weak and slowly rising onset appears at 737 Å (16.8_2 eV) followed by a much sharper and more intense onset at 657 Å (18.8_7 eV). Subtracting the ionization energy of atomic oxygen [28] from the minimum threshold gives 3.2_2 eV for the heat of reaction compared with the above calculated value of 3.115 eV. Apparently about 0.1 eV of excess energy is included in this reaction Transition to the ground state is forbidden by spin-conservation rules.

N_2O: Relative intensities of the N_2O^+, NO^+, N_2^+, O^+, and N^+ ions were found to be 1.00, 0.59, 0.16, 0.02, and 0.03, respectively, at 584 Å (21.33 eV). Relative intensities of the fragment ions measured at 600 Å by Weissler et al. [13], are much larger and suggest the possibility of impurities due to inadequate pumping facilities.

An O^- ion was observed with a maximum intensity at about 800 Å. Unfortunately, the abundance (estimated to be about 0.001 relative to the molecule ion abundance) is too weak to permit satisfactory measurements of the ionization efficiency curve. Curves were obtained for all the observed positive ions although only the molecule and the N_2^+ ions are shown in figure 2, and the NO^+ ion curve is shown in figure 3. The remaining curves are omitted in order to simplify the figures. Various progressions and Rydberg series observed by Tanaka et al. [19], and the onsets of ionization by means of photoelectron spectroscopy reported by Al-Joboury et al. [22], and by Vroom [15] are indicated in figure 2 in the same manner as in figure 1.

The minimum threshold of ionization for the N_2O^+ ion appears to be a sharp, intense onset with a total energy spread of about 2 Å. As this is essentially the band width of the photon beam, we take the midpoint, 962 Å ($12.88_7 \pm 0.007$ eV) to be the value of the initial ionization energy. This is in excellent agreement with the value of 12.88_9 eV obtained by extrapolation of Rydberg absorption series [19] and of 12.882 ± 0.008 eV [21] and 12.90 ± 0.01 eV [20] obtained by photoionization without mass analysis. These concordant results apparently rule out the lower value of 12.712 eV obtained by Duncan [18]. The two values obtained by photoelectron spectroscopy, 12.82 eV [22] and 12.90 ± 0.01 eV [15] are not consistent within the uncertainties suggested by the number of significant figures, although our measurements agree with the second value. We are not in agreement with recent electron impact values of 13.09 ± 0.05 eV [8] and 12.63 ± 0.05 eV [16].

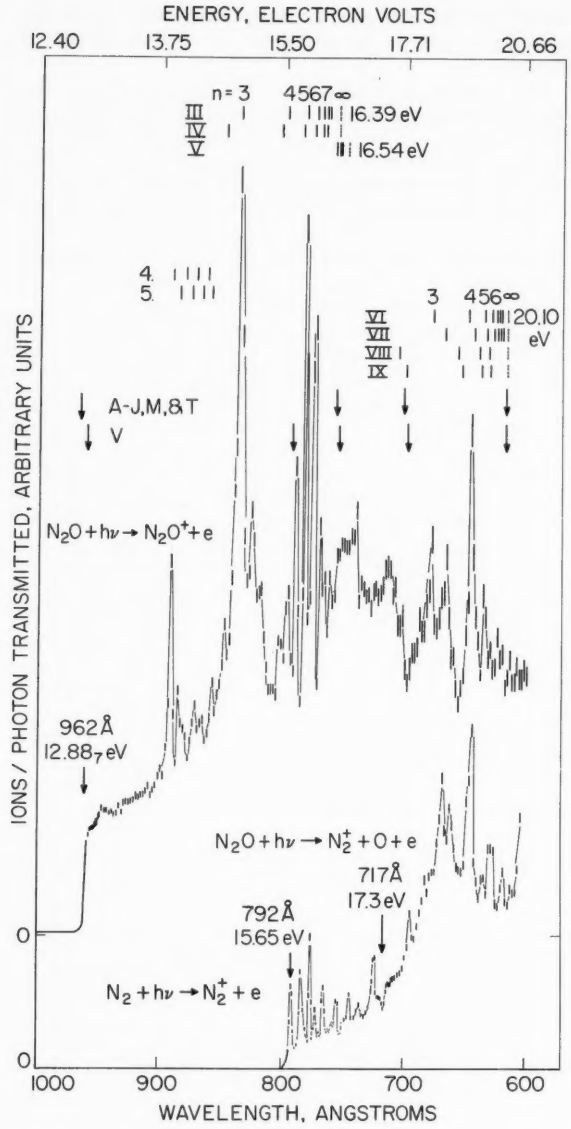

FIGURE 2. *Photoionization yield curves for the* N_2O^+ *and* N_2^+ *ions of* N_2O.

Tanaka et al. [19], observed two Rydberg series of absorption bands converging to 104,000 and 104,300 cm^{-1}, respectively, which they ascribed to the two components of the $^2\Pi$ ground state of the N_2O^+ ion. Although their $\Delta\nu = 300$ cm^{-1} is in poor agreement with the value of 133.1 cm^{-1} obtained by Callomon [29] for the splitting of the $^2\Pi$ state, the discrepancy is ascribed [30] to the fact that the second Rydberg series could not be followed to very high members. It is not possible to resolve this matter in the present work, although there is evidence for two additional onsets at about 950 and 935 Å. These may represent doubly excited bending frequencies or totally symmetric stretching frequencies. However, no previous observations of Rydberg series leading to vibrationally excited ground states of the ion have been reported.

Below 900 Å, partially resolved peaks ascribed to autoionization are observed at wavelengths that are in excellent agreement with those of the weak, diffuse progressions numbered 4 and 5 by Tanaka et al. This is followed by two groups of intense autoionization peaks in the region 850 to 770 Å which are easily correlated with the Rydberg absorption series III, IV, and V converging to the limits of 16.39 eV and 16.54 eV. These limits are not apparent in the present work but the first of these is in good agreement with a threshold of ionization observed by photoelectron spectroscopy [15, 22].

Other autoionization peaks are observed in the region 700 to 630 Å. These are also correlated with the Rydberg absorption series VI and VII. It is interesting to note that there is also evidence for minima in the photoionization curve in this region that apparently correspond to Rydberg levels in the emission series VIII and IX as reported by Tanaka. Again, there is no appearance of an onset [31] at the convergence limit of 20.10 eV although it is apparently confirmed by photoelectron spectroscopy [15, 22].

The photoionization efficiency curve for the N_2^+ ion shown in figure 2 is of particular interest. The midpoint of a sharply rising onset first appears at 796 Å (15.576 eV) with a peak maximum at 792 Å (15.65 eV). The full-width at half maximum is approximately equal to the optical resolution. Other peaks follow at about 10 Å intervals to 720 Å. A sharp increase in continuum occurs at 717 Å (17.29 eV) and again at 700 Å (17.71 eV) followed by considerable autoionization in the region 670 to 600 Å. Assuming the onset at 17.29 eV to represent the threshold for the dissociative ionization process, $N_2O + h_n \rightarrow N_2^+ + O + e$, subtracting the ionization energy, $I(N_2) = 15.576$ eV [32] gives the bond dissociation energy, $D(N_2 - O) = 1.71$ eV. Within the obvious uncertainty of evaluating and interpreting the threshold, this value is in agreement with $D(N_2 - O) = 1.671$ eV calculated from thermochemical heats of formation [27] at 0 °K.

Unfortunately, the interpretation of the low energy threshold and the origin of the autoionization peaks in the wavelength region 792 to 722 Å is somewhat ambiguous. One possible interpretation is the dissociative ionization of Rydberg levels in the N_2O molecule (predissociation) to yield ion-pairs according to the process, $N_2O + h\nu \rightarrow [N_2O^*] \rightarrow N_2^+ + O^-$. In which case the minimum threshold will appear at an energy lower than the ion-neutral process by an amount equal to the electron affinity of the oxygen atom, $EA(0) = 1.48$ eV [33] or at 15.81 eV (784 Å). The discrepancy in the observed value is -0.16 eV.

Curran and Fox [16] reported an analogous observation in an electron-impact study of N_2O. They observed an onset of ionization below that of the ion-neutral process but ascribed it to the ionization of molecular nitrogen formed by the pyrolysis of

N_2O in their heated ion source. Pyrolysis is ruled out in the present experiments as the ion source operates at ambient room temperature. Formation by multiple photon collision or by means of a bimolecular reaction is also excluded as indicated in the section on experimental procedure. Thus the possibility remains that the threshold for the ion-neutral process includes excess energy and that the N_2-O bond dissociation energy (1.671 eV) calculated from heats of formation is too high by at least 0.16 eV. There is some evidence in support of this suggestion [16, 23, 34].

In the present measurements, however, it is possible to compare the wavelengths of the autoionizing Rydberg levels for the several molecular species involved. For example, if the N_2^+ ion is due to ion-pair formation by dissociative autoionization of Rydberg levels in the N_2O molecule, then peaks in the molecule ion curve, reflected in the ion pair curves, should appear at the same wavelength in the latter (N_2^+, O^-) curves. Table 1 lists wavelengths and estimated relative intensities for principal peaks observed in the wavelength region 790 to 690 Å of the N_2^+ and N_2O^+ ion curves of figure 2. It also includes the wavelengths and ionization coefficient (k_i) values of the maxima previously observed in total photoionization curves of N_2O [35] and N_2 [36].

TABLE 1. *Comparison of maxima observed in the 792–694 Å region of the ionization efficiency curves of N_2O and N_2*

Mass analysis				Total ionization			
N_2^+		N_2O^+		N_2O [a]		N_2 [b]	
λ	I[c]	λ	I[c]	λ	k_i(cm^{-1})	λ	k_i(cm^{-1})
792	0.6	790	.7	789.5	810	792.0	1000
784	.7	782	1.0	782.5	1000	783.5	1040
776	1.0	774	0.9	774.0	850	776.0	1060
772	0.4	770	.6	769.5	600	771.5	750
765	.6	767	.5	767.0	540	765.0	940
758	.4	762	.5	762.5	485	758.5	600
754	.5	750	.6	750.0	500	754.3	940
744	.5	740	.6	740.0	540	743.7	680
736	.4	730	.5	730.0	530	736.8	570
723	.8	.....	.....	.....	.....	723.4	1100
694	[d].4	.....	.....	.....	.....	694.9	800

[a] Reference [35].
[b] Reference [36].
[c] Relative intensities estimated from peak heights.
[d] Corrected for estimated N_2^+ from ion-neutral process.

Although the relative intensities of the maxima observed in the present work are of qualitative significance only, it is clear that the wavelength positions for the maxima in the N_2^+ ion (fig. 2) in the region 792 to 694 Å correspond within 0.5 Å to maxima in the absorption curve of molecular nitrogen and that they differ by 2 Å or more from the maxima observed in the molecule-ion curve. Furthermore, we have obtained the photoionization curve for the molecule ion of nitrogen and, in the wavelength region 792 to 694 Å, we find the onset and maxima to be identical with that region of the N_2^+ curve in figure 2 whereas the peaks at shorter wavelengths are due to N_2O, only. We must conclude, that the low-energy process observed here is due principally to the photoionization of molecular nitrogen. The ion-pair process may occur with low probability but it is obscured by the ionization of nitrogen.

The ionization coefficients for N_2O and N_2 in the above wavelength region have been tabulated [35, 36]. For example, at 733 ± 1 Å the minimum k_i − values for N_2O and N_2 are approximately equal (500 cm^{-1}). From that fact and the observed intensity of the N_2^+ ion, we estimate the presence of about 3 mole percent nitrogen in the ion source. As this is an order of magnitude greater than anticipated from the purified sample or measured as background (without introduction of sample), the origin is presently unexplained.

The ionization efficiency curve of the NO^+ ion from N_2O is plotted in figure 3 in the same manner as figure 2. A sharp but relatively weak onset at 828 Å (15.01 eV) is followed by autoionization peaks at intervals of about 8 Å in the region 820 to 770 Å. These are ascribed to Rydberg levels apparently converging to a second, more intense onset at 750 Å (16.53 eV). The associated continuum shows some evidence of autoionization and a third onset at 699 Å (17.74 eV).

The threshold at 15.01 eV, ascribed to the process $N_2O + h\nu \rightarrow NO^+(X'\Sigma^+) + N(^4S°)$, is in good agreement with the less precise electron impact value of 15 eV [8] but considerably higher than the more recent value of 13.75 ± 0.01 eV [16]. Subtracting the ionization energy, I(NO) = 9.250 eV [21] from 15.01 eV gives D(N − NO) = 5.76 eV (132.4 kcal mol^{-1}). The appropriate heats of formation [27] at 0 °K result in a value of 4.924 eV (113.55 kcal mol^{-1}). Thus the observed threshold includes 0.84 eV excess energy and this is consistent with the expectation that a transition to the ground state of the products from $N_2O(X'\Sigma^+)$ is forbidden by spin conservation rules. The excess energy probably appears as a vibrationally excited ion as Nicholson [21] reports the 0–3 vibrational interval of the $NO^+(X'\Sigma^+)$ to be 0.855 eV.

The second and third thresholds at 16.53 and 17.74 eV are ascribed to the formation of NO^+ in the ground state and N atoms in the $^2D°$ and $^2P°$ states, respectively. The observed threshold of 16.53 eV for the reaction $N_2O(X'\Sigma^+) + h\nu \rightarrow NO^+(X\Sigma^+) + N(^2D°) + e$ is in excellent agreement with the calculated value of 16.557 eV using heats of formation of the ground state species and the ($^4S° - ^2D°$) interval of 2.383 eV [28]. Similarly, the observed threshold at 17.74 eV for the reaction, $N_2O(X'\Sigma^+) + h\nu \rightarrow NO^+(X'\Sigma^+) + N(^2P°) + e$ is in good agreement with 17.749 eV calculated by means of the ($^4S° - ^2P°$) interval of 3.575 eV [28].

The O^+ ion curve (not shown) has a weak onset at 810 Å (15.31 eV) followed by considerable autoionization in the range 800 to 740 Å. The well-defined peaks appeared at about 7–Å intervals and at wavelengths identical with peaks observed in the molecule ion curve (see fig. 2). The threshold at 15.31 eV is in good agreement with electron impact values of 15.33 ± 0.02 eV [8], and 15.49 ± 0.10 eV [16] and with the threshold of 15.289 eV at 0 °K calculated from heats of formation for the reaction, $N_2O + h\nu \rightarrow O^+ + N_2 + e$.

The N^+ ion is measurable only over a relatively short wavelength region. However, a very sharp onset

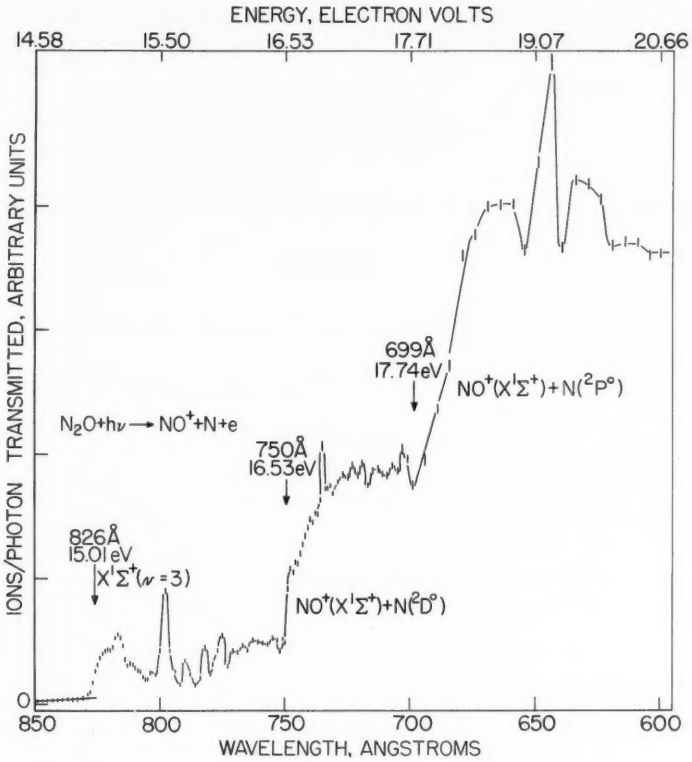

FIGURE 3. *Photoionization yield curve for the* NO^+ *ion of* N_2O.

is observed at 618 Å (20.06 eV) followed by a fairly smooth increase in continuum to 600 Å. The heats of formation result in a calculated threshold of 19.456 eV at 0 °K for the reaction, $N_2O + h\nu \rightarrow N^+ + NO + e$. Thus about 0.6 eV excess energy is included in the dissociative ionization process.

4. References

[1] R. S. Mulliken, J. Chem. Phys. **3,** 720 (1935).
[2] R. S. Mulliken, Revs. Mod. Phys. **14,** 204 (1942).
[3] W. C. Price and D. M. Simpson, Trans. Faraday Soc. **37,** 106 (1941).
[4] T. Nakayama, M. Y. Kitamura, and K. Watanabe, J. Chem. Phys. **30,** 1180 (1959).
[5] L. Harris and G. W. King, J. Chem. Phys. **8,** 775 (1940).
[6] S. Claesson, J. Donoghue, and V. Schomaker, J. Chem. Phys. **16,** 207 (1948).
[7] D. C. Frost, D. Mak, and C. A. McDowell, Can. J. Chem. **40,** 1064 (1962).
[8] J. Collin and F. P. Lossing, J. Chem. Phys. **28,** 900 (1958).
[9] R. W. Kiser and I. C. Hisatsune, J. Phys. Chem. **65,** 1444 (1961).
[10] R. W. Kiser and E. J. Gallegos, J. Phys. Chem. **66,** 947 (1962).
[11] R. J. Kandel, J. Chem. Phys. **23,** 84 (1955).
[12] J. Collin, J. Chem. Phys. **30,** 1621 (1959); Nature **196,** 373 (1962).
[13] G. L. Weissler, J. A. R. Samson, M. Ogawa, and G. R. Cook, J. Opt. Soc. Am. **49,** 338 (1959).
[14] M. I. Al-Joboury and D. W. Turner, J. Chem. Soc. **1964,** 4434.
[15] D. A. Vroom, private communication and Doctoral Thesis, Univ. British Columbia, Vancouver, B.C., 1966.
[16] R. K. Curran and R. E. Fox, J. Chem. Phys. **34,** 1590 (1961).
[17] F. H. Dorman, J. Chem. Phys. **43,** 3507 (1965).
[18] A. B. F. Duncan, J. Chem. Phys. **4,** 638 (1936).
[19] Y. Tanaka, A. S. Jursa, and F. J. LeBlanc, J. Chem. Phys. **32,** 1205 (1960).
[20] K. Watanabe, T. Nakayama, and J. Mottl, J. Quant. Spectrosc. Radiat. Transfer **2,** 369 (1962).
[21] A. J. C. Nicholson, J. Chem. Phys. **43,** 1171 (1965).
[22] M. I. Al-Joboury, D. P. May, and D. W. Turner, J. Chem. Soc **1965,** 6350.
[23] F. C. Fehsenfeld, E. E. Ferguson, and A. L. Schmeltekopf, J. Chem. Phys. **45,** 1844 (1966).
[24] For preceding paper in this series, see: V. H. Dibeler and J. A. Walker, J. Opt. Soc. Am.
[25] V. H. Dibeler and R. M. Reese, J. Res. NBS, **68A** (Phys. and Chem.), No. 4, 409 (1964).
[26] Y. Tanaka and A. S. Jursa, J. Chem. Phys. **36,** 2493 (1962).
[27] D. D. Wagman, W. H. Evans, I. Halow, V. B. Parker, S. M. Bailey and R. H. Schumm, NBS Tech. Note 270–1 (Oct. 1, 1965).
[28] C. E. Moore, NBS Circ. 467 (June 15, 1949).
[29] J. H. Callomon, Proc. Chem. Soc. **1959,** 313.
[30] G. Herzberg, Molecular Spectra and Molecular Structure. III. Electronic Spectra and Electronic Structure of Polyatomic Molecules, p. 506, et seq (D. Van Nostrand Co., Inc., Princeton, N.J., 1966).
[31] For a discussion of the appearance or absence of such onsets, see reference 24.

[32] T. Namioka, M. Ogawa, Y. Tanaka, Paper No. B208–1, Molecular Structure and Spectroscopy Symposium, Tokyo, 1962.
[33] R. S. Berry, J. C. Mackie, R. L. Taylor, and R. Lynch, J. Chem. Phys. **43,** 3067 (1965).
[34] G. L. Schulz, J. Chem. Phys. **34,** 1778 (1961).
[35] G. R. Cook and B. K.-Ching, Rept. No. TDR–469 (9260–01)–4 Aerospace Corp., El Segundo, Calif. (30 January, 1965).
[36] G. R. Cook and P. H. Metzger, J. Chem. Phys. **41,** 321 (1964).

(Paper 71A5–467)

JOURNAL OF RESEARCH of the National Bureau of Standards—A. Physics and Chemistry
Vol. 71A, No. 5, September–October 1967

Ionization Constants of Substituted Benzoic Acids in Ethanol-Water*

G. M. Brauer, George Durany, and Harold Argentar

Institute for Materials Research, National Bureau of Standards, Washington, D.C. 20234

(May 11, 1967)

The thermodynamic ionization constants of meta and para substituted allyl- and propenylbenzoic acids were determined potentiometrically in aqueous ethanol of varying ethanol concentration. The pK values increase with increasing ethanol content. The relative acid strength does not vary with change in solvent concentration. The $\Delta pK/\Delta$ percent ETOH increases with ethanol content of the medium until a maximum is reached around 40 weight-percent ethanol. A plot of $pK + \log [H_2O]$ versus the reciprocal of the dielectric constant of the solvent gives a nearly linear relationship to about 44 weight-percent ethanol. From pK values found in the literature a similar linear relationship exists for other benzoic acids. With the exception of the p-propenylbenzoic acid the σ-substituent constants of the Hammett equation do not change greatly with ethanol concentration. This behavior may be indicative that the solvation shell surrounding the p-propenyl-acid differs from that of other benzoic acids.

Key Words: Allyl- and propenylbenzoic acids, change of pK with dielectric constant, Hammett sigma constants, ionization constants, pK values in ethanol-water, sigma constants in ethanol-water, substituted benzoic acids.

1. Introduction

Previous results [1][1] have shown that a relationship exists between the reactivity and the presence of substituent groups in phenols. This relationship applies to the ionization constants of substituted *o*-methoxyphenols (substituted guaiacols) as well as to the rate of the setting reaction of 4-allyl-2-methoxyphenol (eugenol) and 5-allyl-2-methoxyphenol (chavibetol) with zinc oxide. One of the objectives of this study was to determine the ionization constants of meta- and para-allyl- and propenylbenzoic acids. These constants were determined in aqueous ethanol solutions of varying ethanol content to study the effect of the composition of the solvent medium on ionization constants, relative acid strength, solvent-solute interaction, and the free energy of ionization. Data from this and other investigations were used to examine the validity of existing relationships between the dielectric constant of the solvent and ionization constants, and to calculate ion size-parameters.

Another aim of this study was to obtain accurate values for the substituent constants of the Hammett equation for allyl ($-CH_2-CH=CH_2$) and propenyl ($-CH=CH-CH_3$) groups. These constants may be very valuable in predicting rate or equilibrium parameters such as chelate stability constants of aromatic compounds containing allyl or propenyl groups. The results of this and previously published works were also used to calculate the substituent constants of various functional groups in aqueous ethanol solutions.

2. Experimental Procedures

2.1. Materials

The benzoic acid and potassium acid phthalate were standard samples of the National Bureau of Standards.

The allyl- and propenylbenzoic acids were synthesized as previously described [1]. In addition, p-propenylbenzoic acid was prepared by isomerization from p-allylbenzoic acid. To 15 ml of a saturated solution of KOH in 90 percent ethanol, 0.1 g of p-allylbenzoic acid was added in a 50 ml flask. The solution was saturated with argon and refluxed for 48 hr, cooled and neutralized with 6*N* HCl solution. The precipitate was filtered, washed with water, decolorized with activated charcoal, and recrystallized repeatedly from a 30 percent ethanol-water solution. Yield: 0.04 g (40%) of p-propenylbenzoic acid, mp = 215 °C.

* The dental research program at the National Bureau of Standards is carried on in cooperation with the Council on Dental Research of the American Dental Association; the National Institute for Dental Research; the Army Dental Corps; the Dental Sciences Division of the School of Aerospace Medicine, USAF; and the Veterans Administration.

† This paper was presented at the 152d meeting of the American Chemical Society, New York, September 1966.

[1] Figures in brackets indicate the literature references at the end of this paper.

707-984 O-67—3

2.2. Procedures

The thermodynamic ionization constants at 25.0 ± 0.2 °C were determined potentiometrically in an inert atmosphere with a carbonate-free aqueous ethanol solution of sodium hydroxide in the buffer region where the degree of ionization is between 25 percent and 75 percent. Further *p*H values were obtained in the vicinity of the end point. A Radiometer *p*H meter with scale expander was used. Before each titration the instrument was standardized with 0.05 *M* potassium acid phthalate (*p*H = 4.008) and 0.025 *M* $KH_2PO_4 - Na_2HPO_4$ (*p*H = 6.865).

A 40 ml ethanol-water solution of the acid (2 to $4 \times 10^{-3} M$) was used in the titrations with the exception of *p*-propenylbenzoic acid, where 100 ml of a nearly saturated solution was employed.

A slow stream of nitrogen or argon saturated with the solvent used in the titration was passed through the liquid in the reaction vessel for at least 10 min. The inert gas was also passed through the solution before each *p*H reading. All solutions were protected from carbon dioxide contamination by sodium hydroxide-asbestos absorbent. Details of the experimental procedures are given by Brauer, Argentar, and Durany [1]. The precise end point was obtained by plotting $\Delta pH/\Delta$ ml or its reciprocal versus milliliters of NaOH added and taking as the end point the number of milliliters of NaOH at which $\Delta pH/\Delta$ ml is a maximum or Δ ml/Δ *p*H is a minimum [2]. From the law of mass action and assuming (1) the validity of the Debye-Hückel equation, (2) that the activity coefficient of the unchanged, undissociated acid molecule is unity, and (3) that the hydroxyl ion concentration may be neglected, the following equation that was employed to calculate *pK* values can be derived.

$$pK = pH + \log \frac{C_A - ([Na^+] + [H^+])}{[Na^+] - [H^+]} + \frac{A\sqrt{[Na^+] + [H^+]}}{1' + B\sqrt{[Na^+] + [H^+]}} \quad (1)$$

where C_A = [HA] + [A⁻] = total concentration of all acid species,

[HA] = concentration of the undissociated acid, and

[A⁻] = concentration of anion of the acid.

The constants A and B which are dependent on the solvent composition were calculated from the expressions by Bates, Paabo, and Robinson [3] $A = 1.825 \times 10^6 (\epsilon T)^{-3/2}$ and $B = 1.5 \ (78.3/\epsilon)^{1/2}$ where T = absolute temperature and ϵ = dielectric constant of the solvent, obtained by interpolation from the values given by Åkerlof [4]. The calculations were made using the National Bureau of Standards Omnitab program [5].

3. Results and Discussion

3.1. Ionization Constants

The apparent thermodynamic *pK* values of benzoic acid and the substituted benzoic acids in 0 to 64.8 weight percent (0 to 70 volume percent) aqueous ethanol solutions (including the number of runs and the standard error of the mean of the *pK* values) are given in table 1. The *pK* values were corrected for liquid junction potential and medium effect by graphic interpolation of the average values of $\delta = (\bar{E}_j - \log_m \gamma_H)$ from data of Gutbezahl and Grunwald [6] and Bates, Paabo, and Robinson [3] where $\bar{E}_j$ is the liquid junction potential expressed in *p*H units and $_m\gamma_H$, the medium effect, measures the difference in the standard free energy of the proton in water and aqueous ethanol. The estimated standard deviations for *pK* values obtained during one run were about 0.004 *pK* units. With increasing ethanol concentration the *pK* values increase markedly from around 4.2 in water to 6.4 for the 64.8 weight percent ethanol solution. As has been shown by Grunwald [6] $\Delta pK = \log {}_m\gamma_H + \log (\gamma_{A^-}/\gamma_{HA})$ where $_m\gamma_H$, γ_{A^-} and γ_{HA} are the degenerate activity coefficients of the proton, anion, and undissociated acid referred to the infinitely dilute aqueous state. Since ΔpK is a function of both solvent and acid structure and $\log \gamma_H$ is a function of solvent only, $\log \gamma_{A^-}/\gamma_{HA}$ must be a function at least of the acid structure and possibly of the solvent. On increasing the ethanol concentration the nature of the ionization equilibrium is changed, partially because the ethanol-solvated carboxylate moiety differs from the corresponding water-solvated group.

TABLE 1. pK *Values of substituted benzoic acids in aqueous ethanol solution*

Temperature = 25.0 ± 0.2 °C.

Substituent	Weight percent ethanol in solution																			
	0.0				12.2				25.2				44.1				64.8			
	n [a]	$pK_{app.}$	$S/\sqrt{n}$ [b]	$pK_{cor.}$ [c]	n	$pK_{app.}$	$S/\sqrt{n}$	$pK_{cor.}$	n	$pK_{app.}$	$S/\sqrt{n}$	$pK_{cor.}$	n	$pK_{app.}$	$S/\sqrt{n}$	$pK_{cor.}$	n	$pK_{app.}$	$S/\sqrt{n}$	$pK_{cor.}$
Hydrogen	17	4.210	0.002	4.210	14	4.444	0.002	4.46	16	4.918	0.003	4.89	8	5.692	0.004	5.55	15	6.424	0.012	6.21
m-Allyl	9	4.266	.004	4.266	8	4.514	.007	4.53	4	5.035	.010	5.01	5	5.808	.003	5.66	4	6.532	.009	6.32
p-Allyl	9	4.326	.004	4.326	8	4.563	.003	4.58	5	5.061	.007	5.04	3	5.811	.003	5.67	3	6.537	.013	6.32
m-Propenyl	5	4.248	.006	4.248	7	4.485	.007	4.50	4	4.972	.001	4.95	7	5.763	.008	5.62	2	6.478	.008	6.26
p-Propenyl	4	4.487	.003	4.487	3	4.785	.039	4.80	4	5.154	.016	5.13	2	5.854	.014	5.71	6	6.614	.028	6.40

[a] n = number of runs.

[b] Standard error of the mean = $\frac{S}{\sqrt{n}}$.

Estimated standard deviation = $\sqrt{\frac{n\Sigma x^2 - (\Sigma x)^2}{n(n-1)}}$.

[c] $pK_{cor.}$ is corrected for liquid junction potential and the medium effect for hydrogen ion; $pK_{cor.} = pK_{app.} - \delta$.

Figure 1 shows the pK values as a function of the ethanol-water composition. For the *m*- and *p*-allyl- and propenylbenzoic acids, the relative acid strength does not vary with solvent composition and the pK versus ethanol content curves have the same general shape. Ion solvating power is the dominant factor in the dissociation of the acids. Increases in the ion solvating power should favor the creation and concentration of charge [7]. Kilpatrick [8] has pointed out that estimation of acid strength in mixed solvents such as water-ethanol is difficult since two bases are competing for the proton and two solvated protons may be formed. In addition, the solvent dipoles will be oriented differently around the ions and solute molecules. Thus, it is conceivable that a local unmixing of the solvent may occur.

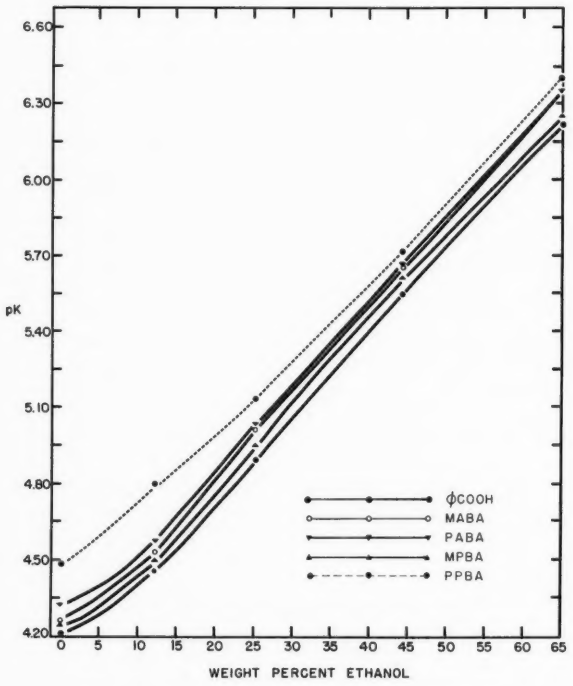

FIGURE 1. *Change of ionization constants of benzoic acid with change in ethanol content of the solvent.*

The change in free energy, ΔG, is likely to be a measure of the relative affinity of ion-solvent interaction arising mainly in the primary solvation zone. The pK values are directly proportional to the free energy change in the ionization reaction at any given temperature. In table 2, ΔG, the change in free energy of ionization for the benzoic acids, calculated from their pK values, are tabulated. The ΔG values increase with the increasing ethanol concentration.

In table 3, the rates of change of pK with change in solvent composition are given. The $\Delta pK/\Delta$ (percent EtOH) increases with ethanol content of the medium

TABLE 2. ΔG *values for the dissociation of substituted benzoic acids in aqueous ethanol solutions*

Temperature = 25.0 ± 0.2 °C

Wt. % Ethanol	ΔG in cal/mole				
	Substituent				
	H	*m*-Allyl	*p*-Allyl	*m*-Propenyl	*p*-Propenyl
0	5740	5820	5900	5790	6120
12.2	6080	6180	6240	6140	6540
25.2	6670	6830	6870	6750	6990
44.1	7570	7720	7730	7660	7790
64.8	8470	8620	8620	8540	8730

TABLE 3. *Rate of change of* pK *values of substituted benzoic acids with change in solvent composition*

Substituent	$(\Delta pK)/\Delta$ (percent EtOH)			
	0–12.2%	12.2–25.2	25.2–44.1	44.1–64.8
Hydrogen	1.92×10^{-2}	3.65×10^{-2}	4.10×10^{-2}	3.54×10^{-2}
m-Allyl	2.03×10^{-2}	4.01×10^{-2}	4.09×10^{-2}	3.50×10^{-2}
p-Allyl	1.94×10^{-2}	3.83×10^{-2}	3.97×10^{-2}	3.57×10^{-2}
m-Propenyl	1.94×10^{-2}	3.75×10^{-2}	4.19×10^{-2}	3.45×10^{-2}
p-Propenyl	2.43×10^{-2}	2.84×10^{-2}	3.70×10^{-2}	3.68×10^{-2}

until a maximum is reached around 40 weight-percent ethanol. This maximum appears to be in the vicinity of the solvent composition where the nature of the interaction of the binary components of the medium may be altered (so that the benzoate ion becomes more soluble in ethanol than in water) as indicated by the change in the slope of the $pK + \log [H_2O]$ versus the reciprocal of the dielectric constant (see next paragraph) and where the differential heats of dilution for ethanol reach a minimum [9].

3.2. Ion Size Parameters

The change of free energy, ΔG, on transfer of ions from one solvent medium to another results from a change in the type of solvation shell. The electrostatic part of the free energy change can be estimated by the Born equation [10], if the ions are treated as spheres of finite radius r immersed in a continuum of uniform dielectric constant ϵ. Plots of pK versus the reciprocal of the dielectric constant are not linear since the Born equation does not take into account the specific interaction between ions and the solvent which must contribute significantly to the nonelectrostatic part of the free energy change. Yasuda [11] showed that linearity of the pK versus $1/\epsilon$ plot is improved for partially aqueous solvents by the addition of a water concentration term to account for the variation of the amount of water in the mixed solvent. With the exception of media containing high concentrations of organic solvents the acids investigated by Yasuda had relatively almost the same dissociation constants in various mixed solvents with the same dielectric constant.

267-984 O-67—4

Shedlovsky [12] assumes that in mixed solvents, such as ethanol-water, on dissolving a weak organic acid the following competitive reactions take place:

$$HA + H_2O \overset{K_1}{\rightleftarrows} HA \cdot H_2O \overset{K_2}{\rightleftarrows} H_3O^+ \cdot A^- \overset{K_3}{\rightleftarrows} H_3O^+ + A^- \tag{2}$$

$$HA + ROH \overset{K_4}{\rightleftarrows} RA \cdot ROH \overset{K_5}{\rightleftarrows} ROH_2^+ \cdot A^- \overset{K_6}{\rightleftarrows} ROH_2^+ + A^- \tag{3}$$

where K_1 to K_6 are the corresponding mass action constants. The overall constants for each solvent are K_H and K_R where

$$K_1K_2K_3 = \frac{[H_3O^+][A^-]f^2}{[HA][H_2O]} = K_H \tag{4}$$

$$K_4K_5K_6 = \frac{[ROH_2^+][A^-]f^2}{[HA][ROH]} = K_R. \tag{5}$$

Assuming that the concentrations of all the electrically neutral species can be taken as their activities and that the last step in the ionic dissociation is controlled by simple coulombic forces, then

$$K_H = B_He^{-b} \tag{6}$$

and

$$K_R = B_Re^{-b} \tag{7}$$

where B_H and B_R are empirical constants; $b = e^2/\epsilon kTa$ in which e is the electronic charge, k is the Boltzmann constant, T is the temperature in degrees K. The parameter, a, may be interpreted as the distance between the centers of charge in the ion-pairs. It can be shown [13] that if $B_H \gg B_R$ and hence $K_H \gg K_R$ then the observed ionization constant is given by the following equation

$$pK + \log [H_2O] + \log B_H = \frac{1}{2.303}\frac{e^2}{kTa}\left(\frac{1}{\epsilon}\right); \tag{8}$$

thus a plot of $pK + \log [H_2O]$ against $1/\epsilon$ should be linear (at least in the water-rich region of solvent composition) and the ion size parameter, a, can be obtained from the slope. For acetic acid in water-ethanol, the linear relationship applies up to nearly 50 weight percent (28 mole percent) ethanol [12].

On plotting $pK + \log [H_2O]$ versus $1/\epsilon$ for the benzoic acids investigated, a nearly linear relationship was obtained from 0 to about 44 weight percent ethanol. The values of a and $-\log B_H$ (the intercept on the ordinate when $1/\epsilon = 0$) and their estimated standard deviations were obtained by the method of least squares and are given in table 4. With the exception of *p*-propenylbenzoic acid, the ion size parameter and the $-\log B_H$ values for the benzoic acids are the same within experimental error. Unexpectedly, the ion size parameter for acetic acid is 2.56 Å [12] which is considerably larger than the values obtained for benzoic acid in this study. It is conceivable that the larger ratio of charge to mass of the acetate ion compared to the benzoate ion may lead to an increase in hydration.

TABLE 4. *Ion size parameters and values of* $-\log B_H$ *for benzoic acids*

Substituent	Ion size parameter		$-\log B_H$	
	Å			
Hydrogen	1.25	0.10 [a]	3.46	0.17 [b]
m-Allyl	1.19	0.07	3.40	0.18
p-Allyl	1.25	0.07	3.57	0.17
m-Propenyl	1.22	0.06	3.43	0.15
p-Propenyl	1.44	0.10	4.10	0.18

[a] Estimated standard deviation calculated from the estimated variance of the slope of the $pK + \log [H_2O]$ against $1/\epsilon$ plot using the method given in reference 22.
[b] Estimated standard deviation calculated from the estimated variance of the intercept using the method given in reference 22.

To check further validity of the $pK + \log [H_2O]$ versus $1/\epsilon$ relationship, literature values of the ionization constant of benzoic acid in aqueous ethanol were collected. The values of Bright and Briscoe [13] were corrected by eq (1) where *p*H was taken as the observed *p*H and the second term was omitted since it was found to be negligible. The value of $[Na^+]$ was 0.01 mol/l and the $[H^+]$ terms were neglected. The volume percent ethanol was converted to weight percent for the pK values of Bright and Briscoe [13] and Tabagua [14]. The values of Grunwald and Berkowitz as given in reference 5 were also plotted in figure 2. The earlier values given in the literature [15, 16] were not used since it was either impossible to calculate the exact weight percentage of ethanol or not enough data were available to calculate the thermodynamic ionization constants. Up to about 44 weight percent ethanol, the thermodynamic pK values of the different investigators are seen to be in quite good agreement despite the fact that in this work and that of Grunwald, glass electrodes were used, whereas Tabagua and Bright and Briscoe employed hydrogen-AgCl and hydrogen-calomel electrodes, respectively. At concentrations exceeding 80 weight-percent alcohol the differences in the pK values are considerable. A possible cause for this discrepancy is that the glass electrode may not always measure hydrogen ion activity accurately at high ethanol concentrations. The nearly linear relationship of $pK + \log [H_2O]$ versus $1/\epsilon$ up to 44 weight-percent ethanol is clearly seen from figure 2. A similar relationship should exist for anisic acid (*p*-methoxybenzoic acid) (also plotted in fig. 2) the pK of which was accurately determined by Sager and Bower [17] and for the eight substituted benzoic acids studied by Bright and Briscoe [13]. The approximately linear relationship up to around 45 weight-percent is not unexpected since the molar concentration of water in this region is always much

larger than that of ethanol. In view of the larger dipole moment of water compared to ethanol, preferential hydration of the substituted benzoate ions should occur and, therefore, their effective diameter should be practically constant over a considerable concentration range. On increasing the ethanol concentration, substitution of water by ethanol in the solvent cloud surrounding the substituted benzoate ion takes place. It would be interesting to determine if a transition from the hydrated ion to an ethanol solvated complex takes place around 45 weight-percent ethanol.

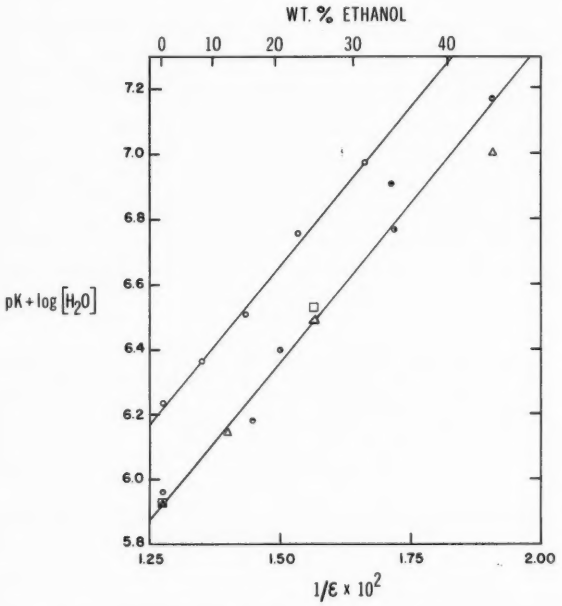

FIGURE 2. *Plot log* pK + *log* [H_2O] *versus* $1/\epsilon$.
Benzoic acid: △ this study, ◑ Grunwald and Berkowitz [6], ◓ Bright and Briscoe [13], ⊡ Tabagua [14]. Anisic acid: ⊙ Sager and Bower [17].

3.3. Hammett Sigma Constants

Among the linear free energy relationships, the equation first proposed by Hammett has been very successful for correlating rate and equilibrium constants. This equation describes the effect of a meta or para substituent on the rate or equilibrium constant of an aromatic side chain reaction provided that the resonance interaction between the substituent and the reaction center is either small or proportional to the polar effects.

For acid dissociation equilibria, the Hammett equation may be written

$$pK_0 - pK = \sigma\rho \tag{9}$$

where pK_0 and pK are the negative logarithms of the ionization constants for the corresponding unsubstituted compound and the meta or para substituted benzene derivative respectively; σ is a substituent constant which is a measure of the ability of the substituent to donate or withdraw electrons; and ρ is the solvent-dependent reaction constant characteristic of the reaction under consideration. The reaction constant ρ has been defined as unity for the acid dissociation equilibrium of benzoic acid in water at 25 °C so that σ can be defined as the difference between the logarithm of the ionization constant in water of the substituted benzoic acid and benzoic acid itself.

Only limited data are available on the change of σ or ρ with solvent. For ethanol-water systems Grunwald and Berkowitz [6] showed that

$$\rho = \rho^w + \beta Y_- \tag{10}$$

where ρ^w is the reaction constant which by definition is 1.000 for benzoic acids and its derivatives in water, Y_- is a solvent-dependent activity function and the parameter $\beta = 0.628$. By interpolation of the data given in reference 6 values at the respective weight concentrations of ethanol were found and the corresponding ρ values were calculated. These ρ values are in reasonably good agreement with other values given in the literature for the ethanol concentrations investigated [18–20].

It is interesting to note that up to 45 percent ethanol content the product of ρ and ϵ is constant within ±2.3 percent. According to Bowden [21]

$$\rho = (A + B/\epsilon)/RT \tag{11}$$

where the constants A and B respectively describe the susceptibility of the reaction to polar effects independent of and dependent on the medium. If A is negligible compared to B/ϵ then ρ is inversely proportional to ϵ. In the 0–45 weight-percent ethanol range where the reaction constant varies inversely with the dielectric constant of the medium any effect caused by preferential solvation of the anion or the undissociated acid by the two solvents appears to be negligible.

Using the calculated ρ values, the σ values of the Hammett equation were obtained and are tabulated in table 5 and plotted in figure 3. With the exception of the *p*-propenylbenzoic acid the σ values do not change greatly with change in ethanol concentration.

TABLE 5. *Hammett sigma constants*

Ethanol concentration	ρ [a]	Sigma constant							
		m-Allyl		*p*-Allyl		*m*-Propenyl		*p*-Propenyl	
Wt %									
0	1.000	−0.056	0.004 [b]	−0.116	0.004 [b]	−0.038	0.006 [b]	−0.277	0.023 [b]
12.2	1.128	−.062	.006	−.105	.003	−.036	.006	−.302	.035
25.2	1.266	−.092	.008	−.113	.006	−.043	.002	−.187	.013
44.1	1.465	−.079	.003	−.081	.003	−.048	.006	−.111	.009
64.8	1.578	−.068	.010	−.072	.011	−.034	.009	−.121	.019

[a] Calculated from $\rho = 1.000 + 0.628\ Y_-$, where Y_-, which is a characteristic parameter of carboxylate-carboxylic acid equilibria, was obtained by interpolation of the values given by Grunwald and Berkowitz [6].

[b] Standard error of the mean $\frac{\sqrt{S^2_{pK_H} + S^2_{pK_X}}}{\rho}$ where $S_{\overline{pK}_H}$ is the standard error of the mean for benzoic acid and $S_{\overline{pK}_X}$ is the corresponding value for the substituted benzoic acid.

It is possible that the solvation shell surrounding the *p*-propenylbenzoic acid differs from that of the other benzoic acids.

To check further the effect of solvent composition on σ the corrected *pK* values of Bright and Briscoe [13] and ρ constants obtained by the equation given by Grunwald and Berkowitz [6] were used to calculate σ for ten substituents. These data including the estimated standard deviation of the σ values for all ethanol concentrations are given in table 6. Only for the NH_2, OH and NO_2 groups, where the electron distribution is altered because of solvation of the substituent is the substituent constant markedly dependent on solvent. For these substituents, the dependence of σ on solvent is of the same order of magnitude as that found for the *p*-propenyl group in this study.

The ionization constants for benzoic acids are recommeded for calculating primary Hammett substituent constants [19]. This is especially true for the *p*-propenyl group since *p*-propenylphenol is not very stable in basic media. A comparison of the secondary σ constants determined previously from the *pK* values in water of guaiacol and substituted guaiacols [1], and the primary constants obtained from the respective benzoic acids are given in table 7. These values for the allyl groups agree within ± 0.02. For the *m*-propenyl group the σ constant decreases by 0.08 when benzoic acids are used instead of guaiacols. The greatest change in σ occurs for the *p*-propenyl group (σ values are 0.05 and -0.28 as calculated from the *pK*'s of guaiacols and benzoic acids, respectively). This difference may be explained by noting that in *p*-propenylguaiacols the propenyl group is in direct conjugation with the acidic OH while in the corresponding benzoic acid any resonance effect of the propenyl group would likely be transmitted to the para carbon atom of the ring and the acidic OH group by induction.

TABLE 6. *Sigma constants for various substituents* [a]

Wt % ETOH	ρ	Sigma constants									
		m-CH_3	*p*-CH_3	*m*-NH_2	*p*-NH_2	*m*-OH	*p*-OH	*m*-Cl	*p*-Cl	*m*-NO_2 [b]	*p*-NO_2 [b]
0	1.00	−0.07	−0.19	−0.61	−0.74	0.14	−0.32	0.37	0.14	0.72	0.78
16.5	1.17	−0.12	−0.31	−0.42	−0.64	−0.05	−0.42	.....	.....	.....	.....
34.4	1.36	−0.04	−0.11	−0.13	−0.55	0.05	−0.30	0.38	.....	1.13	1.04
44.1	1.46	−0.05	−0.11	−0.13	−0.54	0.02	−0.29	0.36	0.30	0.77	0.88
64.8	1.58	−0.10	−0.08	−0.18	−0.60	−0.08	−0.35	0.33	0.27	0.75	0.85
75.9	1.60	−0.09	−0.08	.....	−0.62	−0.08	−0.39	0.34	0.30	0.71	0.81
87.7	1.61	−0.14	−0.11	.....	−0.66	−0.12	−0.47	0.33	0.26	0.67	0.77
93.7	1.62	.....	.....	.....	.....	.....	.....	.....	.....	0.82	0.90
100*	1.63	−0.14	−0.14	.....	−0.66	−0.13	−0.48	0.34	0.28	0.86	0.96
Average ...		−0.09	−0.14	−0.29	−0.63	−0.03	−0.38	0.35	0.26	0.80	0.87
Estimated standard deviation.		0.04	0.08	0.21	0.06	0.09	0.07	0.02	0.06	0.15	0.09

[a] From extrapolated *pK* values.
[b] Uncorrected *pK* values using quinhydrone electrode for benzoic acid and substitued benzoic acids.
[c] Calculated from Bright and Briscoe [13].

TABLE 7. *Sigma values of allyl and propenyl groups in water*

Substituent	Sigma	
	Primary [a]	Secondary [b]
m-Allyl	−0.056	−0.02
p-Allyl	−.116	−.10
m-Propenyl	−.038	+.04
p-Propenyl	−.277	+.05

[a] From benzoic acids.
[b] From guaiacols.

4. Summary

The thermodynamic *pK* values of allyl- and propenylbenzoic acids in aqueous ethanol increase with increasing ethanol content the *pK* values are dependent on the dielectric constant of the medium. For mixed solvents up to 44 percent water an approximately linear relationship between $pK + \log [H_2O]$ and the reciprocal of the dielectric constant exists. The Hammett substituent constant, σ for the *m*- and *p*-allyl and *m*-propenyl groups do not vary greatly with composition of the solvent. However, for the *p*-propenyl group the σ constant is affected by the medium.

The authors thank Robert A. Robinson for his valuable suggestions and Mrs. Ruth Davenport for the computer programing.

5. References

[1] G. M. Brauer, H. Argentar, and G. Durany, J. Res. NBS **68A** (Phys. and Chem.) No. 6, 619 (1964).
[2] G. Gran, Acta Chem. Scand. **4,** 559 (1950).
[3] R. G. Bates, M. Paabo, and R. A. Robinson, J. Phys. Chem. **67,** 1833 (1963).
[4] G. Åkerlöf, J. Am. Chem. Soc. **54,** 4125 (1932).
[5] J. Hilsenrath, G. G. Ziegler, C. G. Messina, P. J. Walsh, and R. J. Herbold, Omnitab. A Computer Program for Statistics and Numerical Analysis, NBS Handbook 101 (U.S. Government Printing Office, Washington, D.C., 1966).
[6] E. Grunwald and B. J. Berkowitz, J. Am. Chem. Soc. **73,** 4939 (1951); B. Gutbezahl and E. Grunwald, J. Am. Chem. Soc. **75,** 565 (1953).
[7] E. D. Hughes and C. K. Ingold, J. Chem. Soc. **1935,** 244.
[8] M. Kilpatrick, Chem. Rev. **30,** 159 (1942).
[9] G. L. Bertrand, F. J. Millero, C. Wu, and L. G. Hepler, J. Phys. Chem. **70,** 699 (1966).
[10] M. Born, Z. Physik **1,** 45 (1920).
[11] M. Yasuda, Bull. Chem. Soc. Japan **32,** 429 (1959).
[12] T. Shedlovsky, in Pesce, B. Ed., Symposium on Electrolytes, p. 146, Trieste 1959 (Pergamon Press, New York, 1962).
[13] W. L. Bright and H. T. Briscoe, J. Phys. Chem. **37,** 787 (1933).
[14] I. D. Tabagua, Russ. J. Phys. Chem. **37,** 828 (1963).
[15] J. O. Halford, J. Am. Chem. Soc. **55,** 2272 (1933).
[16] L. Michaelis and M. Mizutami, Z. Phys. Chem. **116,** 134 (1925).
[17] E. E. Sager and V. E. Bower, J. Res. NBS **64A** (Phys. and Chem.) No. 4, 351 (1960).
[18] H. H. Jaffé, Chem. Rev. **53,** 191 (1953).
[19] D. H. McDaniel and H. C. Brown, J. Org. Chem. **23,** 420 (1958).
[20] H. Van Bekkum, P. E. Verkade, and B. M. Wepster, Rec. trav. chim. **78,** 815 (1959).
[21] K. Bowden, Can. J. Chem. **41,** 2781 (1963).
[22] M. G. Natrella, Experimental Statistics, NBS Handbook **91,** pp. 5–10 (U.S. Government Printing Office, Washington, D.C., 1963).

(Paper 71A5–467)

JOURNAL OF RESEARCH of the National Bureau of Standards—A. Physics and Chemistry
Vol. 71A, No. 5, September–October 1967

Dissociation Constants of Some Substituted Nitrophenols in Aqueous Solution at 25 °C

R. A. Robinson

Institute for Materials Research, National Bureau of Standards, Washington, D.C. 20234

(May 9, 1967)

The dissociation constants of twelve substituted phenols with a nitro group in the *o*- or *p*-position have been determined by spectrophotometric measurements in aqueous solution at 25 °C.

Key Words: Dissociation constant, nitrophenols, substituted phenols.

1. Introduction

The determination of the dissociation constants of a number of substituted phenols by the spectrophotometric method has been described recently [1, 2, 3, 4, 5, 6, 7].[1] The purpose of this paper is to present data for twelve substituted phenols with an indicator range *p*H 2.1–5.5.

2. Experimental Procedure

2.1. Materials

With the exception of 2,6-diiodo-4-nitrophenol, the materials were commercial products. I am indebted to Dr. Marion M. Davis for the following details of their purification.

2-Chloro-4, 6-dinitrophenol was recrystallized twice from benzene-cyclohexane, mp 111.0–111.5 °C. 4-Chloro-2,6-dinitro-3-methylphenol was recrystallized once from benzene-cyclohexane and then from ligroin, mp 68.0–68.5 °C; 2-chloro-6-nitrophenol first from 95 percent ethanol and then from benzene-cyclohexane, mp 70.0–70.5 °C. 2,4-Dibromo-6-nitrophenol was purified in the same way, mp 117.0–117.5 °C. 2,6-Dibromo-4-nitrophenol was recrystallized three times from benzene-cyclohexane, then from aqueous ethanol and then from benzene-cyclohexane, mp 141.8–142.0 °C, 2,6-dichloro-4-nitrophenol twice from benzene-cyclohexane, mp 125 °C (dec.). 2,6-Diiodo-4-nitrophenol was synthesized by the method of Datta and Prosad [8] by adding *p*-nitrophenol in an excess of ammonia to a solution of iodine in aqueous potassium iodide, recrystallized from aqueous ethanol and then from benzene-cyclohexane, mp 156.5–157.0 °C. 2,4-Dinitro-6-methylphenol was recrystallized twice from benzene-cyclohexane mp 86.0–86.7 °C; 2,6-dinitro-4-methylphenol from benzene-cyclohexane and then from cyclohexane, mp 80.7–81.2 °C; 2,4-dinitro-3-methyl-6-*iso*propylphenol from aqueous ethanol and then from ligroin, mp 55.0–55.7 °C. 2,4-Dinitro-6-phenylphenol recrystallized from methyl ethyl ketone and then from ethyl acetate, mp 206.6–207.0 °C; 2,4-dinitro-6-*iso*propylphenol from 95 percent ethanol and then from hexane, mp 54.0–55.0 °C.

Table 1 gives some characteristics of the absorption spectra of these compounds, recording the wavelengths and extinction coefficients at maximum absorption in both acid and alkaline solution, and also those at the isosbestic points. Figure 1 shows the absorption spectrum of one of these phenols, 4-chloro-2,6-dinitro-3-methylphenol, in alkaline solution where the phenol is present in the form of the phenolate anion, in strongly acid solution where it exists as the undissociated molecule, and in a dilute solution of hydrochloric acid were both species are present; the isosbestic point is at 378 mμ with an extinction coefficient $\epsilon = 2{,}740$.

TABLE 1. *Characteristics of the absorption spectra of substituted phenols in aqueous solution at 25 °C.*

	Alkaline solution ϵ_2 mμ	Acid solution ϵ_1 mμ	Isosbestic point ϵ mμ
2-Chloro-4,6-dinitrophenol	14,910 370	10,100 268	4,250 326
4-Chloro-2,6-dinitro-3-methylphenol	5,660 425	3,950 355	2,740 378
2-Chloro-6-nitrophenol	4,580 420	2,620 350	2,200 372
2,4-Dibromo-6-nitrophenol	4,180 430	2,370 365	2,110 383
2,6-Dibromo-4-nitrophenol	15,720 402	7,650 312	3,900 344
2,6-Dichloro-4-nitrophenol	13,850 399	7,020 312	3,500 343
2,6-Diiodo-4-nitrophenol	15,620 409	6,550 318	3,570 351
2,4-Dinitro-6-methylphenol	14,210 377	13,630 272	5,330 333
2,6-Dinitro-4-methylphenol	7,250 450	5,100 365	2,390 393
2,4-Dinitro-3-methyl-6-*iso*propylphenol	14,630 396	5,500 300	3,900 335
2,4-Dinitro-6-phenylphenol	14,990 380	8,290 265	4,280 334
2,4-Dinitro-6-*iso*propylphenol	13,400 375	5,680 265	5,220 335

[1] Figures in brackets indicate the literature references at the end of this paper.

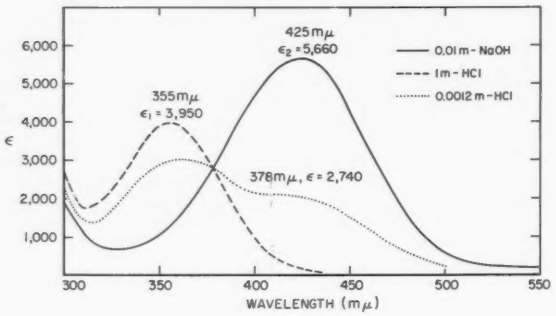

FIGURE 1. *Absorption spectra of 4-chloro-2,6-dinitro-3-methylphenol.*

2.2. Method

The spectrophotometric method of determining the dissociation constant of a weak acid has been described many times [1, 2, 3, 4, 5, 6, 7]. For the five phenols with *pK* values less than 3.5, dilute solutions of hydrochloric acid were found to be suitable media in which to make measurements; for the other seven, with *pK* values greater than 3.8, succinate buffers were used. In some cases a small correction was needed for the effect of the phenol on the acidity of the buffer solution; this correction has already been described [9].

3. Results and Discussion

Details of the spectrophotometric measurements are given in tables 2 to 13. The results are summarized in table 14.

It is known that ortho and para substitution of a nitro group in phenol have effects which are by no means additive. Thus, if the *pK* value of phenol itself is 9.99_8 [10], that of *o*-nitrophenol 7.23_0 [11], and that of *p*-nitrophenol 7.15_6 [12], then *o*- and *p*-nitro substitution lowers the *pK* value of phenol by 2.76_8 and 2.84_2, respectively. We might, therefore, expect $pK = (9.99_8 - 2.76_8 - 2.84_2) = 4.38_8$ for 2,4-dinitrophenol, whereas

TABLE 2. *Dissociation constant of 2-chloro-4,6-dinitrophenol in aqueous solution at 25 °C*

Concentration of phenol: 1.18×10^{-5} M, cell length 4 cm, wavelength 372 mμ, D_1 0.073, D_2 0.660

$m_{HCl} \times 10^3$	D	$m_{H^+} \times 10^3$	$-2 \log \gamma$	pK
2.210	0.542	2.221	0.046	2.100
3.206	.508	3.216	.054	2.090
4.967	.454	4.976	.065	2.101
7.389	.403	7.397	.081	2.103
10.05	.359	10.06	.089	2.108
Average				2.10_0

TABLE 3. *Dissociation constant of 4-chloro-2,6-dinitro-3-methylphenol in aqueous solution at 25 °C*

Concentration of phenol: 2.6×10^{-5} M, cell length 4 cm, wavelength 425 mμ, D_1 0.012, D_2 0.583

$m_{HCl} \times 10^4$	D	$m_{H^+} \times 10^4$	$-2 \log \gamma$	pK
2.192	0.420	2.378	0.016	3.241
6.048	.293	6.176	.025	3.248
8.084	.257	8.196	.029	3.239
10.28	.228	10.38	.032	3.232
12.06	.205	12.15	.034	3.241
Average				3.24_0

TABLE 4. *Dissociation constant of 2-chloro-6-nitrophenol in aqueous solution at 25 °C*

Concentration of phenol: 3×10^{-5} M, cell length 4 cm, wavelength 430 mμ, D_1 0.014, D_2 0.538
Buffer solution: Sodium hydrogen succinate and disodium succinate, each at molality *m*

m	D	$p(a_H\gamma_{Cl})$	pK	pK (corr.)
0.0100	0.294	5.553	5.493	5.491
.0175	.290	5.532	5.485	5.483
.0250	.285	5.511	5.481	5.480
.0375	.281	5.499	5.482	5.481
.0500	.274	5.477	5.483	5.483
Average				5.48_3

TABLE 5. *Dissociation constant of 2,4-dibromo-6-nitrophenol in aqueous solution at 25 °C*

Concentration of phenol: 4.5×10^{-5} M, cell length 4 cm, wavelength 430 mμ, D_1 0.067, D_2 0.757
Buffer solution: sodium hydrogen succinate and sodium chloride, each at molality *m*

m	D	$p(a_H\gamma_{Cl})$	pK	pK (corr.)
0.02	0.467	4.853	4.713	4.712
.04	.461	4.833	4.709	4.708
.06	.458	4.821	4.704	4.704
.08	.454	4.811	4.705	4.705
.10	.449	4.802	4.709	4.709
Average				4.70_8

TABLE 6. *Dissociation constant of 2,6-dibromo-4-nitrophenol in aqueous solution at 25 °C*

Concentration of phenol: 2.05×10^{-5} M, cell length 4 cm, wavelength 402 mμ, D_1 0.005, D_2 1.274

$m_{HCl} \times 10^4$	D	$m_{H^+} \times 10^4$	$-2 \log \gamma$	pK
2.013	0.855	2.150	0.015	3.376
3.106	.726	3.222	.018	3.391
4.018	.649	4.122	.020	3.392
4.980	.584	5.073	.023	3.394
6.057	.527	6.141	.025	3.393
6.999	.482	7.076	.027	3.397
8.015	.447	8.086	.028	3.392
9.003	.415	9.069	.030	3.393
9.996	.385	10.06	.031	3.397
Average				3.39_2

TABLE 7. *Dissociation constant of 2,6-dichloro-4-nitrophenol in aqueous solution at 25 °C*

Concentration of phenol: 2.4×10^{-5} M, cell length 4 cm, wavelength 400 mμ, D_1 0.002, D_2 1.340

$m_{HCl} \times 10^4$	D	$m_{H^+} \times 10^4$	$-2 \log \gamma$	pK
1.987	0.792	2.129	0.015	3.528
2.989	.655	3.106	.018	3.547
4.033	.562	4.133	.020	3.548
5.008	.497	5.097	.023	3.547
6.314	.426	6.390	.025	3.553
6.583	.415	6.657	.026	3.553
7.786	.370	7.852	.028	3.554
8.773	.340	8.834	.030	3.555
9.973	.308	10.03	.031	3.558
Average				3.54_9

TABLE 8. *Dissociation constant of 2,6-diiodo-4-nitrophenol in aqueous solution at 25 °C*

Concentration of phenol: 2.5×10^{-5} M, cell length 4 cm, wavelength 409 mμ. D_1 0.005, D_2 1.540

$m_{HCl} \times 10^4$	D	$m_{H^+} \times 10^4$	$-2 \log \gamma$	pK
2.019	1.065	2.192	0.015	3.324
2.975	0.946	3.128	.018	3.323
3.861	.864	4.001	.020	3.314
4.144	.823	4.277	.020	3.332
4.965	.764	5.089	.023	3.326
6.063	.691	6.175	.025	3.327
7.791	.614	7.890	.028	3.313
8.959	.557	9.059	.030	3.324
9.984	.513	10.07	.032	3.335
Average				3.32_4

TABLE 9. *Dissociation constant of 2,4-dinitro-6-methylphenol in aqueous solution at 25 °C*

Concentration of phenol: 8.3×10^{-5} M, cell length 1 cm, wavelength 400 mμ, D_1 0.028, D_2 0.969

Buffer solution: sodium hydrogen succinate and sodium chloride each at molality m

m	D	$p(a_H\gamma_{Cl})$	pK	pK (corr.)
0.02	0.691	4.853	4.476	4.471
.03	.688	4.840	4.469	4.466
.05	.680	4.826	4.473	4.471
.07	.675	4.816	4.474	4.473
.10	.669	4.802	4.472	4.471
Average				4.47_0

TABLE 10. *Dissociation constant of 2,6-dinitro-4-methylphenol in aqueous solution at 25 °C*

Concentration of phenol: 2.25×10^{-5} M, cell length 4 cm, wavelength 450 mμ, D_1 0, D_2 0.650

Buffer solution: mixture of sodium hydrogen succinate (m) and hydrochloric acid ($0.6667m$) equivalent to a mixture of sodium hydrogen succinate ($0.3333m$), succinic acid ($0.6667m$), and sodium chloride ($0.6667m$)

m	D	$p(a_H\gamma_{Cl})$	pK [a]
0.02	0.206	3.898	4.232
.04	.203	3.887	4.230
.06	.202	3.882	4.228
.08	.199	3.878	4.233
.10	.199	3.875	4.230
Average			4.23_1

[a] The correction to pK is negligible.

the observed value is 4.09 [13]. In the same way, $pK = 4.46_2$ might be predicted for 2,6-dinitrophenol, compared with the observed value of 3.71 [14].

An additivity principle works much better with meta substitution; $pK = 8.35_5$ has been found [15] for *m*-nitrophenol and hence one would predict pK 6.71 for 3,5-dinitrophenol, compared with the observed value of 6.69 [1].

The substitution of a methyl group in the para position to give *p*-cresol *raises* the pK value of phenol by 0.26_4 [16]; $pK = 7.49_4$ might be predicted for 4-methyl-2-nitrophenol compared with the observed value of 7.59_7 [6]. The difference between the observed and calculated value is not large, but the

observed value is higher than the calculated, whereas for the dinitrophenols mentioned above the observed value was lower than the calculated. A quantitative explanation of this anomaly, the difference between the observed and calculated *pK* values, is not yet possible, but the change in sign of the difference in going from 4-methyl-2-nitrophenol to 2,4- or 2,6-dinitrophenol suggests that the anomaly increases with a decrease in the *pK* value of the phenol into which an *o*- or *p*-nitro group is introduced.

TABLE 11. *Dissociation constant of 2,4-dinitro-3-methyl-6-isopropylphenol in aqueous solution at 25 °C*

Concentration of phenol: 1.09×10^{-4} M, cell length 1 cm, wavelength 396 mμ, D_1 0.032, D_2 1.594

Buffer solution: mixture of sodium hydrogen succinate (m) and hydrochloric acid (0.6667m) equivalent to a mixture of sodium hydrogen succinate (0.3333m), succinic acid (0.6667m), and sodium chloride (0.6667m)

m	D	$p(a_H\gamma_{Cl})$	pK	pK (corr.)
0.02	0.758	3.898	3.959	3.954
.03	.752	3.892	3.960	3.957
.04	.749	3.887	3.958	3.955
.05	.746	3.884	3.959	3.957
.06	.743	3.882	3.961	3.959
.08	.738	3.878	3.961	3.960
.10	.735	3.875	3.962	3.961

Average..... 3.95_8

TABLE 12. *Dissociation constant of 2,4-dinitro-6-phenylphenol in aqueous solution at 25 °C*

Concentration of phenol: 1.79×10^{-5} M, cell length 4 cm, wavelength 380 mμ, D_1 0.142, D_2 1.070

Buffer solution: mixture of sodium hydrogen succinate (m) and hydrochloric acid (0.6667m) equivalent to a mixture of sodium hydrogen succinate (0.3333m), succinic acid (0.6667m), and sodium chloride (0.6667m).

m	D	$p(a_H\gamma_{Cl})$	pK	pK (corr.)
0.01	0.634	3.906	3.854	3.852
.02	.629	3.898	3.855	3.851
.03	.627	3.892	3.853	3.852
.04	.626	3.887	3.850	3.849
.05	.628	3.884	3.843	3.843
.06	.627	3.882	3.843	3.843
.07	.627	3.880	3.841	3.841
.08	.620	3.878	3.852	3.852
.09	.620	3.877	3.851	3.851

Average..... 3.84_8

TABLE 13. *Dissociation constant of 2,4-dinitro-6-isopropylphenol in aqueous solution at 25 °C*

Concentration of phenol: 9.6×10^{-5} M, cell length 1 cm, wavelength 400 mμ D_1 0.029, D_2 0.791

Buffer solution: sodium hydrogen succinate and sodium chloride each at molality m.

m	D	$p(a_H\gamma_{Cl})$	pK	pK (corr.)
0.02	0.541	4.853	4.542	4.536
.03	.539	4.840	4.534	4.530
.05	.529	4.826	4.545	4.543
.07	.528	4.816	4.538	4.536
.10	.524	4.802	4.534	4.533

Average..... 4.53_6

TABLE 14. *Summary of the* pK *values of substituted phenols in aqueous solution at 25 °C*

	pK
2-Chloro-4,6-dinitrophenol	2.10_0
4-Chloro-2,6-dinitro-3-methylphenol	3.24_0
2-Chloro-6-nitrophenol	5.48_3
2,4-Dibromo-6-nitrophenol	4.70_8
2,6-Dibromo-4-nitrophenol	3.39_2
2,6-Dichloro-4-nitrophenol	3.54_9
2,6-Diiodo-4-nitrophenol	3.32_4
2,4-Dinitro-6-methylphenol	4.47_0
2,6-Dinitro-4-methylphenol	4.23_1
2,4-Dinitro-3-methyl-6-*iso*propylphenol	3.95_8
2,4-Dinitro-6-phenylphenol	3.84_8
2,4-Dinitro-6-*iso*propylphenol	4.53_6

The available literature values have been used to study this possibility. Data are available for *p*-nitro substitution in the following compounds, *pK* values being known for the phenols before and after substitution:

Parent phenols	*pK* Parent phenols	*pK* Nitro derivatives		Differences
		Predicted	Observed	
o-Chlorophenol	8.53_4 [10]	5.69_2	5.45 [17]	0.24
o-Nitrophenol	7.23_0 [11]	4.38_8	4.09 [13]	0.30
2,6-Dichlorophenol	6.79_1 [4]	3.94_9	3.54_9	0.40
2,6-Dibromophenol	6.67_4 [7]	3.83_2	3.39_2	0.44
2-Chloro-6-nitrophenol	5.48_3	2.64_1	2.10_0	0.54
2,6-Dinitrophenol	3.71 [14]	0.87	0.33 [18]	0.54

Thus, *o*-chlorophenol, with a *pK* value of 8.53_4, can be converted to 2-chloro-4-nitrophenol, whose predicted *pK* value (pK 5.69_2) is 2.84_2 lower, the observed value being 5.45 and the anomaly 0.24. The absence of a literature reference in the above table means that the datum was taken from the present paper.

For *o*-nitro substitution the following data have been found, assuming 2.76_8 for the effect of the nitro group:

Parent phenols	*pK* parent phenols	*pK* nitro derivatives		Differences
		Predicted	Observed	
p-Cresol	10.26_2 [16]	7.49_4	7.59_7 [6]	−0.10
p-Chlorophenol	9.41_8 [10]	4.38_8	4.09 [13]	0.30
o-Chlorophenol	8.53_4 [11]	5.77_6	5.48_5	0.29
2,4-Dibromophenol	7.79_0 [7]	5.02_2	4.70_8	0.31
o-Nitrophenol	7.23_0 [11]	4.46_2	3.71 [14]	0.75
p-Nitrophenol	7.15_6 [12]	4.38_8	4.09 [13]	0.30
4-Chloro-2-nitrophenol	6.46 [17]	3.69	2.96_9 [5]	0.72
2-Chloro-4-nitrophenol	5.45 [17]	2.68	2.10_6	0.58
2,4-Dinitrophenol	4.09 [13]	1.32	0.33 [18]	0.99

These anomalies, ($\Delta pK = pK_{calcd.} - pK_{obsd.}$), are plotted in figure 2 against the *pK* value of the phenol into which the nitro group is introduced. It can be seen that, in general, the anomaly increases in magnitude as the acid strength of the phenol increases (*pK* decreases). For *p*-nitro substitution, the value for the formation of picric acid from 2,6-dinitrophenol seems somewhat small.

For *o*-nitro substitution, the anomaly seems to be uniformly greater as the *pK* value of the phenol decreases but there are three peculiar cases, the formation of 2,6-dinitrophenol from *o*-nitrophenol, that of 4-chloro-2,6-dinitrophenol from 4-chloro-2-nitrophenol, and that of picric acid from 2,4-dinitrophenol. In each case the anomaly seems to be somewhat large. It should be noted that in each case the synthetic process is one in which an *o*-nitrophenol is converted into a 2,6-dinitrophenol, each of which has adjacent NO_2-OH-NO_2 groups. In such cases marked steric inhibition of resonance would be expected.

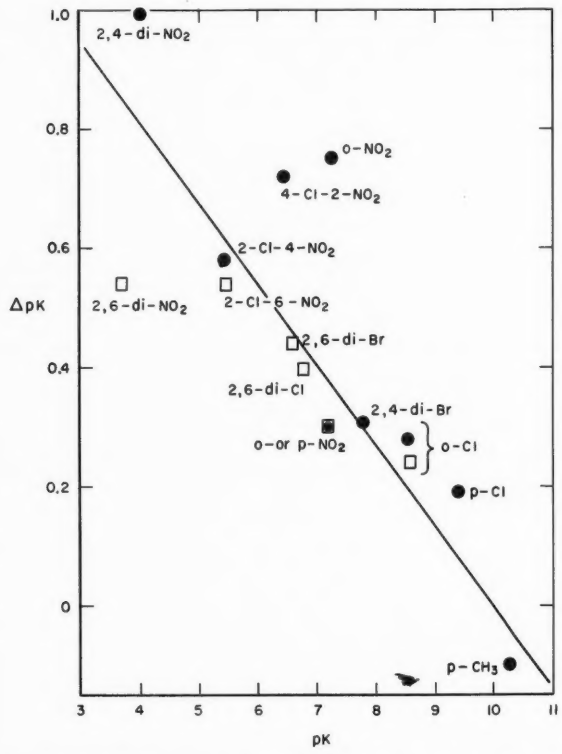

FIGURE 2. $\Delta pK = pK$ (*calcd.*) $- pK$ (*obsd.*), *where* pK (*calcd.*) *is derived on the assumption that (1) o-nitration of a substituted phenol lowers the* pK *value by* 2.76_8, *identical with the lowering of* pK *found for the o-nitration of phenol itself; (2) p-nitration of a substituted phenol lowers the* pK *value by* 2.84_2, *identical with the lowering of* pK *found for the p-nitration of phenol itself.*

The lettering within the figure indicates the structure of the parent substituted phenol which undergoes *o*-nitration (●) or *p*-nitration (□). The abscissa gives the *pK* value of the parent phenol.

My sincere thanks are expressed to Dr. Marion M. Davis for providing the purified chemicals used in this work.

4. References

[1] R. A. Robinson, M. M. Davis, M. Paabo, and V. E. Bower, J. Res. NBS **64A**, (Phys. and Chem.) No. 4, 347 (1960).
[2] M. M. Davis, M. Paabo, and R. A. Robinson, J. Res. NBS **64A**, (Phys. and Chem.) No. 6, 531 (1960).
[3] M. M. Davis and M. Paabo, J. Res. NBS **64A**, (Phys. and Chem.) No. 6, 533 (1960).
[4] R. A. Robinson, J. Res. NBS **68A** (Phys. and Chem.) No. 2, 159 (1964).
[5] E. E. Sager, R. A. Robinson, and R. G. Bates, J. Res. NBS **68A** (Phys. and Chem.) No. 3, 305 (1964).
[6] R. A. Robinson and R. G. Bates, J. Res. NBS **70A** (Phys. and Chem.) No. 6, 553 (1966).
[7] R. A. Robinson, J. Res. NBS **71A** (Phys. and Chem.) No. 3, 217–222 (1967).
[8] R. L. Datta and N. Prosad, J. Am. Chem. Soc. **39**, 441 (1917).
[9] R. A. Robinson and A. K. Kiang, Trans. Faraday Soc. **51**, 1398 (1955).
[10] A. I. Biggs and R. A. Robinson, J. Chem. Soc. (London) 388 (1961).
[11] R. A. Robinson and A. Peiperl, J. Phys. Chem. **67**, 1723 (1963).
[12] G. F. Allen, R. A. Robinson, and V. E. Bower, J. Phys. Chem. 66, 171 (1962).
[13] H. von Halban and G. Kortüm, Z. physik. Chem. **A170**, 351 (1934).
[14] G. Kortüm and H. Wilski, Z. physik. Chem. **2**, 256 (1954).
[15] R. A. Robinson and A. Peiperl, J. Phys. Chem. **67**, 2860 (1963).
[16] A. I. Biggs, Trans. Faraday Soc. **52**, 35 (1956).
[17] V. E. Bower and R. A. Robinson, J. Phys. Chem. **64**, 1078 (1960).
[18] M. M. Davis and M. Paabo, J. Res. NBS **67A** (Phys. and Chem.) No. 3, 241 (1963).

(Paper 71A5–469)

JOURNAL OF RESEARCH of the National Bureau of Standards—A. Physics and Chemistry
Vol. 71A, No. 5, September–October 1967

Publications of the National Bureau of Standards*

Selected Abstracts

Procedure for high precision density determinations by hydrostatic weighing, H. A. Bowman and R. M. Schoonover *with Appendix by* M. W. Jones, *J. Res. NBS* **71C3** (*Engr. and Instr.*), *No. 3, 179–198 (July–Sept. 1967).*

There are several simplifications which can be made in the performance of the hydrostatic experiment which lead to more reproducible results. The operation of single-pan two-knife balances is discussed, and simple modifications suggested to adapt it to hydrostatic work. A data philosophy is presented which will be particularly applicable to a generation of now-developing force measuring instruments when used in hydrostatic work. A simplified formula for air density is presented and a formula for estimating day-to-day variability in the density of water. A simple balance calibration procedure is presented in an appendix, and simplified methods of fabricating suspension wires and degassing sample surfaces are described. The use of these techniques is illustrated by measurements on silicon crystals which indicate process reproducibility of a standard deviation of about one part per million.

Key Words: Air density, balance, balance calibration, balance equilibrium, balance sensitivity, density, double substitution weighing, hydrostatic balance, hydrostatic weighing, silicon density, substitution balance, volumetric measurement, water density, water weighing.

Torsion creep of circular and noncircular tubes, L. Mordfin, *J. Res. NBS* **71C3** (*Engr. and Instr.*), *No. 3, 209–225 (July–Sept. 1967).*

A torsion creep theory for noncircular tubes was developed by applying a multiaxial creep theory to a derived generalization of Bredt's equations.

A review of the literature revealed no torsion creep data on noncircular tubes. Hence, to evaluate the theory, a test program was carried out on twelve specimens of aluminum alloy structural tubing, of four configurations, at 400 °F.

Observed discrepancies between the torsion creep theory and experiment are smaller than variations in the measured creep properties of the specimen material from one tube configuration to another and are not appreciably greater than discrepancies between elastic torsion theory and experiment. Most of the observed discrepancies are consistent with measured anisotropy in the tubes, while other discrepancies are ascribed to nonhomogeneity in creep properties and a hydrostatic stress effect in multiaxial creep. For the calculation of torsion stresses in circular tubes the thin-wall approximation is adequate for thickness-to-radius ratios up to one-tenth. For straight-sided tubes equivalent accuracy is obtained for effective ratios up to only one-twentieth. These criteria apply to creep conditions as well as to elastic conditions.

Key Words: Creep, primary creep, shear, shell, stress analysis, thin wall, torsion, tube.

Digitized low-frequency phasemeter assembled from logic modules, J. E. McKinney, *J. Res. NBS* **71C3** (*Engr. and Instr.*), *No. 3, 227–238 (July–Sept. 1967).*

A digital phasemeter is described which is capable of operating from arbitrarily low frequencies to 10 kHz, for which the lower limit depends essentially upon the time available to the operator to make the measurement. The phasemeter involves a logic circuit which can be assembled easily from commercially available logic modules without the necessity of a proficiency in electronics. The output of the logic circuit is read into a conventional digital preset frequency-ratio meter. The determination is absolute and utilizes a time base. Accordingly, no calibration against a phase standard is necessary. The agreement between this phasemeter and a quality phase shifter was found to be within $\pm .01°$ at 400 Hz, which is the accuracy specified by the manufacturer of the phase shifter. Considerable ability to ignore signal imperfections is inherent in this device.

Key Words: Digital, logic circuit, low frequency, measurements, phase, phasemeter.

The viscosity and thermal conductivity coefficients of dilute neon, krypton, and xenon, H. J. M. Hanley and G. E. Childs, *Tech. Note 352 (Mar. 23, 1967), 25 cents.*

The coefficients of viscosity and thermal conductivity for dilute neon, krypton, and xenon were examined by a method already proved successful for dilute argon, oxygen, and nitrogen. This method selects a suitable potential function, and its parameters, which is then used to correlate theory with experimental data, given the kinetic theory expressions for the transport coefficients. The method has recently been expanded and generalized and the results of this general study are applied in this note. The potential functions examined were members of the m-6, Kihara, Exp: 6, and Morse families. It was found that the Kihara was most suitable for neon, and the m-6, with $m=17$ and $m=24$, was most suitable for krypton and xenon, respectively. Viscosity and thermal conductivities were calculated from these functions and tables are given between 100 and 1000 °K.

Key Words: Dilute gases, neon, krypton, xenon, transport coefficients, correlations, m-6, Kihara, Exp: 6, Morse, potential functions.

Connector for saturated standard cells, J. J. Barth, *Tech. Note 353 (April 21, 1967), 10 cents.*

This paper describes a connector used for making electrical connections to saturated standard cells in oil baths. The connector has at least three advantages over other methods in common use. These advantages are namely: (1) it does not generate thermoelectromotive forces; (2) it allows cell racks to be placed close together in the bath; and (3) it is economical to fabricate since it can be made from a common inside caliper.

Key Words: Connector, electromotive force, oil baths, standard cells, thermoelectric.

Quantum mechanical calculations of the second virial coefficients for hydrogen, M. E. Boyd and S. Y. Larsen, *Tech. Note 412 (April 10, 1967), 15 cents.*

Quantum mechanical second virial coefficients of dilute ortho and para hydrogen have been calculated for the case of a Lennard-Jones potential. These computations cover the temperature range from 0 °K to 80 °K. Special attention is paid to the behaviour of the Boltzmann and exchange contributions. The purely statistical contribution to the ortho-para difference is shown to vanish to three decimal places by about 10.5 °K. Comparison with experimental data indicates that considerable improvement in the potential function and inclusion of non-spherical terms will be required at the low temperatures considered here.

Key Words: Second virial coefficient, quantum mechanics, hydrogen, equation of state, statistical mechanics, intermolecular potential.

Thermal radiation property measurement techniques, S. T. Dunn, J. C. Geist, D. G. Moore, H. E. Clark, and J. C. Richmond, *Tech. Note 415 (April 27, 1967), 50 cents.*
This is an annual summary report of work completed on NASA Contract R-09-022-032. The work comprised (1) completion of the development and calibration of a rotating cylinder procedure for measuring normal spectral emittance of non-conducting materials at temperatures in the range of 1200 to 1600 °K, (2) analysis and calibration of an ellipsoidal mirror reflectometer, and (3) a study of the relation between surface roughness and geometric distribution of flux reflected from a surface.

Key Words: Averaging spheres, diffuse reflectance, emissivity, emittance, flux averaging devices, infrared reflectance, spectral reflectance, spectral emittance, specular reflectance.

Flash photolysis of methane in the vacuum ultraviolet. II. Absolute rate constants for reactions of CH with methane, W. Braun, J. R. McNesby, and A. M. Bass, *J. Chem. Phys,* **46,** *No. 6,* 2071–2079 (*Mar. 15, 1967*).
By means of kinetic spectroscopy, the concentration of CH has been measured in the flash photolysis of methane. Measurements were made by following the attenuation of $C^2\Sigma^+ \leftarrow X^2\Pi$ Q branch at 3143 Å where the disappearance of CH is of the first order in CH. Experiments were conducted with pure methane, methane + H_2 and methane + N_2. The reactions and the corresponding rate constants in mol^{-1} cm^2 sec^{-1} are:

$CH + CH_4 \rightarrow C_2H_5 + H$	$k = 2.0 \times 10^{12}$
$CH + H_2 \rightarrow CH_3$	$k = 6.2 \times 10^{11}$
$CH + N_2 \rightarrow$ products	$k \simeq 4.3 \times 10^{10}$
$CH + CH \rightarrow C_2H_2$	$k \simeq 1.6 \times 10^{14}$

Key Words: CH, flash photolysis, hydrogen, kinetic spectroscopy, methane, nitrogen, rate constant, vacuum ultraviolet.

Initial kinetic parameters from thermogravimetric rate and conversion data, J. H. Flynn and L. A. Wall, *J. Polymer Sci. Letters* **5B,** *No. 2, 191–196 (Feb. 1967).*
A new method for determining the initial activation energy for volatilization process is developed from the limiting characteristics of rate vs. conversion plots and a few simple variants thereof. At low conversion, the energy of activation of linear polyethylene was $E(0.003 < C < 0.025;\ 630\ °K < T < 680\ °K) \cong 36$ kcal/mol, while a sample preheated at 200 °C in a vacuum for an hour gave $E(0.003 < C < 0.04;\ 640\ °K < T < 685\ °K) \cong 60$ kcal/mol.

Key Words: Energy of activation, thermogravimetry, polymer degradation, initial kinetic parameters, non-isothermal kinetics, stability of polymers, polyethylene.

Neutron-scattering study of the motions of water molecules in hydrated salts of transition metals, J. J. Rush, J. R. Ferraro, and A. Walker, *Inorg. Chem.* **6,** *No. 2, 346–351 (Feb. 1967).*
The low-frequency motions of water molecules in a series of hydrated transition-metal salts have been investigated by the energy-gain scattering of cold neutrons. The compounds studied include $CuSO_4 \cdot H_2O$, $CuSO_4 \cdot 5H_2O$, $Co(NO_3)_2 \cdot 2H_2O$, $Co(NO_3)_2 \cdot 6H_2O$, $Cu(NO_3)_2 \cdot 3H_2O$, and $UO_2(NO_3)_2 \cdot 6H_2O$. Broad bands observed in the spectra at neutron energy gains of 500 to 800 cm^{-1} are assigned to the wagging and rocking modes of the coordinated and hydrogen-bonded water molecules. Bands around 400 to 500 cm^{-1} are attributed both to M-OH_2 stretching modes, and to the H_2O torsional vibrations around the bisectrix. Maxima are also observed at energy transfers below 300 cm^{-1}, which are tentatively assigned to hydrogen bond stretching vibrations and possibly to H_2O-M-OH_2 deformation modes. Comparison of the various spectra appears to indicate that the average strength of binding of the water molecules does not change significantly in proceeding from the higher to the lower hydrates. The neutron results are compared in detail with previous infrared and structure results.

Key Words: Cold neutrons, neutron scattering, hydrates, hydrated salts, water librations, coordination, hydrogen-bonding, vibration spectra.

Stress-corrosion cracking of cold-reduced austenitic stainless steels, H. L. Logan and M. J. McBee, *Mater. Res. Std.* **7,** *No. 4, 137–145 (Apr. 1967).*
The effects of specimen orientation with respect to the direction of rolling or prior rolling on the susceptibility to stress-corrosion cracking in a boiling $MgCl_2$ solution were determined for both annealed and cold reduced types 301, 304, 310 and 321 stainless steels. Threshold stresses for the most susceptible orientations were determined in a boiling 0.5 N NaCl, 0.1 N $NaNO_2$ solution to be 60 to 110 percent of the yield strengths of the materials. None of the steels cracked in a marine atmosphere during 15 months exposure stressed at 90 percent of their yield strengths. The effects on the threshold stresses of varying amounts of cold work differed from steel to steel and are reported. The effects of internal stress patterns and welding were also investigated for some of these steels and are described.

Key Words: Stress-corrosion cracking, stainless steel types 301, 304, 310, 321, cold work, rolling orientation, threshold stresses, laboratory corrodents, marine exposure.

Autoionization spectra of the noble gases, R. P. Madden and K. Codling, (*Proc. Symp. Atomic Interactions and Space Physics, Goddard Space Flight Center, Greenbelt, Maryland, Aug. 10–11, 1965*), *Book, Autoionization: Astrophysical, Theoretical, and Laboratory Experimental Aspects, pp. 129–151 (Mono Book Corp., Baltimore, Md., 1966).*
The absorption spectra of the noble gases He through Xe have been studied extensively in the region 20–180 eV (600–70 Å), utilizing as a background source the pure continuum radiated by the orbiting electrons in the NBS 180 MeV electron synchrotron. Discrete structures or resonances, have been observed in the photoionization continua of each of these gases. These resonances are due to the existence of autoionizing states of the neutral atoms lying at energies in general, well above their first ionization limits. The structures have been classified into two types of transition; on the one hand, one-electron excitation involving either an outer-shell, sub-shell or inner-shell electron, on the other involving the excitation of any two electrons simultaneously, such that the energy required was appropriate for the present region of observation.

Key Words: Far ultraviolet absorption spectra, 20–180 eV, He, through Xe, autoionization, one and two electron excitation, synchrotron light source, resonance profiles.

An intercomparison of hydrogen and cesium frequency standards, R. Vessot, H. Peters, J. Vanier, R. Beehler, D. Halford, R. Harrach, D. Allan, D. Glaze, C. Snider, J. Barnes, L. Cutler, and L. Bodily, *IEEE Trans. Instr. Meas.* **IM-15,** *No. 4, 165–176 (Dec. 1966).*
Intercomparisons of average frequency and of frequency stability were made among one Hewlett-Packard 5060A cesium beam, two Varian Associates H–10 atomic hydrogen masers, and the National Bureau of Standards NBS III cesium beam designated as the United States Frequency Standard. Each of the standards displayed a white noise frequency fluctuation behavior with a transition into an approximate flicker of frequency fluctuation behavior for longer time intervals. The rms fractional frequency fluctuation between adjacent samples, $\sigma(\tau, N=2)$, was $6 \times 10^{-11}\tau^{-1/2}$ down to a flicker level of about 3×10^{-13} for the hp 5060A cesium beam ($10^2 \leq \tau \leq 10^4$s), $1 \times 10^{-11}\tau^{-1/2}$ down to a flicker level of less than 1×10^{-13} for NBS III cesium beam ($10^2 \leq \tau \leq 10^4$s), and $5 \times 10^{-13}\tau^{-1/2}$ down to a flicker level of about 1×10^{-14} for the H–10 hydrogen masers ($10^0 \leq \tau \leq 10^4$s). The accuracy capabilities of NBS III and H–10 #4 are now 1.1×10^{-12} and 0.47×10^{-12}, respectively (1σ estimate).
A discrepancy of only 1.1 parts in 10^{12} was observed between the average frequencies of the hp 5060A cesium beam and the NBS III cesium beam, with the former being higher in frequency.
In terms of the frequency of the Cs^{133} hyperfine transition $(F=4,\ m_F=0) \leftrightarrow (F=3,\ m_F=0)$, defined as 9192 631 770.0000 Hertz, the measured frequency of the H^1 hyperfine transition

$(F=1, m_F=0) \leftrightarrow (F=0, m_F=0)$ was $\nu_H = 1420\,405\,751.7864 \pm 0.0017$ Hertz. This is the most accurate and precise measurement of any physical quantity.

Key Words: Atomic clocks, cesium beam, clocks, frequency fluctuations, frequency standards, hydrogen maser, hyperfine separation, maser, noise, standards, time standards, wall shift.

Dislocation node determinations of the stacking fault energy in silver-tin alloys, A. W. Ruff, Jr. and L. K. Ives, *Acta Met.* **15,** *189–198 (Feb. 1967).*
Direct measurements by transmission electron microscopy on extended dislocation nodes in alloys of tin in silver have led to values for the intrinsic stacking fault energy. The values decreased smoothly from 23 erg/cm² for pure silver to 4.5 erg/cm² for 7.8 at .% tin, near the fcc phase limit. The results are compared with previous determinations in other silver-base alloys, and sources of systematic error are discussed. A comparison of different theoretical analyses is included.

Key Words: Dislocations, silver-tin alloy, stacking fault energy, electron microscopy.

Estimate of extrinsic stacking-fault energies from dislocation configurations, W. F. Hartl, R. deWit, and R. E. Howard, *J. Appl. Phys.* **38,** *No. 1, 1–4 (Jan. 1967).*
In this paper we use straight line models of observed extrinsic nodes to estimate extrinsic stacking fault energies. Using isotropic elasticity theory and neglecting interactions we find easily applicable expressions for the energy in terms of the inscribed radii of the nodes. We apply the results to be observed extended nodes in a silver −8 at .% tin alloy and find a ratio of extrinsic to intrinsic stacking fault energy of 3.0.

Key Words: Stacking fault energy, extrinsic faults, dislocations, silver-tin alloy.

Interpretation of ferromagnetic resonance measurement made in a nonresonant system, A. S. Risley and H. E. Bussey, *IEEE Trans. Instr. Meas.* **IM-15,** *No. 4, 393–396 (Dec. 1966).*
The loaded line width, ΔH_m (loaded by the coupling), and the resonator coupling coefficient, β, assuming a cavity resonator model, were measured on ferrimagnetic resonant YIG spheres in a (nonresonant) short circuited waveguide. The coupling was varied over a wide range by changing the angle ϕ between the dc and driving rf magnetic fields. The results showed that the unloaded line width, $\Delta H = \Delta H_m/(1+\beta)$, was essentially constant during changes in coupling. It is therefore tentatively concluded that the cavity resonator model furnishes an accurate model for separating unloaded from loaded line width. Other methods for obtaining ΔH, namely using a matched waveguide, or a pick-up loop, or the usual cavity perturbation method were less satisfactory.
The coupling coefficient was 1.06 times theoretical for widely different sample sizes and all reasonable angles ϕ. It follows that line width can be determined very simply from a simple reflection measurement without measuring the width.

Is proton channeling a diffraction process? H. A. Fowler and C. Erginsoy, *Physics Letters* **24A,** *No. 7, 390–391 (Mar. 27, 1967).*
Some stopping-power limitations are suggested on a dynamical-diffraction model of proton channeling at 1–5 MeV.

Key Words: Channeling, diffraction, energy loss, protons, stopping power.

Kinetics of solute-enhanced diffusion in dilute face-centered-cubic alloys, R. E. Howard and J. R. Manning, *Phys. Rev.* **154,** *No. 3, 561–568 (Feb. 1967).*
A theory of the effect of solutes on solvent self-diffusion in dilute f.c.c. alloys is given based on the model of nearest-neighbor interactions between solute impurities and vacancies. The parameters of the theory are the four vacancy jump frequencies in the neighborhood of an impurity and the vacancy jump frequency in the pure crystal. No assumptions are made about the relative magnitudes of these frequencies. This distinguishes the present theory from previous theories based on the same model. The theory is used to deduce for each of nine dilute Ag-based alloys sets of jump frequency ratios (and corresponding impurity correlation factors) that are consistent with measured values of the solute enhancement coefficient and of the impurity diffusion coefficient. The desirability of isotope effect measurements to determine the impurity correlation factors is emphasized.

Key Words: Correlation factors, diffusion, dilute alloys, impurities, jump frequencies, vacancies, solute atoms.

Molecular thermodynamics of simple liquids, pure components, H. Renon, C. A. Eckert, and J. M. Prausnitz, *I & EC Fundamentals* **6,** *No. 1, 52–58 (Feb. 1967).*
Thermodynamic properties of simple liquids are calculated from an analytical partition function based on a modification of Prigogine's cell theory and on a three-parameter theorem of corresponding states. The partition function gives an excellent representation of the configurational properties of 15 liquids ranging in molecular complexity from argon to neopentane. Three characteristic molecular parameters are sufficient to calculate the configurational energy and entropy, volume, coefficient of expansion, and compressibility. These parameters are a molecular size, a pair-potential energy, and a term closely related to noncentral intermolecular forces; this last parameter is a nearly linear function of Pitzer's acentric factor. The main application of this statistical thermodynamic treatment follows from its straightforward extension to liquid mixtures.

Molecular thermodynamics of simple liquids, mixtures, C. A. Eckert, H. Renon, and J. M. Prausnitz, *I & EC Fundamentals* **6,** *No. 1, 58–67 (Feb. 1967).*
The analytical partition function for pure, simple liquids is generalized for liquid mixtures containing any desired number of components. The properties of liquid mixtures are calculated from standard statistical mechanical relations on the basis of Scott's two-liquid theory coupled with a three-parameter theorem of corresponding states. The effect of three molecular parameters on solution excess function is investigated, and it is shown that these are very sensitive to the characteristic energy for two unlike molecules; in general, this energy is not sufficiently well approximated by the geometric-mean assumption but must be determined by some mixture property such as the second virial cross coefficient, B_{12}. Calculated excess Gibbs energies, enthalpies, and volumes agree very well with experimental results for 17 binary systems containing simple, nonpolar molecules.

Rare-gas collision broadening in the lowest $^3P_1$ level of Cd, R. L. Barger, *Phys. Rev.* **154,** *No. 1, 94–97 (Feb. 5, 1967).*
Alignment depolarization collision cross sections have been measured for the $^3P_1$ level of cadmium broadened by the rare gases. Cross sections obtained with the Hanle effect (zero-field level crossing) and the method of modulated light double resonance agree within approximately 10 percent, but differ from theoretical predictions by approximately 50 percent. Average experimental values (units of 10^{-15} cm²) for He, Ne, Ar, Kr, and Xe, respectively, are 2.6, 2.7, 4.1, 5.9, and 8.3.

Key Words: Cadmium, cross sections, double resonance, level crossing.

Some aspects of the photodisintegration of light nuclei, E. Hayward, *Proc. Intern. School of Physics "Enrico Fermi," Course 565 (Academic Press Inc., London, England, 1966).*
The photonuclear giant resonance is discussed from the point of view of isotopic spin mixing and intermediate structure.

Key Words: Isotopic spin, intermediate structure, photodisintegration.

Some experiments with Zeeman shifted levels, K. G. Kessler (*Proc. Zeeman Centennial Conf., Amsterdam, The Netherlands, Sept. 9–11, 1965*), *Physica* **33,** *29–46 (1967).*
A review of some applications of the Zeeman effect to studies of the resonance line of mercury. Techniques discussed include Zeeman scanning of an atomic beam, double resonance, level

crossing and the Zeeman filter. Examples are drawn in large part from the work of Dr. Bitter's group at MIT and by the author and his colleagues at NBS. Fundamental data obtained in these studies include the hyperfine structure, isotope shifts and Zeeman splitting, in both naturally occurring and short-lived isotopes, the Lande g-factor and the lifetime of the $^3P_1^0$ states.

Key Words: Atomic beams, double resonance, isotope shifts, Lande *g*-factor, mercury hyperfine structure, Zeeman filter.

Some relations for straight dislocation, R. deWit, *Phys. Stat. Sol.* **20,** *567–573 (1967).*
Expressions are presented for the stress, strain, dilatation, and displacement due to a straight dislocation, as well as the force per unit length and the total force on a straight dislocation due to another straight dislocation. They differ from previous expressions in the literature in that they are given completely in tensor or vector notation. They are limited to the case of a *linear, isotropic, infinite* continuum.

Key Words: Continuum, crystal, defect, dislocation, displacement, interaction, isotropic, strain, stress.

Specific heat of natural rubber and other elastomers above the glass transition temperature, L. A. Wood and N. Bekkedahl, *J. Polymer Sci. Letters* **5,** *169–175 (1967).*
A survey is given of literature values of the specific heat C_p as a function of temperature (above the glass transition temperature) for the elastomers, including natural rubber, polyisobutylene, polybutadiene, several butadiene-styrene copolymers, and a butadiene-acrylonitrile copolymer. The values of dC_p/dt (where t is the temperature) found for natural rubber were abnormally low in the range −68 to +2 °C and abnormally high in the range 17° to 47 °C. The most probable explanation is that crystallization of the unvulcanized rubber was predominating in the first range, and melting of these crystals was predominating in the second range.

Key Words: Specific heat, elastomers, rubber, polyisobutylene, polybutadiene, butadiene-styrene copolymers, butadiene-acrylonitrile copolymer, polyethelene, crystallization of rubber.

The self-energy of dislocation configurations made up of straight segments, R. deWit, *Phys. Stat. Soc.* **20,** *575–580 (1967).*
Three general expressions are presented: the first is the interaction energy between two nonparallel straight dislocation segments, the second is the interaction energy between two parallel straight segments, and the third is the self-energy of a straight segment. These can be used to determine the total energy of any dislocation configuration made up of piecewise straight segments. They differ from previous expressions in the literature primarily in that they are given completely in vector notation and in that the self-energy includes a core traction term. The expressions are limited to the case of a *linear, isotropic, infinite* continuum. As an example, the formulas are applied to the case of a stacking-fault-tetrahedron.

Key Words: Continuum, crystal, defect, dislocation, energy, interaction, isotropic, straight.

The small-angle limit for twice-scattered gamma rays from a point-isotropic source, E. E. Morris and L. V. Spencer, *Nucl. Sci. Eng.* **27,** *485–488 (Feb. 1967).*
The small-angle limit of the twice-scattered flux from a point isotropic, monoenergetic source of gamma radiation is calculated. Importance is attached to this limit because of a logarithmic divergence of the angular distribution of the twice-scattered flux. Comments intended to facilitate the application to neutrons are given at the end.

Key Words: Angular distribution, gamma radiation, logarithmic divergence, point isotropic, small-angle limit, twice-scattered.

The stacking-fault energy in alpha-silver-tin alloys, A. W. Ruff, Jr. and L. K. Ives, *Can. J. Phys.* **45,** *787–795 (1967).*
Direct measurements by transmission electron microscopy on extended dislocation nodes in alloys of tin in silver have led to values for the intrinsic stacking fault energy. The values decreased smoothly from 23 erg/cm² for pure silver to 4.5 erg/cm² for 7.8 at .% tin. The results are compared with previous determinations in other silver-base alloys.

Key Words: Dislocations, stacking faults, silver-tin alloys, electron microscopy, stacking fault energy, dislocation nodes.

Vibrational analysis of SeF_6 and WF_6, S. Abramowitz and I. W. Levin, *Inorg. Chem.* **6,** *538–541 (1967).*
The gas phase infrared vibration-rotation spectra of SeF_6 and WF_6 have been measured in the region of their fundamental absorption bands. Coriolis constants, evaluated from the observed contours, are used as constraints for the general force field for these molecules.

Key Words: Force field, SeF_6, WF_6, Coriolis constants, vibration-rotation, infrared.

Other NBS Publications

J. Res. NBS 71B2 & 3 (Math. and Math. Phys.), No. 2 & 3 (Apr.–Sept. 1967), 75 cents.
Poincaré's conjecture is implied by a conjecture on free groups. R. D. Traub.
Construction of *EPr* generalized inverses by inversion of nonsingular matrices. J. Z. Hearon.
A generalized matrix version of Rennie's inequality. J. Z. Hearon.
Polar factorization of a matrix. J. Z. Hearon.
Two classical theorems on commuting matrices. M. Newman.
A converse to Banach's contraction theorem. P. R. Meyers.
E-transforms (II). F. M. Ragab.
Criterion for the stability of numerical integration methods for the solution of systems of differential equations. A. I. A. Karim.
Discrete complex functions with prescribed boundary values and residues. E. L. Peterson.
Numerical solution of second-order linear difference equations. F. W. J. Olver.
Indefinite integrals involving Bessel functions. B. A. Peavy.

J. Res. NBS 71C3 (Engr. and Instr.), No. 3 (July–Sept. 1967), 75 cents.
Procedure for high precision density determinations by hydrostatic weighing. H. A. Bowman and R. M. Schoonover with Appendix by M. W. Jones. (See above abstracts.)
Study of the storage stability of the barium fluoride film electric hygrometer element. F. E. Jones.
Torsion creep of circular and noncircular tubes. L. Mordfin. (See above abstracts.)
Digitized low-frequency phasemeter assembled from logic modules. J. E. McKinney. (See above abstracts.)

Bibliography of temperature measurement, July 1960 to December 1965, L. O. Olsen and C. Halpern, Mono. 27, Supplement 2 (April 28, 1967), 35 cents (supersedes Supplement 1 to Monograph 27).
Colors of signal lights: Their selection, definition, measurement, production, and use, F. C. Breckenridge, Mono. 75 (April 3, 1967), 40 cents.
Automatic typographic-quality typesetting techniques: a state-of-the-art review, M. E. Stevens and J. L. Little, Mono. 99 (April 7, 1967), 70 cents.
Technical highlights of the National Bureau of Standards, annual report 1966, Misc. Publ. 283 (April 1967), 60 cents.
Technology and world trade. Proceedings of a symposium, edited by R. L. Stern, Misc. Publ. 284 (1967), $1.25.
Units of weight and measure. International (metric) and U.S. Customary, L. J. Chisholm, Misc. Publ. 286 (May 1967), $1.50 (supersedes Miscellaneous Publication 233).
Report of the 51st National Conference on weights and measures, 1966, Report editor L. J. Chisholm, Misc. Publ. 290 (May 15, 1967), $1.00.
Softwood plywood, construction and industrial, Prod. Std. 1–66 (November 1, 1966), 20 cents (supersedes Commercial Standards 45–60, 122–60, and 259–63).
Standard stock light-duty 1⅜- and 1¾-inch thick flush-type interior steel doors and frames, Prod. Std. 4–66 (November 1, 1966), 10 cents (supersedes Commercial Standard 211–57).

Discussion of errors in gain measurements of standard electromagnetic horns, R. W. Beatty, Tech. Note 351 (March 1967), 30 cents.

Quantitative methods for management, G. Suzuki, Tech. Note 414 (May 23, 1967), 25 cents.

Adhesive bonding of various materials to hard tooth tissues. IV. Forces developing in direct-filling materials during hardening, R. L. Bowen, J. Am. Dental Assoc. **74,** No. 3, 440–445 (Feb. 1967).

Bonding porcelain teeth to acrylic resin denture bases, G. C. Paffenbarger, W. T. Sweeney, and R. L. Bowen, J. Am. Dental Assoc. **74,** 1018–1023 (Apr. 1967).

Comparison of direct and sensitized photolysis of 3-methylpentanal in vapor phase, R. E. Rebbert and P. J. Ausloos, J. Am. Chem. Soc. **89,** No. 7, 1573–1579 (Mar. 29, 1967).

Conformation of polyesters adsorbed on solid surfaces, P. Peyser, D. J. Tutas, and R. R. Stromberg, J. Polymer Sci. **5,** Pt. A-1, 651–663 (1967).

Effects of packing pressures on the properties of spherical alloy amalgams, G. T. Eden and R. M. Waterstrat, J. Am. Dental Assoc. **74,** No. 5, 1024–1029 (Apr. 1967).

Flow properties of aqueous suspensions containing kaolins of varying degrees of crystallinity, W. C. Ormsby and J. H. Marcus, J. Am. Ceramic Soc. **50,** No. 4, 190–195 (Apr. 1967).

NBS hunts for better ways to control corrosion, S. Lichtenstein, Mater. Eng. **65,** No. 5, 21–23 (May 1967).

Reactions of ethylidene in the vacuum ultraviolet photolysis of ethylene, E. Tschuikow-Roux, J. R. McNesby, W. M. Jackson, and J. L. Faris, J. Phys. Chem. **71,** No. 5, 1531–1532 (Apr. 1967).

The effect of other metallic ions on the electrocrystallization of silver from nitrate solutions, J. P. Young, Plating **54,** No. 3, 272–274 (Mar. 1967).

The relationship between laboratory tests on solubility of zinc oxide-eugenol type cement and their behavior in the mouth, G. M. Brauer, N.Y. J. Dentistry **37,** No. 4, 146 (Apr. 1967).

A new service by NBS. An aid in making the Bureau's technical resources available to private standards organizations, manufacturers, and government agencies, G. S. Gordon, Proc. 15th Annual Meeting Standards Engineering Society, Atlantic City, N.J., Sept. 14, 1966, pp. 73–75 (1966).

Absolute calibration of vibration generators with time-sharing computer as integral part of system, B. F. Payne, Shock Vibration Bull. **36,** Pt. 6, 183–194 (Feb. 1967).

Cathodic protection of copper in a severely corrosive soil, W. J. Schwerdtfeger, IEEE Trans. Ind. Gen. Appl. **IGA-3,** No. 1, 66–69 (Jan.–Feb. 1967).

Electrical feedthrough for pressures to 10 kbar, P. L. M. Heydemann, Rev. Sci. Instr. Laboratory Notes **38,** No. 4, 558–559 (Apr. 1967).

Ellipsometric errors due to multiple reactions in mica quarter-wave plates, H. T. Yolken, R. M. Waxler, and J. Kruger, J. Opt. Soc. Am. **57,** No. 2, 282–284 (Feb. 1967).

Evaluation of a stark voltmeter, Y. Beers and T. W. Russell, IEEE Trans. Instr. Meas. **IM-15,** No. 4, 380–388 (Dec. 1966).

Improved transfer standard for vibration pickups, E. Jones, D. Lee, and S. Edelman, J. Acoust. Soc. Am. **41,** No. 2, 354–357 (Feb. 1967).

Introduction, J. M. Richardson, (Proc. 1966 Conf. Precision Electromagnet Measurements, Boulder, Colorado, June 21–23, 1966), IEEE Trans. Instr. Meas. **IM-15,** No. 4, 138 (Dec. 1966).

Anniversaries in 1966–67 of interest to statisticians Part I: Introduction and summary, C. Eisenhart, Am. Stat. **21,** No. 2, 32–34 (Apr. 1967).

Classification of normal subgroups of the modular group, M. Newman, Trans. Am. Math. Soc. **126,** No. 2, 267–277 (Feb. 1967).

Comments on presentation by Albert A. Anctil, J. R. Rosenblatt, (Proc. 11th Conf. Design of Experiments in Army Research Development and Testing, Dover, N.J., Oct. 20–22, 1965), U.S. Army ARO–D Report 66–2, pp. 509–510 (U.S. Army Research Office, Durham, N.C., May 1966).

Note on normal subgroups of the modular group, L. Greenberg, Proc. Am. Math. Soc. **17,** No. 5, 1195–1198 (Oct. 1966).

Interval scales, ratio scales, and additive scales for the sizes of differences perceived between members of a geodesic series of colors, D. B. Judd, J. Opt. Soc. Am. **57,** No. 3, 380–386 (Mar. 1967).

Reflectance spectrophotometry, D. B. Judd, Encyclopedia of Industrial Chemical Analysis, **3,** 376–392 (John Wiley and Sons, Inc., New York, N.Y., 1966).

The national measurement systems of various countries, H. W. Lance, IEEE Trans. Instr. Meas. **IM-15,** No. 4, 397–403 (Dec. 1966).

The variability of color measurements, I. Nimeroff, Color Eng. **5,** No. 2, 24–29 (Mar.–Apr. 1966).

Thermal converters for audio-frequency voltage measurements of high accuracy, F. L. Hermach and E. S. Williams, IEEE Trans. Instr. Meas. **IM-15,** No. 4, 260–268 (Dec. 1966).

WWV moves to Colorado. Part I, Y. Beers, QST **51,** No. 1, 11–14 (Jan. 1967); Part II, QST **51,** No. 2, 30–35 (Feb. 1967).

An optical power limiter, B. L. Danielson, Appl. Opt. **6,** No. 1, 158–159 (Jan. 1967).

Chromatic changes induced by changes in chromaticity of background of constant lightness, H. Takasaki, J. Opt. Soc. Am. **57,** No. 1, 93–96 (Jan. 1967).

Comments on "Nature of the critical nucleus in heterogeneous vapor-solid nucleation," A. J. Melmed and S. C. Hardy, Surface Sci. **6,** No. 4, 481–482 (April 1967).

Compensation and band tailing effects in high power room temperature GaAs lasers, N. N. Winogradoff and H. K. Kessler, Solid-State Communications **5,** 155–158 (Pergamon Press Ltd., London, England, 1967).

Correlation of spherical aberration of axially symmetrical magnetic lenses, L. Marton, Rev. Sci. Instr. **38,** No. 1, 130–131 (Jan. 1967).

Correlation of large longitudinal deformations with different strain histories, L. J. Zapas and T. Craft, Rubber Chem. Technol. **40,** No. 2, 506–516 (Mar. 1967).

Electron monochromator design, C. E. Kuyatt and J. A. Simpson, Rev. Sci. Instr. **38,** No. 1, 103–111 (Jan. 1967).

Excitation and ionization in arc and spark spectroscopic sources, M. Margoshes, Appl. Spectry. **21,** No. 2, 92–99 (1967).

Measurement of thermal neutron flux, R. S. Carter, C. O. Muehlhause, and V. W. Myers, IEEE Trans. Nucl. Sci. **NS-14,** No. 1, 414–415 (Feb. 1967).

Recombination of He^{+} and He^{++} in the afterglow of a helium discharge, E. R. Mosburg, Jr., Phys. Rev. **152,** No. 1, 166–176 (Dec. 2, 1966).

Second breakdown and crystallographic defects in transistors, H. A. Schafft, G. H. Schwuttke, and R. L. Ruggles, Jr., IEEE Trans. Electron Devices **ED-13,** No. 11, 738–742 (Nov. 1966).

Simultaneous diffraction with the three-circle diffractometer, M. Zocchi and A. Santoro, Acta Cryst. **22,** Pt. 3, 331–334 (Mar. 1967).

**Publications for which a price is indicated are available by purchase from the Superintendent of Documents, U.S. Government Printing Office, Washington, D.C. 20402 (foreign postage, one-fourth additional). The NBS nonperiodical series are also available from the Clearinghouse for Federal Scientific and Technical Information, Springfield, Va. 22151. Reprints from outside journals and the NBS Journal of Research may often be obtained directly from the authors.*

U.S. GOVERNMENT PRINTING OFFICE : 1967 OL—267–984

UNIVERSITY MICROFILMS INC
ATTN SERIALS SECTION
300 NORTH ZEEB RD
ANN ARBOR MICH 48106

UNITED STATES
GOVERNMENT PRINTING OFFICE
DIVISION OF PUBLIC DOCUMENTS
WASHINGTON, D.C. 20402

OFFICIAL BUSINESS

POSTAGE AND FEES PAID
U.S. GOVERNMENT PRINTING OFFICE

JOURNAL OF RESEARCH of the National Bureau of Standards Vol. 71A, No. 5 September–October 1967
A. Physics and Chemistry

Contents

Page

Zeeman effect in positronium annihilation at low temperatures. William C. Sauder and Richard D. Deslattes. 347

Surface-layer relaxation in the dielectric spectrum of CaF_2 doped with GdF_3. A. D. Franklin, S. Marzullo, and J. B. Wachtman, Jr. 355

Thermal expansion of rutile from 100 to 700 °K. Richard K. Kirby. 363

Mass spectrometric study of photoionization. VII. Nitrogen dioxide and nitrous oxide. Vernon H. Dibeler, James A. Walker, and Susan K. Liston. 371

Ionization constants of substituted benzoic acids in ethanol-water. G. M. Brauer, George Durany, and Harold Argentar. 379

Dissociation constants of some substituted nitrophenols in aqueous solution at 25 °C. R. A. Robinson. 385

Publications of the National Bureau of Standards. 391

Library of Congress Catalog Card Number: 62–37059

For sale by the Superintendent of Documents, U.S. Government Printing Office, Washington, D.C. 20402. Price $1.00 (single copy).
Subscription price: $5 a year; $1.00 additional for foreign mailing.
UNITED STATES GOVERNMENT PRINTING OFFICE, WASHINGTON : 1967